Physical-Layer-Impairment-Aware Routing and Spectrum Allocation in Flexible Optical Networks

Cao Chen

AVIGNON UNIVERSITÉ

ACADÉMIE D'AIX-MARSEILLE
UNIVERSITÉ D'AVIGNON ET DES PAYS DE VAUCLUSE

THÈSE

présentée à l'Université d'Avignon et des Pays de Vaucluse
pour obtenir le diplôme de DOCTORAT

SPÉCIALITÉ : Informatique

École Doctorale 536 « Sciences et Agronomie »
Laboratoire d'Informatique (EA 4128)

Routage et Allocation de Spectre en Tenant Compte de l'Interférence de la Couche Physique dans les Réseaux Optiques Flexibles

Présentée par
Cao Chen

Soutenue publiquement Octobre 2021 devant un jury composé de :

Mme.	Catherine Lepers	Professeur, Télécom SudParis	Rapporteur
M.	Mario Pickavet	Professeur, Université de Gand	Rapporteur
M.	Ahmed Meddahi	Professeur, IMT Nord Europe	Examinateur
M.	Yvan Pointurier	Ingénieur de Recherche, Huawei France	Examinateur
M.	Laurent Clavier	Professeur, IMT Nord Europe	Examinateur
M.	Shilin Xiao	Professeur, Université Shanghai Jiao Tong	Co-directeur
M.	Fen Zhou	Professeur, IMT Nord Europe & Université d'Avignon	Directeur

Laboratoire d'Informatique d'Avignon

LABORATOIRE INFORMATIQUE D'AVIGNON

AVIGNON UNIVERSITÉ

ACADÉMIE D'AIX-MARSEILLE
UNIVERSITÉ D'AVIGNON ET DES PAYS DE VAUCLUSE

THESIS

A thesis submitted at the University of Avignon
for the degree of Doctor of Philosophy

In : Computer Science

Doctoral School 536 « Sciences et Agroscience »
Laboratoire d'Informatique (EA 4128)

Physical-Layer-Impairment-Aware Routing and Spectrum Allocation in Flexible Optical Networks

Presented by

Cao Chen

Defended publicly October 2021 before the jury members:

Ms.	Catherine Lepers	Professor, Telecom SudParis	Reviewer
M.	Mario Pickavet	Professor, Ghent University	Reviewer
M.	Ahmed Meddahi	Professor, IMT Nord Europe	Examiner
M.	Yvan Pointurier	Research Engineer, Huawei France	Examiner
M.	Laurent Clavier	Professor, IMT Nord Europe	Examiner
M.	Shilin Xiao	Professor, Shanghai Jiao Tong University	Co-supervisor
M.	Fen Zhou	Professor, IMT Nord Europe & Avignon University	Supervisor

LABORATOIRE INFORMATIQUE D'AVIGNON

Laboratoire d'Informatique d'Avignon

Résumé

La croissance constante du trafic Internet constitue un défi pour les réseaux de cœur actuels, nous motivant à tirer pleinement parti de l'équipement optique en place pour augmenter la capacité de transmission dans les réseaux optiques flexibles (FONs). Cependant, les paramétrages efficaces de réseau sont strictement et prudemment limités par des dégradations complexes de la couche physique (PLI). Ainsi, il est nécessaire d'établir un modèle d'estimation PLI approprié pour intégrer la prise en compte de ces paramètres de réseau pour exploiter la capacité potentielle.

Dans cette perspective, nous établissons d'abord un modèle PLI. Un modèle PLI précis implique moins d'erreurs d'estimation des PLI subis et plus de chances d'utiliser le paramètre efficace. En particulier, l'interférence complexe entre les chemins optiques est modélisée sous forme de graphes non orientés, dans lesquels le nœud représente un chemin optique tandis que le lien entre les nœuds désigne l'interférence non linéaire ou la diaphonie des nœuds. En outre, la capacité réalisable et l'exigence de rapport signal sur bruit (SNR) d'un format de modulation (MF) et d'une correction d'erreur directe (FEC) donnés sont également évaluées afin que chaque chemin optique puisse utiliser les paramètres appropriés en fonction de ses PLI. En utilisant ce modèle PLI établi, nous réalisons trois études, qui visent à optimiser différents paramètres de la couche physique, tels que la bande passante du signal, l'espace entre des canaux, MF, FEC et la densité spectrale de puissance (PSD), ainsi que l'avantage de services élastiques.

La première étude porte sur la maximisation des revenus en tirant parti des MF et FEC. Nous formulons un modèle de programmation linéaire en nombres entiers mixtes qui peut fournir le chemin optique incorporant à la fois les PLI sur les liens et au niveau des optiques nœuds. Les résultats de la simulation valident l'amélioration des revenus avec les paramètres optimisés. En outre, les résultats révèlent également que l'utilisation du MF adaptatif permet d'augmenter les revenus dans le scénario de SNR élevé, tandis que l'utilisation du FEC adaptatif est rentable pour les scénarios à faible SNR, ce qui élargit un nouvel aperçu des MF et des FEC.

Dans la deuxième étude, nous étudions le gain de performances tout en optimisant le débit en bauds et l'espacement simultanément. En particulier, l'espacement des canaux est optimisé de manière peu complexe sans utiliser de bandes de garde candidates. Ensuite, l'amélioration des performances SNR d'une telle optimisation est convertie en débit du réseau en utilisant un algorithme de réglage de rétroaction itératif. Les résultats de la simulation vérifient l'amélioration de l'optimisation de l'espacement

des canaux pour les charges de trafic faible et moyenne en termes de débit du réseau et de performances SNR, qui surpassent tous deux la stratégie d'espacement de canaux fixe existante. En outre, la stratégie d'espacement fixe des canaux n'est même pas compatible pour les réseaux avec une charge élevée. Ces résultats mettent en évidence le scénario d'application potentiel de l'optimisation de l'espacement des canaux et des débits en bauds flexibles dans les FONs.

Dans la troisième étude, nous nous concentrons sur les performances de revenus lorsque le réseau prend en charge des services avec des débits, par exemple, acceptables avec un débit de 100%, 80% ou 50%, plutôt qu'un débit simplement 100%. Un modèle de programmation linéaire en nombres entiers et une méthode de décomposition sont proposés pour maximiser les revenus en résolvant le problème des sélections de débit du service, de route, de MF, de FEC, et de débit en bauds, ainsi que l'allocation de spectre. En outre, nous étudions également la stratégie de reconfiguration du réseau appropriée pour prendre en charge les services élastiques dans le scénario de charges incrémentielles. À cette fin, nous proposons un schéma d'auto-dégradation pour déclencher l'accord ou le réacheminement du spectre dans une charge de réseau élevée. En utilisant ce schéma, nous sommes en mesure de déterminer les stratégies de reconfiguration de réseau appropriées pour un réseau spécifié lors de la prise en charge de services élastiques.

Mots-clés: Réseaux optiques flexibles (FONs), Routage et allocation de ressource spectrale (RSA), Altération de la couche physique (PLI), Espacement des canaux

Abstract

The constant Internet traffic growth poses a challenge for the current backbone networks, motivating us to take full advantage of the incumbent optical equipment to increase the transmission capacity in flexible optical networks (FONs). However, the efficient network parameters are strictly and conservatively constrained by complex physical layer impairments (PLIs). Thus, it is required to establish a proper PLI estimation model to incorporate the consideration of these network parameters to exploit the potential capacity.

From this perspective, we first establish a PLI model. An accurate PLI model implies less estimation error of the suffered PLIs and more chance of using the efficient parameter, thus we simultaneously incorporate the PLIs on links and at nodes to numerically reflect PLIs for the changes of different lightpaths. In particular, the complex interference between lightpaths is modeled as undirected graphs, in which the node represents a lightpath while the link between nodes denotes the nonlinear interference or node crosstalk. In addition, the achievable capacity and the signal-to-noise ratio (SNR) requirement of a given modulation format (MF) and Forward Error Correction (FEC) are also evaluated so that each lightpath can use appropriate parameters according to its experienced PLIs. By using this established PLI model, we carry out three studies, which investigate the benefit of optimizing different physical layer parameters, such as signal bandwidth, channel spacing, MF, FEC, and power spectral density (PSD), as well as the benefit of elastic services.

The first study investigates the revenue maximization problem leveraging adaptive MFs and multiple FECs. We formulate a mixed-integer linear programming model that can provision the lightpath incorporating both the PLIs on links and at nodes. Simulation results validate the revenue improvement with the optimized parameters. Besides, the results also reveal that using adaptive MF enables to increase the revenue in the scenario of high SNR while using adaptive FEC is profitable for scenarios with low SNR, which broadens a new insight of the MFs and FECs.

In the second study, we investigate the performance gain when optimizing baudrate and channel spacing. More importantly, the channel spacing is optimized in a low-complexity way without using candidate guard bands. Then, the SNR performance improvement of such optimization is converted into network throughput by using an iterative feedback tuning algorithm. Simulation results verify the improvement of channel spacing optimization of low traffic and medium traffic loads in terms of network

throughput and SNR performance, which both outperform the existing fixed channel spacing strategy. Besides, it is allowed for the proposed channel spacing strategy to be employed in the high traffic load scenario that is unable for the fixed channel spacing strategy. These findings highlight the potential application scenario of channel spacing optimization and flexible baud-rates in FONs.

In the third study, we focus on the revenue performance when the network supports elastic services, e.g., acceptable with 100%, 80%, or 50%, rather than merely 100%. An integer linear programming model and a decomposition method are proposed to maximize the revenue by solving the service level, route, MF, FEC, baud-rate, spectrum assignment problem. In addition, we also investigate the suitable network reconfiguration strategy for accommodating elastic services in the scenario of incremental loads. To this end, we propose an auto-degrading scheme to trigger the spectrum tuning or rerouting in a high network traffic load. Using this scheme, we are able to determine the proper network reconfiguration strategies for a specified network when accommodating elastic services.

Key-words: Flexible Optical Networks (FONs), Routing and Spectrum Assignment (RSA), Physical Layer Impairment (PLI), Channel Spacing.

Acknowledgements

This work is supported by China Scholarship Council, Campus France, and special doctoral contract (Covid-19) of Avignon University.

First and foremost, I offer my gratitude to Prof. Fen Zhou, who supported me throughout my thesis with his kindness, patience, guidance and encouragement. Without his effort, patience and availability during the four years, I would not have been able to complete this work.

I would like to thank Prof. Shilin Xiao. He always gives me good advice and encouragement in my work. I also appreciate his guideline on the participation of the joint-supervision program.

I would like to thank Prof. Massimo Tornatore for his invaluable suggestions, patience, kindness, and kind encouragement. I really appreciate the opportunity to work with him.

I also would like to thank my committee members for their prompt evaluation and comments to improve the quality of this dissertation.

I would like to thank my friends Min Ju, Haitao Wu, Weijie Lan, Xuwei Liu, Linyuan Li, Xu Zhang, Jiabao Yu, Yi Yu, Yuanhao Liu, and all the fellow graduate students for their friendship during my four years in France (Avignon, Paris, and Lille). Special thanks to Min Ju and Yuanhao Liu for the valuable discussions and collaborations.

I would like to thank fellow graduate students and friends Zhengtao Jin, Yunhao Zhang, Lu Zhang, Ling Liu, Hanlin Feng, Yinan Hou, Shaojie Zhang, Yuankai Xue, Meihua Bi, Yinghong Yu, Wansheng Pan, and Jiafei Fang in Shanghai Jiao Tong University for their friendship during my work.

Last but not least, I would like to thank my family, my relatives in China, as well as my girlfriend Xiaoyin, for their kindness, patience, encouragement, and support in these years.

List of Figures

List of Tables

Introduction

According to recent traffic reports, network traffic (fueled by network services like video on demand, file sharing, online gaming, and video conferencing) is growing exponentially on today's Internet[36]. What is more important is that busy hour traffic peaks are expected to grow almost five times from 2017 to 2022 (average Internet traffic will increase only about four times)[36]. The problem of coping with sudden resource crunches will become even more a matter of concern in the following years, especially during peak usage periods. Such heavy traffic loads will bring significant challenges to the current network.

A solution to accommodate the tremendous traffic growth is using the optical network. It has become an essential technology for modern core networks with the help of enormous bandwidth, low latency, and long transmission reach. In optical networks, the network traffic is transported along a selected lightpath that connects the source node to the destination node. An adequate amount of spectrum resources to establish a lightpath is required. Traditionally, in coarse wavelength division multiplexing (CWDM or coarse WDM) networks, the spectral resources were divided by rigid 20 nm over the optical wavelength ranging from 1,270 nm to 1,610 nm. Recently, in the dense wavelength division multiplexing (DWDM) networks with a narrower channel spacing of 100 GHz or 50 GHz, the frequency grid of spectral resources has shifted from the rigid 20 nm to the fine-grained 0.8 nm or 0.4 nm. More recently, in flexible optical networks (FONs), finer-grained frequency slot (FS, e.g., 12.5 GHz or 6.25 GHz) is available, and multiples contiguous FSs can form into a super-channel[49]. This new form of spectrum utilization makes it possible for on-demand bandwidth provisioning, and dramatically cuts the unused spectrum resources of CWDM and DWDM. With the mature of coherent detection technology and the commercially available analog-to-digital converters (ADCs) and digital-to-analog converters (DACs), advanced modulation formats (e.g., modulation format (MF)[147], Forward Error Correction (FEC)[50], probabilistic shaping[43], and time-domain hybrid modulation (TDHM)[156]) are also available for the optical channel to obtain the theoretical spectral efficiency predicted by Shannon theory. The opportunity created by the flexibilities of the route, flexible spectrum resources, and advanced MFs, allows the network to reach its maximum capacity. However, it also poses challenges for network management.

One of the challenges is that network operators should be aware of the physical layer impairments (PLIs) when employing various flexibilities. The PLIs of a lightpath

are influenced by the bandwidth, by power spectral density (PSD), by the route length, by the number of crossed nodes, by the crossed fiber links, etc. Due to the impact of all the parameters just mentioned, the quality of transmission (QoT, e.g., expressed by lightpath's signal-to-noise ratio, SNR) may degrade and fall below acceptable threshold for correct signal reception after a long distance. Traditionally, a simple method to avoid the complex impact of PLIs is to employ a large margin calculated by the worst-case, and then restrict the maximum transmission reaches or the maximum spectral efficiencies. The overestimation of PLIs can guarantee uninterrupted communication, which however leads to waste network spectral resources, and consequently fail to exploit the advantage of these flexibilities. Moreover, since the interference between lightpaths depends on their center frequencies, the channel spacing and channel order problems omitted in traditional non-PLI-aware routing will act as a new degree of freedom for optimization[92, 140].

Another challenge is that network operator should consistently provision the incoming services with guaranteed quality of service (QoS), even when the network is approaching saturation during rush hours. The capacity crunch problem will occur in the near future due to the impact of PLIs[12]. We are expected to use the current network resources for a long time before new optical fibers (low loss in multi-band or low crosstalk in multiple spatial modes), new transmission bands (O, E, S, C, and L band), and new optical equipment (the supported optical amplifiers and lasers) are deployed before 2025[134]. With such limited resources, the optical network will become heavily loaded and fail to satisfy all requests, thus leading to a revenue loss.

The two above-mentioned problems will be studied in this thesis. The rest of this chapter is organized into three parts: motivations and objectives, contributions of the thesis, and the organization of the thesis.

Motivations and Objectives

Given a set of requests or a certain network load, the objective of this thesis is to explore how to optimize the route, flexible spectrum resources, and different flexibility of advanced MF in an effort to maximize the overall network performance (network throughput or total revenue) in static FONs.

Motivation 1: To make full use of the potential performance, a PLI-aware resource allocation is required, which relies on two modeling techniques. One is the PLI model to describe the actually suffered impairments, the other is the resource allocation model to optimize the network parameters. The optimal solution depends on the accuracy of the two models.

- On one hand, for each lightpath, the PLIs on the links mainly stem from the fiber and the optical amplifiers, whereas the PLIs at the nodes stem from the optical filters of each optical cross-connect (OXC). The PLIs of fiber are often described by the Schrödinger equation or the derived physical layer impairment model (Gaussian Noise (GN) model[5, 99], inter-channel stimulated Raman scattering model [121]). Incorporating a PLI model, related studies on the resource allocation tech-

niques have been developed in the past few years[17, 105, 139, 149]. However, in these studies, the impact of OXC crosstalk between lightpaths is either assumed with a constant penalty or seldom considered. As depicted in [46, 101], the OXC crosstalk, especially in-band crosstalk, is related with the overlapping spectrum and cannot be omitted. Thus, an integrated PLI model that can quantitatively calculate the different PLIs on links and at nodes is required so as to improve the efficiency of spectrum resources.

- On the other hand, since FONs can support heterogeneous bandwidths, the routing and wavelength assignment problem (RWA) in WDM networks has evolved into the routing and spectrum assignment (RSA) in FONs[71, 84, 108, 139]. Furthermore, if incorporating the traffic provisioning with multiple MFs and FECs, it maps into a problem of routing, MF, FEC, and spectrum assignment (RMFSA) [124]. Although some researchers have proposed heuristic algorithms[69, 84, 111], like *congestion-aware sequential loading* algorithm[114], and *adaptive FEC selection*[76], there is no complete mathematical model for the lightpath provisioning in FONs with both MF and FEC, which also accounts for PLI model. While the optimal combination of MF and FEC has been investigated at the transmission layer in [73], in this thesis we investigate how the combination of MF and FEC can be used to maximize revenues through appropriate traffic provisioning strategies.

Motivation 2: When implementing the previous study, we observe an interesting fact about the channel spacing setting: in a single fiber, the best spectrum position for the uniform bandwidth channels is not uniform. This can be explained by the channel spacing-dependent feature of interference. The channel in the center experiences the most interference from both sides, which needs to keep a larger channel spacing than the channel at the edge. However, such flexibility of channel spacing optimization cannot be easily implemented by the existing studies that only provide the fixed and candidate guard bands [88, 90, 136]. It motivates us to study how much performance gain can be achieved using the optimized continuous channel spacing strategy instead of using candidate guard bands. In addition, the optimization of the channel spacing will be more complicated in the FON where the spectrum non-overlapping constraint should also be considered for the heterogeneous bandwidths. Moreover, the complexity of channel spacing optimization could also increase with the number of lightpaths and the heterogeneous bandwidths.

Mitigating the system margin (typical margin includes nonlinear interference (NLI) and aging) can improve the network performance[100, 117]. Similar to the optimization of other physical layer parameters (launch power optimization in[17, 62, 106]), the channel spacing optimization is also able to mitigate the NLI in the physical layer (increasing the SNR margin). How about the network performance gain of channel spacing optimization? Answering this question requires an efficient algorithm to convert the enhanced SNR margin into throughput.

Motivation 3: After investigating the flexibility in physical layer in previous two studies (route, MF, FEC, channel spacing, baud-rate, PSD), let us look at the flexibility of network layer. When the network is heavily loaded, the new coming request will

face difficulty in finding enough spectrum resources. Luckily, the video services that account for the majority of network traffic are operational with a lower bit-rate while the QoS is weakly impaired. These services that can be degraded at a lower bit-rate are called *elastic services* or *elastic requests* in this thesis. For example, the traditional rigid requests only allow 100% bit-rate, while the elastic service can tolerate the bit-rate of {100%, 80%, 50%}. The management of such elastic services will become a key to network operators for cost-efficient resource management.

One of the greatest benefits of elastic services is to spare the spectrum resources. Such resources are especially important in a high load scenario, in which the revenue will probably be lost if the network fails to provision a lightpath for the coming requests. The release of spectrum resources requires network operators to reconfigure the existing lightpaths with different techniques, such as rerouting and spectrum retuning. The two techniques differ in cost, speed, service quality, and hardware implementation[25]. In order to make full play of the network reconfiguration, an intuitive method is to use these two techniques simultaneously. However, it is time-consuming, costly, and difficult for network operators. Thus, the first question is that *how to reconfigure the network to maintain a high revenue when part of these reconfiguration techniques is available*. In addition, network reconfiguration seems only desired for revenue improvement in a high traffic load scenario, while it is too complex to operate in a low network load scenario for the frequent reconfiguration. Thus, another question arises, *2) when to reconfigure the existing lightpaths in order to avoid the frequent network reconfiguration*. Therefore, it is required to investigate the performance of different reconfiguration schemes to choose the right strategy to maintain the revenue for a specified optical network.

Contributions of the Thesis

The studies of this thesis cover two aspects of the spectrum resource crunch, namely before and after the resource crunch happens. In addition, the flexibility offered by the FONs is combined to exploit the maximum potential network performance. The three major contributions in this thesis are listed and explained in detail below.

1. Revenue maximization leveraging adaptive MF and FEC

- This study proposes a novel lightpath's PLI evaluation model based on the channel bandwidth, and incorporates different PSDs, FECs, and MFs. By tracing the relationship between the PSD and SNR, we observe that using MFs enables to increase revenues with high SNR, while using multiple FECs is preferred for the scenarios of low SNR. Besides, compared to the wavelength-related or FS-related method, the bandwidth-related method enables a more accurate estimation of PLIs. Thus, the spectrum resources of fiber are assumed to be continuous rather than discrete FS.
- Furthermore, this study also devises novel traffic provisioning strategies to maximize the total revenue with different combinations of MF and FEC. With this strategy, the lightpaths can adopt different combinations with higher spectral

efficiency or longer transmission reach to guarantee the bit-rate under resource crunch. Compared to single MF or single FEC, the combination provides just-enough spectral efficiency and transmission reach, thus improve traffic provisioning. Using a piece-wise linear fitting function to model the nonlinear interference and calculating the crosstalk of intermediate nodes, we can linearize the PLIs then model the studied problem as a mixed-integer linear programming (MILP) model. The MILP model is based on flow rather than pre-calculated route. Without using the candidate route, this method can obtain the optimal solution irrespective of the number of routes. Besides, a fast and near-optimal heuristic algorithm is also proposed to solve the revenue maximization problem.

2. Throughput maximization leveraging just-enough SNR margin and channel spacing optimization:

- This study proposes the throughput maximization problem that leverages the just-enough SNR margin and channel spacing optimization. Unlike the conventional lightpath provisioning constrained by the stringent QoT through preserving an excessive SNR margin, leveraging the just-enough SNR margin permits increasing the network throughput by exploiting the stranded transmission capacity of each channel. Through analyzing and evaluating the impact of different lightpath's parameters, we are allowed to determine the value of just-enough SNR margin accordingly. The flexible parameters (route, MF, FEC, baud-rate, spectrum assignment) are jointly optimized while considering the nonlinear interference.

- We introduce a partial neighbor channel spacing optimization method for optimizing the channel spacing, resulting in a low-complexity method that applies to a large number of lightpaths. The performance improvement (SNR performance and the throughput) is validated by comparing with the widely used channel spacing strategies (fixed, candidate channel spacing) under the same network load.

- Finally, this study devises an iterative feedback tuning algorithm that can efficiently solve the throughput maximization leveraging just-enough SNR margin and channel spacing optimization problem for a given resource over-provisioning scenario. Specifically, it reduces the SNR margin by adjusting a slack variable iteratively to obtain the just-enough SNR margin.

3. Revenue maximization leveraging elastic services: We formulate the lightpath provisioning problem for the elastic services in a static FON that supports variable MF, FEC, and baud-rate. The objective is to maximize the total revenue of a network supporting elastic services. Then, we design an integer linear programming (ILP) model. An efficient decomposition method is also proposed. Next, we propose an auto-degrading provisioning scheme to load the elastic services incrementally. With this scheme, we can compare the revenue difference of different lightpath provisioning strategies and different network configuration strategies[38, 63, 115], thus addressing the issue of when and how to reconfigure the network.

Organization of the Thesis

The thesis carried out studies on PLI-aware routing and spectrum assignment for FONs. Background of FONs is presented in the **Chapter** 1. Next, following the different flexibilities, this thesis is divided into four parts, PLI model in **Chapter** 2, revenue maximizing leveraging the MF and FEC in **Chapter** 3, throughput maximization leveraging the just-enough SNR margin and channel spacing optimization in **Chapter** 4, and revenue maximization leveraging elastic service in **Chapter** 5. Finally, **Chapter** 6 concludes this thesis and envisions the future work.

In **Chapter** 1, we introduce the backgrounds of the current Internet as well as the enabling technologies of FONs. First, we present the internet traffic growth and the revenue issue of the current network. Second, as a comparison, we present the evolution of optical networks from the conventional WDM networks to the current FONs. After that, we present the key-driven technologies in FONs, including flexible transceivers, flexible OXCs, and flexible grids. Then, we investigate the problems, (i) routing and spectrum assignment, namely RSA, (ii) routing, MF, and spectrum assignment (RMSA), as well as (iii) its variant (PLI-aware RSA). Finally, the related studies on the resource allocation are also presented.

In **Chapter** 2, we describe PLI model of a lightpath and present how we calculate the QoT metric in this thesis. The required SNR threshold and the achievable spectral efficiency for different MFs are also devised through the classical digital communication theory.

In **Chapter** 3, we study the revenue maximization problem leveraging adaptive MF and multiple FEC. Specifically, we first provide the SNR threshold and the spectral efficiency for different combinations of MFs and FECs. Then, we formulate the problem of traffic provisioning with adaptive MFs and multiple FECs. This problem is constrained by the network flow constraints, spectrum non-overlapping constraints, and SNR constraints. To solve this problem, we present an MILP model, as well as a heuristic algorithm that consists of two subproblems (routing, transmission mode assignment (RMTA), and spectrum assignment problem (SA)). Followed by that, we present a benchmark method. Extensive simulations are conducted to 1) validate the solution efficiency of MILP; 2) investigate the revenue impact of different physical layer parameters (PSD, MF, and FEC); 3) study the impact of different traffic loads. The work of this chapter can be found in the publications **[C4]** and **[S1]**.

In **Chapter** 4, we present the throughput maximization problem that leverages the just-enough SNR margin, baud-rate selection, and channel spacing optimization. The objective is to improve the network throughput for a given network traffic load. Before presenting the throughput maximization problem, we describe the necessary notations and the SNR calculation for the resource allocation. Then, we compare the lightpath provisioning leveraging the just-enough SNR margin and traditionally leveraging excessive SNR margin. As an illustration, a simple instance for a point-to-point link is also shown. To conduct the optimization in a large network, we present an iterative feedback tuning algorithm that iteratively reduces the excessive SNR margin and optimizes

the channel spacing. As the throughput maximization is challenging to solve, we derive a fast and time-efficient heuristic algorithm. Extensive numerical simulations are conducted to compare the throughput difference between excessive SNR margin provisioning and just-enough SNR margin provisioning, between different channel spacing strategies, and between different baud-rate selection strategies. The work of this chapter can be found in the publications [**C3**] and [**S2**].

In **Chapter** 5, we present the elastic service provisioning problem of FONs. The objective is also to maximize the network revenue from another aspect. The resource allocation problem for elastic service is presented first. An integer linear programming (ILP) model and a decomposition method are both proposed too. Specifically, the decomposition method includes two subproblems. The first subproblem includes the route, QoS level selection, and transmission mode selection, while the second subproblem includes the spectrum assignment. Since the decomposition method is still time-consuming for the high network load scenario, we develop an auto-degrading provisioning scheme to trigger the network reconfiguration to maintain the total network revenue. Simulation results of the static network and the various incremental network loads are compared in terms of time efficiency and revenue improvement. The work of this chapter can be found in the publication [**C1**].

Contents

Chapter 1

Background and Technological Context

Contents

The organization of this chapter is as follows.

- In Section 1.1, we describe the trend of the Internet traffic and revenue of network operators.
- In Section 1.2, we present the background of optical network that can accommodate the majority of Internet traffic. The key enabling technologies of FONs are also presented, including flexible transceiver, flexible OXC, and flex-grid.
- In Section 1.3, we describe the routing and resource allocation problem in FONs, namely RSA. The objective and constraints are also presented. In addition, we also depict the PLI-aware constraint.
- In Section 1.4, we review related works on the PLI-aware RSA problem.

1.1 Introduction

The Internet traffic is still increasing over the past decades. Overall, the average broadband speed will increase from 45.9 Mbps to 110.4 Mbps with a traffic growth rate of 19% per year from 2018 to 2023, as predicted by Cisco Annual Internet Report for the global[36]. In France, the mean download speed of broadband connection over the period from 2017 to 2019 has increased from 13.43 to 30.44 Mbps with an increase of approximately 50% per year[82].

Figure 1.1 shows the number of fixed broadband connections in France[59]. Since 2000, the number has increased rapidly but slowed to approximately 10% per year after 2008, and now with almost 44 among 100 inhabitants [3, 59]. Meanwhile, the number of 4K TV sets will increase from 268 to 891 million over the period of 2018 to 2023[36]. YouTube already supports the 8K and 16K Full ultra-high definition (UHD) video services [1]. Among the connected flat-panel TV, the ratio of UHD (15-18Mbps) will also increase from 33% to 66%. It is anticipated that with the move to higher video resolution, 4K and 8K video content will continue to grow not only in the screen quality but also in data usage. Furthermore, the average number of requests for television program per month is increasing from 60 million in 2009 to 270 million in 2017, as indicated by Fig. 1.3. Through the above analysis, we can conclude that the current traffic growth is caused by the following three factors: the increasing users, the increasing requests per user, and the increasing bit-rate services per request.

The increasing network traffic is not only an opportunity but also a challenge for network operators. On one hand, the network operators can meet greater user needs, gain a greater market share, and obtain higher user revenues. From 2010 to 2016, global network operators have witnessed the steady revenue growth brought about by Internet traffic growth, as illustrated in Fig. 1.4. On the other hand, the related studies have shown that the transmission performance of the existing infrastructure is approaching the Shannon limit that describes the ultimate capacity of a communications system [12, 40]. When user demands exceed the available capacity, network operators cannot

[1] https://youtu.be/sLprVF6d7Ug

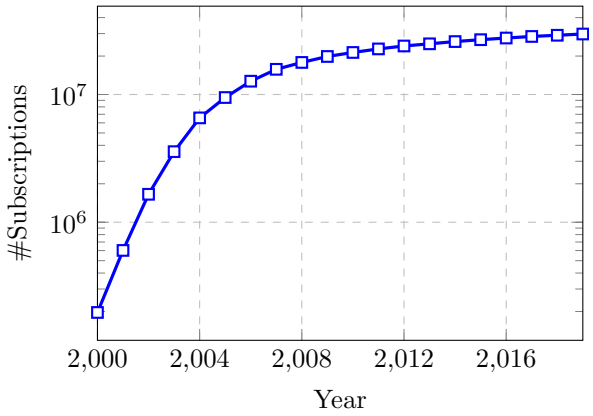

Figure 1.1: *Fixed broadband subscriptions in France 2000-2019[59].*

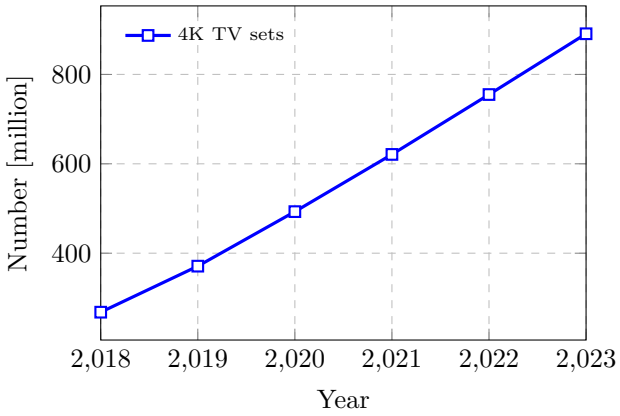

Figure 1.2: *Trend of 4K TV sets. Cisco predicts that by 2023, 66 percent of connected flat-panel TV sets will be 4K[36].*

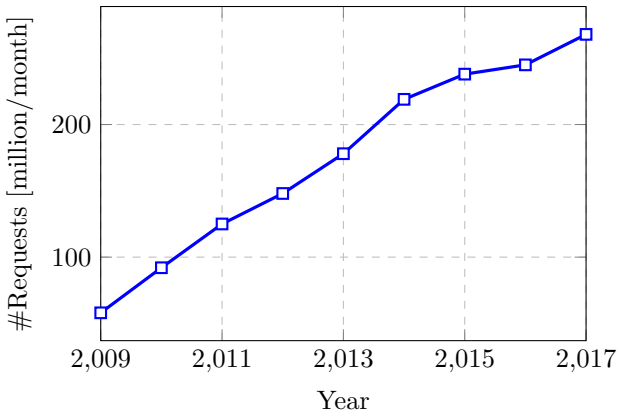

Figure 1.3: *Number of requests of television programs of BBC iplayer per month 2009-2017[57].*

easily maintain the high revenue growth anymore. Moreover, due to regulatory policy and market competition, the Average Revenue Per User (ARPU) in the network is gradually declining. Figure 1.4 shows this trend in China since 2012.

To solve the problems mentioned above, the optical community is moving towards increasing the cores, increasing the number of fibers, and expanding optical bands[135]. Nevertheless, these technologies cannot be implemented in the short term, which prompts us to think about how to increase revenue through efficient management of the existing optical network infrastructure. Therefore, this thesis focuses on how to increase the total revenue performance for the network with limited network resources.

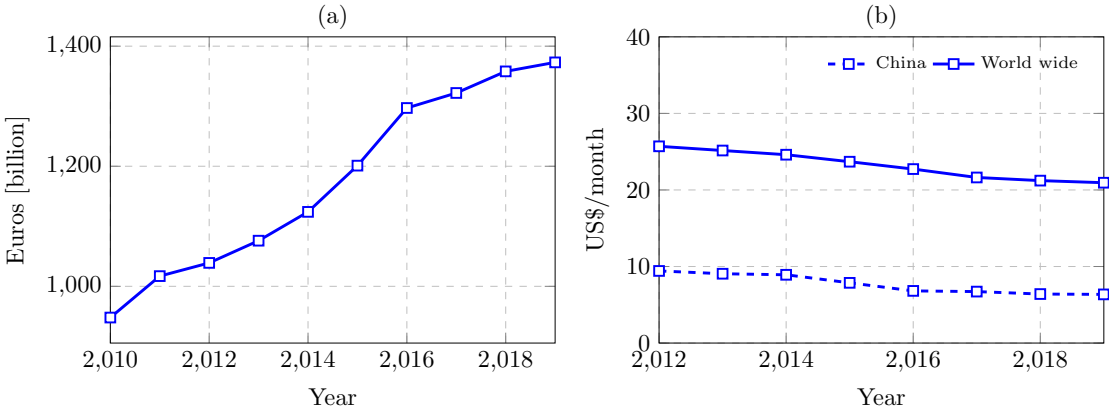

Figure 1.4: *Revenue of telecom operators in the world [55, 78] (a) global revenue of telecom operators; (b) ARPU in China.*

1.2 Enabling Technologies of FONs

As an important transport network of the modern Internet, optical networks support long-haul transmission with huge transmission capacity. The optical network can be viewed as a three-layered network, as shown in Fig. 1.5. The core optical network connects several important cities at different scales, e.g., national, continental, or transcontinental. The signal in a transparent core network is kept always in the optical domain during the transmission, while it is only encoded or decoded in the electrical domain at the source/destination node. The metro optical network connects one or two core nodes to the local access networks in order to aggregate and exchange the traffic of a city, which is generally an optical ring. The access network directly connects the users from either a passive optical network (e.g., fixed broadband service) or a radio access network (e.g., 5G service). The access network usually employs the tree topology. This thesis focuses on the studies of core optical networks, which have the most important and high-capacity connection. As for the network operators, the core optical network provides central support to the rest system that connects the users. Besides, the routing problem is more complex.

Today's optical network is evolving from WDM network to FON[49, 125]. In traditional WDM optical networks, each lightpath should establish the connection at a fixed

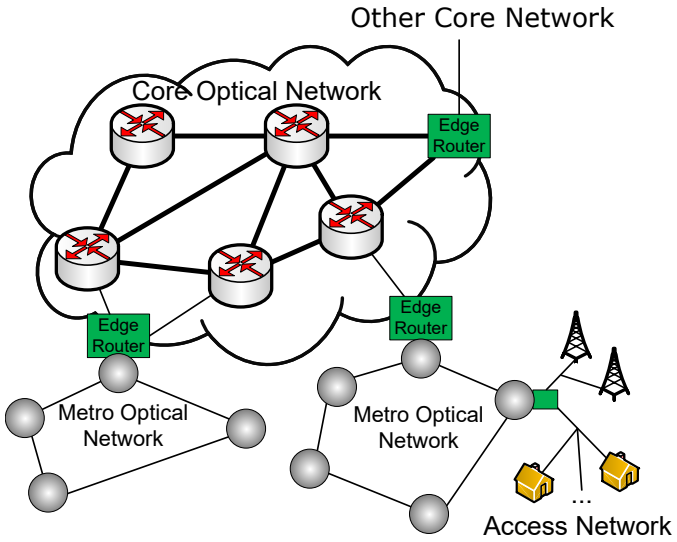

Figure 1.5: *Three-layered optical network[60, 125].*

grid separated by 50 or 100 GHz. Moreover, the bit-rates of each transceiver are fixed at 10, 40, or 100 Gbps, which is realized by a fixed MF, e.g PM-BPSK or PM-QPSK. As a result, the transmission capacity of spectrum resources will be heavily wasted due to such coarse granularity and rigid bandwidth. For example, in the conventional WDM network illustrated in Fig. 1.6, there is a large portion of spectrum resources that have not been used with the 10 Gbps channel.

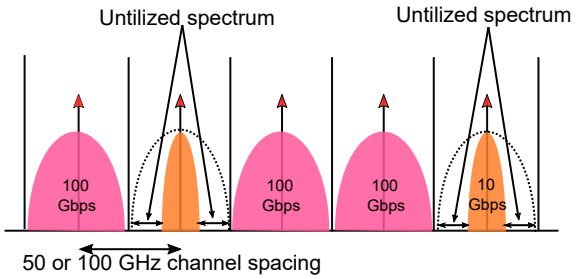

Figure 1.6: *Fixed-grid mode in WDM network.*

With the advance of optical transmission technologies, FON is proposed to solve the aforementioned issues and increase network flexibility. Specifically, FON enables the aggregation of the low bit-rate channels by using various transmission techniques, such as optical orthogonal frequency-division multiplexing (O-OFDM), Nyquist WDM (N–WDM), and so on. Besides, the term "flexibility" indicates the ability to dynamically adjust network parameters[128], such as *bandwidth (baud rate)*, *channel spacing*, *power*, *MF*, and *FEC*. The advantage of FON could be summarized into three aspects: flexible transceiver, flexible optical switch, and flexible grid. Figure 1.7 illustrates the relationship of the three components of FONs as well as their flexibilities.

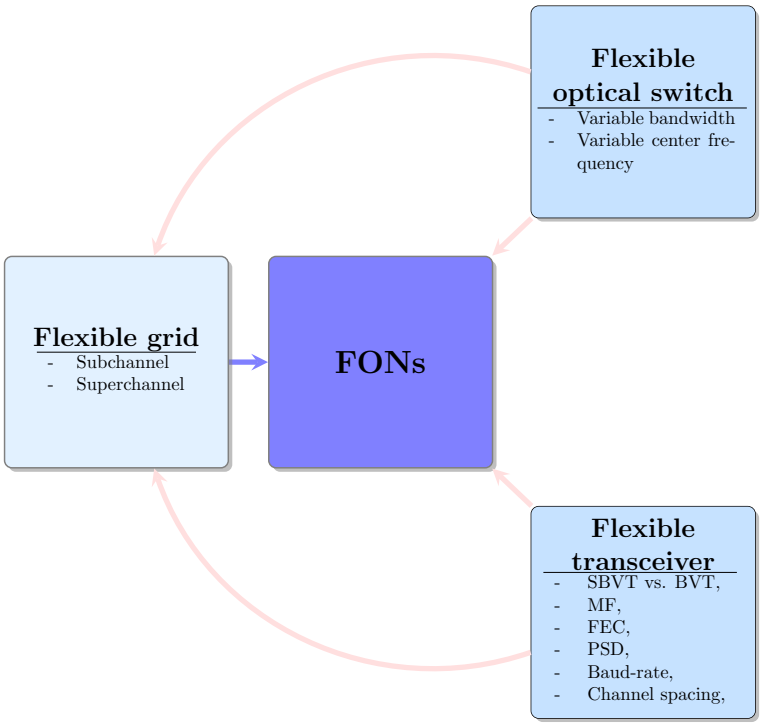

Figure 1.7: *Enabling technologies of FONs.*

1.2.1 Flexible transceiver

The transceiver in WDM only fits one or several data rates, while the transceiver in FON can fit almost all data rates[147]. One of the key enabling techniques is done by aggregating multiple subcarriers with lower symbol rates, which enables the flexible signal bandwidth. It can be implemented by three different approaches, optical OFDM, Nyquist WDM, and Time and Frequency Packing (TFP) [110]. Besides, thanks to the commercially available DAC as well as the coherent detection technologies, each subcarrier can be individually employed with advanced digital signal processing (DSP) technology with higher transmission capacity[34, 35].

- **Nyquist WDM**: This technology can generate the signals with an almost rectangular spectrum, which is implemented by using a pulse-shaping filter at the sender side (e.g., root raised cosine filter) [91, 110]. The advantage of such technology is that only a few subcarriers will be enough to implement the superchannels, e.g., 10 subcarriers of 28 GBaud using PM-QPSK are enough for 1 Tbps connection [20]. Besides, the inter-symbol interference between signals can be greatly reduced with a matched filter at both sender and receiver sides[91]. However, the required filter is also a challenge, which should be sharp enough to remove the narrow filtering effect of the cascaded reconfigurable optical add drop multiplexer (ROADM)[41, 118]. The channel types considered in this thesis are all assumed to be the Nyquist WDM channels.

- **Optical OFDM**: Different from the Nyquist WDM, the key enabling technology of O-OFDM is the overlapped orthogonal carriers[126]. These subcarriers are sinc-shape and overlapped in the frequency domain[146], whereas the subcarriers in Nyquist WDM are almost "rectangular"[19]. Nevertheless, the subcarrier also allows each subcarrier to be densely packed. The advantage of O-OFDM is the high scalability, which allows the smooth upgrading from the low bit-rate transmission to high bit-rate transmission without significant modification to the existing system. However, O-OFDM suffers from two implementation problems[126, 146]. The first one is the high peak-to-average power ratio of the orthogonal subcarriers, which disturbs the ADC/DAC converter thus has a detrimental impact on the transmission system. The other one is the strict orthogonality requirement between subcarriers, which will be easily affected by the frequency noise and phase noise. For the performance comparison of O-OFDM and Nyquist WDM, one can refer to [19].
- **TFP**: This technology sends the pulse signals that overlap in time or frequency or both[110], which is quite different from the previous two technologies. The orthogonality condition is not a strict requirement anymore. Thus it can hopefully overcome the Nyquist limit and obtain a higher spectral efficiency[120]. The drawback is that it relies on complex DSP technology to detect and recover the pulse signal, e.g., sequence detection algorithm Bahl-Cocke-Jelinek-Raviv detector[120].

The following figure illustrates the waveforms of these three technologies.

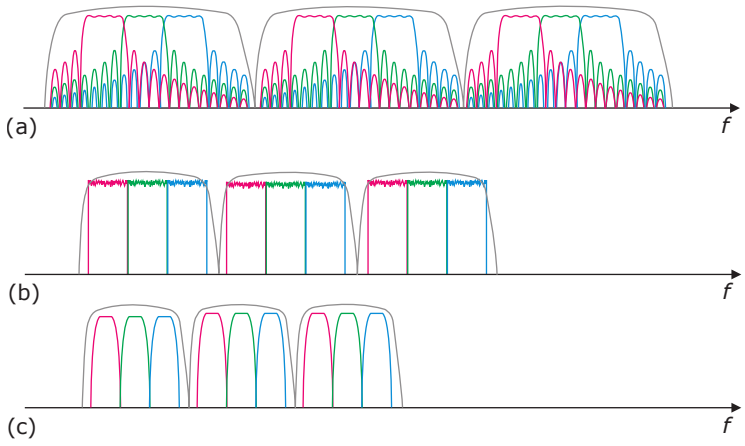

Figure 1.8: *Examples of the spectrum of (a) O-OFDM; (b) Nyquist WDM; (c) TFP[110].*

Furthermore, these subcarriers can be individually employed with different advanced DSP technologies to increase spectral efficiency, including MF, FEC, probabilistic shaping, etc. For example, as long as the length of the lightpath is lower than the maximum reach, each subcarrier can choose the most spectrum-efficient MFs. Besides, different FECs and MFs can be combined to achieve the continuous adaptation of data rate and transmission reach, which is called coded modulation format in recent studies[15]. More advanced DSP technologies, *e.g.*, probabilistic shaping [43] and time-domain hybrid formats[156], have also been proposed to minimize the gap between the

Shannon limit and increase the bit-rate per channel. One commercial transceiver can currently refer to [34, 35], incorporating baud-rate selection and FEC selection.

Besides the bandwidth variable transceiver (BVT), another economically efficient transceiver—sliceable bandwidth variable transceiver (S-BVT)—has also been proposed for FONs[110]. With the sliceable capability, one BVT can be sliced into multiple sub-carriers, "virtual transceivers", each serving a separate traffic flow[49]. Figure 1.9 illustrates and compares the signal flows of BVT and S-BVT. BVT merely serves one traffic for a certain node pair, while S-BVT can split the transmission capacity to multiple flows with a lower bit-rate. From the network operator's view, the operational cost and energy consumption can be greatly saved by using the S-BVT[44].

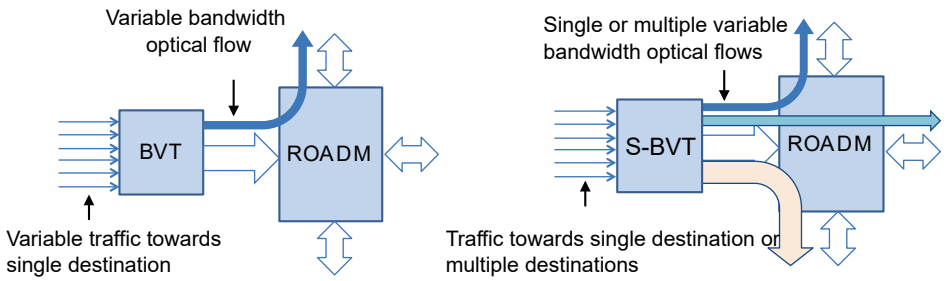

(a) BVT (b) SBVT

Figure 1.9: *Illustration of BVT and S-BVT in FONs[44].*

1.2.2 Flexible optical switch

Currently, there are several typical node architectures that can implement the switch of optical signals using bandwidth variable wavelength selective switches (BV-WSS) [145], e.g., *Broad-and-select* (in 1.10(b)), *Route and couple* (in 1.10(c)), and *Route and select*. Here, to explain how the BV-WSS function in the bandwidth variable cross-connects (BV-OXC), we present two classical node architectures, which use the WSSs and power splitters (PSs). It should be noted that the function of the PS is to broadcast or couple the signal copies to different output ports, while the BV-WSS is to selectively pass or block the signal at a certain frequency (see Fig. 1.10(a)). For the first architecture *broad and select* (in Fig. 1.10(b)), PS will broadcast the input signal. Then, all N copies of the signal will individually flow into the BV-WSSs. Next, the signal will be selectively passed or blocked by the BV-WSSs facing different output ports. For the second architecture *route and couple* (in Fig. 1.10(c)), the BV-WSSs will selectively pass or block the input signals with different frequencies to different output ports. Finally, the signals to a common output port will be coupled by a PS.

1.2.3 Flexible grid

In FONs, the fiber spectrum resources are divided into several chunks that are separated by a minimum 12.5 GHz grid, or even the smaller one with 6.25 GHz, according to the ITU.T standard G.694[2]. This allows each channel to transport data with just-enough spectrum resources rather than multiple 50 GHz bandwidths. Besides, each

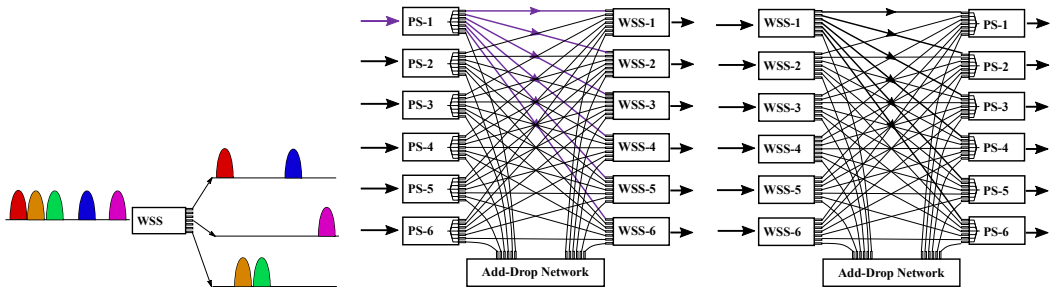

(a) BV-WSS (b) Broad and select (c) Route and couple

Figure 1.10: *Two typical node architectures in FONs[65, 145]*

FS can be individually concatenated to make a larger contiguous FSs block to form the super-channels on demand. By aligning channels on such a minimum grid, the waste spectrum resources can be greatly reduced to improve the spectrum efficiency. Figure 1.11 illustrates the spectrum efficiency improvement of fixed-grid and flex-grid.

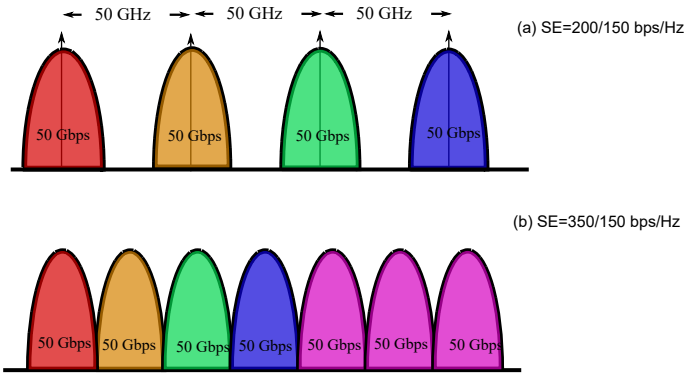

Figure 1.11: *Illustrative examples for fixed-grid and flex-grid mode.*

1.3 Routing and resource allocation in FONs

After having a simple understanding of the key enabling technologies of FON, this part introduces the routing and resource allocation problem. An FON is modeled as a graph $G(V, E)$, where V represents a set of nodes (OXCs), and E denotes a set of optical fiber links. The spectrum resources on each fiber link is denoted by W FSs or F (unit: GHz). Figure 1.12 shows an example network, and Fig. 1.13 shows the spectrum resources of a fiber link. All fiber links have the same amount of spectrum resources. Note that, there are two fibers on a link, each of which is in charge of carrying opposite traffic.

When a request comes, the network will assign a proper lightpath and adequate spectrum resources to establish the communication from the source node to the destination node. In a traditional WDM network, the resource allocation needs to find a proper wavelength on a fixed frequency grid (e.g., typical 50 GHz), while in the FON, it needs to find the right size of contiguous FSs to the request needs. The former is called

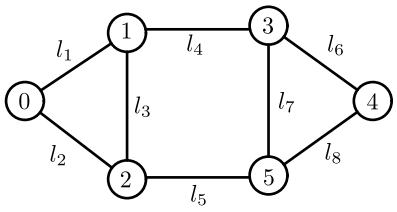

Figure 1.12: *A 6-node network FON.*

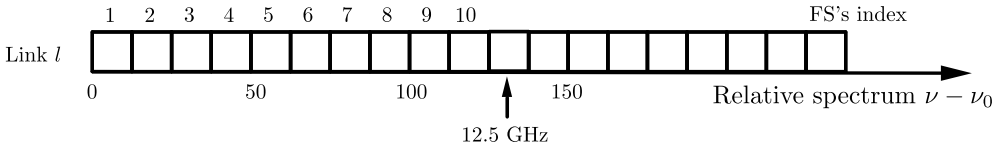

Figure 1.13: *Spectrum resource in a fiber link l.*

as RWA, while the latter is called as RSA[71]. When the flexibility of MFs is available, the RSA problem will upgrade to RMSA[31]. RMSA problem is a simple version of the PLI-aware resource allocation problem. Here, we will briefly present both RSA and the RMSA problem, as well as the classical techniques to solve them.

As for the objective of the RSA problem, there are two variants: min-RSA and max-RSA[26, 64]. The former minimizes the maximum FS index while satisfying all requests. The latter maximizes the number of accepted requests (or the revenue obtained by accepting a request) while rejecting some requests, provided that the spectrum resource is limited. The objective of this thesis takes the latter, max-RSA, which maximizes the total accepted revenue or the bit-rate.

Next, we present several classical techniques to solve the RSA and RMSA problems, respectively.

1.3.1 RSA

RSA is a simple version of the routing and resource allocation in FONs. Two constraints should be satisfied:

- **(1) Routing constraint**: Each lightpath starts from the source node, traverses several links in optical networks, and finally terminates at the destination node.
- **(2) Spectrum assignment constraint:** (i) *continuity constraint*: all traversed links along the lightpath should maintain the same starting FSs and the same number of FSs that satisfy its transmission requirement, e.g., bandwidth requirement or the bit-rate requirement, (ii) *contiguity constraint*: the spectrum resources allocated to lightpath should be contiguous, and (iii) *non-overlapping constraint*: any two lightpaths should not use the same FS on the same fiber link.

The RSA problem can be solved by either a two-step method or a joint optimization method. The two-step method solves the routing problem first and then deals with the spectrum assignment problem, or treats them in the reverse order[26]. Next, we present

three routing-first algorithms (*Fixed routing*, *Candidate routing* and *Least congested routing*[71, 115]), and one spectrum-first algorithm (*Adaptive routing* [132]). As the first-fit (FF) strategy and shortest path algorithm (SP) have been widely used, we use FF and SP to distinguish the following algorithms.

- **Fixed routing:** A single route between a node pair is determined by using the shortest path algorithm, such as Dijkstra's algorithm. Then, available contiguous slots on this route is allocated to the lightpath (SP-FF).
- **Candidate routing:** As a complementary for the fixed routing, $k(k \geq 2)$ candidate routes have been pre-calculated between each node pair. These routes are calculated based on Yen's algorithm taking the distance or distance-related parameters as the metrics [30, 141]. Only one route with available contiguous FSs will be chosen. Generally, when searching the different routes, the route with the minimum cost will be considered first. The request will be blocked when no available spectrum resources on all candidate routes (kSP-FF).
- **Least congested routing:** Different from the previous two algorithms, the least congested routing chooses a route with the minimum metric that can depict the network congestion[71, 115]. Such metric is often denoted by the number of (or the potential) occupied slots on links. The route with the least congestion metric is chosen for the request, which is found by using the shortest path algorithm (congestion metric-FF).
- **Adaptive routing:** Similar to the least congested routing, this algorithm also calculates the route based on the link status. The difference lies in that *adaptive routing* prioritizes the availability of FSs rather than the link metrics. Specifically, for a set of contiguous slots, all candidate lightpaths will be searched until none of them have such desired FSs. Such contiguous slots will scan from the low-indexed FS to the high-indexed FS until the maximum FS is reached (FF-kSP).

The two-step method is mostly adopted because of the high time efficiency. The performance comparison of these algorithms can refer to [26, 132], in terms of the blocking probability, time complexity, configuration time, network throughput, and lightpath distribution.

As for the joint optimization method, it often uses an ILP model in order to obtain the global optimal solution. Generally, a matrix will be used to store the variable that denotes the usage status of the route or links. However, due to the combination nature inherent to the graph coloring problem, it is $\mathcal{NP}$-hard. The studies on this problem can refer [10, 31, 71].

1.3.2 RMSA

In RMSA, the optimization dimension of MF selection is introduced to each lightpath. When a lightpath is short enough, a high-order MF can reduce the spectrum resource consumption while guarantying the same bit-rate. As the physical layer requirement of high-order MF is more sensitive to the noise than the low-order MF, i.e., a higher SNR threshold, the RMSA needs to consider the maximum transmission reach of different

MFs. The optimization with the transmission reach constraint is often regarded as the basic optimization model of the PLI-aware resource allocation. Here, besides the **(1) routing constraint** and **(2) spectrum assignment constraint**, we present the additional constraints of RMSA problem:

- **(3) Bit-rate constraint**: The transmission capacity of each lightpath, determined by the bandwidth and transmission mode, should be no smaller than the required bit-rate. A suitable bandwidth and a suitable transmission mode should be chosen for the lightpath so that the transmission capacity can satisfy the bit-rate requirement. Generally, the spectral efficiency of BPSK, QPSK, 8QAM, 16QAM is assumed with 1, 2, 3, and 4 bps/Hz, respectively. In addition, the adopted MF will be constrained by the following transmission reach constraints;
- **(4) Transmission reach constraint:** The length of each lightpath should not exceed the maximum achievable transmission reach to guarantee the QoT, which is directly given by the equipment vendor or indirectly calculated through experiment. For example, 9,600, 4,800, 2,400, and 1,200 km is respectively adopted for different MFs (BPSK, QPSK, 8QAM, and 16QAM)[67].

The optimization techniques for RSA can be also applied to RMSA seamlessly, where the transmission reach should also be considered for different MFs. Several techniques are also proposed to solve the RMSA in an effort to improve the spectrum efficiency. In [32], they proposed the ILP formulation and a decomposition method that includes (i) routing and MF assignment, and (ii) spectrum allocation (RMA+SA). In [153], they developed a genetic algorithm. Other heuristics that choose the MF first, and then select the candidate route and spectrum can refer to [37].

The transition from RSA to RMSA enables us to select the parameter with higher spectral efficiency. However, the spectral efficiency and transmission reach of each MF are discrete. The coarse granularity of different MFs will lead to stranded capacity. With the advance of spectrum-efficient MFs (such as FEC, probabilistic shaping, and TDHM), it becomes possible to select such an MF that approaches the almost maximum spectral efficiency according to the lightpath's length rather than several predetermined given transmission reaches. **Thus, exploiting the advantage of higher spectral efficiency is one of the main motivations of our thesis**.

It is worth noting the limitation of (4) *transmission reach constraint*, which is a rigid PLI constraint. Such constraints avoid the complex calculation of the interference between lightpaths, by merely restricting the length. To ensure uninterrupted communication with a satisfied QoT, we must tolerate the maximum impairments, including the maximum noise and interference. A typical approach to calculate the transmission reach is assuming the static worst-case of fully occupied network resources. However, the overestimation of PLI will conservatively restrict the actual tolerable reach or the actual achievable spectral efficiency, and consequentially leads to stranded transmission capacity. More expensive optical transceivers may be required to achieve the same transmission rates[33]. **Therefore, it is urgent to incorporate the PLI-aware calculation and resource allocation together, in an effort to better utilize the MFs and other advanced MFs. This will be accomplished by the first study in Chapter 3, in which we**

exploit the adaptive MFs and multiple FECs. In addition, besides the NLI on fibers, the lightpath also experiences the PLI at nodes. As indicated in [46], the node crosstalk between lightpaths depends on the factors of filters, such as passband widths, isolation magnitude, isolation shape, and center frequency detuning. Recent studies consider the node crosstalk by assuming a constant penalty on the impairments[13, 14, 132, 155]. Similar to the overestimation of NLI on fibers, the overestimation of node crosstalk also causes inefficient physical layer performance or spectrum usage [13]. **In light of this, we will present a more accurate PLI model that incorporates both the PLI on links and at nodes in Chapter 2, so that the PLIs could be precisely estimated rather than using a constant worst-case value**.

Furthermore, the PLI among lightpaths depends on several factors, such as PSD, bandwidth, channel spacing, and channel order. These factors have not been mentioned in the conventional RMSA problem. Through the first study, we find that the best channel spacing is distributed unevenly. This corresponds to one of the mentioned factors, channel spacing. However, existing studies only employ and compare the strategy of the candidate or fixed channel spacing[88, 88, 90, 92, 136, 144]. These studies were unable to investigate the performance gain when using the channel spacing optimization without candidates. **In order to achieve the maximum physical layer performance gain by optimizing channel spacing, we will present a novel optimization strategy without candidate channel spacing strategies in Chapter 4. This optimization strategy is implemented in a low-complexity way that can be applied to a large number of lightpaths for mesh and ring networks.**

Finally, in presence of a high traffic load, not all incoming traffic can be satisfied at all time. Luckily, several kinds of services, such as videos, can be accepted at a lower bit-rate. From a network operator's view, degrading the bit-rate of some requests enables us to release the spectrum resources, which thus in turn permits us to maintain a higher revenue although weakly impairing the QoS. This characteristic can be used to enhance network reliability and maintain higher network revenue. **We observe that the current studies mainly investigate the 100% bit-rate provisioning strategy for each request. Therefore, it is required to investigate the service provisioning with elastic bit-rate provisioning. This will be investigated in the third study in Chapter 5. In this study, we propose an MILP as well as a decomposition method, which permit us to provision the lightpath for elastic requests. Meanwhile, an auto-degrading simulation scheme is also proposed to trigger the network reconfiguration for the existing lightpaths to maximize the total network revenue in presence of a high traffic load**.

1.4 Literature review

Different from RWA, the utilization of spectrum resources in RSA has evolved from a single wavelength to the contiguous FSs. Besides, the parameter selection of transceivers also evolves from several line rates to multidimensional parameters' selection, including MF, FEC, and baud-rate. These parameter selections will add additional degrees of freedom to resource allocation.

Meanwhile, the calculation of complex PLIs and the associated resource allocation will make the studied problem more complex, because the impact of bandwidth, spectrum order, and channel spacing has been neglected in non-PLI-aware design. These factors should be carefully designed in PLI-aware resource allocation.

In what follows, we review the recent works from two views: flexibility and PLI-aware network design. These related studies are summarized in Tables 1.1 and 1.2.

1.4.1 Flexibility design in FONs

In [32], Christodoulopoulos et al. first incorporated the flexibility of MF for network design in FONs. Both the joint optimization and decomposition methods of RMSA were presented. The joint optimization method simultaneously determines three parameters (a proper starting frequency, a proper route from the pre-calculated route, and a proper MF that satisfies the transmission reach constraint) for each request. The decomposition method sequentially solves the routing and MF assignment problem, and the spectrum assignment problem. Also, a heuristic algorithm was proposed to assign the request one-by-one by finding the route first and spectrum second. In addition, they demonstrated that the RMSA is NP-complete by using the multiprocessor scheduling problem.

In [37], Costa et al. proposed a heuristic algorithm for solving RMSA, which chooses the MF first, and consequentially finds a proper route with enough spectrum resources. They showed that their algorithm could encourage more usage of high-order MF than the conventional method.

With the requirement of higher spectral efficiency, the rate-adaptive coding was firstly introduced in long-haul WDM networks in [50], which quantifies the achievable bit-rates and distance using different FECs. The hardware implementations for the serially concatenated FEC to implement the variable code rate were also presented. Then, in [87], Mello et al. mainly investigated the benefit of variable FECs in terms of cost, capacity, and survivability. They also evaluated the impact of the number of realizable code rates, denoted by N. Simulation results validate the cost-saving performance of using the variable code-rate transceiver is more significant when N increases.

In [111], Sambo et al. developed a resource allocation strategy that can adaptively choose MF and FEC. Generally, the physical layer performance of different MFs and FEC can be determined through either analytical models or experiments. They evaluated the maximal reach using the latter one. Given a required bit rate, they proposed a heuristic algorithm to find a proper route, choose a proper available code with a satisfied QoT, determine the required spectrum resources with that code rate, and finally perform the spectrum assignment by FF policy. However, due to the experiment limit, they only provided the transmission performance for a small number of parameters.

Different from the previous works investigating the min-RSA, the following studies investigated the max-RSA. In [39], Dai et al. investigated the maximal capacity of a network by utilizing the adaptive bit-rates scheme in WDM networks. Specifically, they adopted the scheme of TDHM to enable the continuous bit-rate and transparent reach

Table 1.1: *Related studies on the resource allocation incorporated with different flexibilities of FON.*[1]

Paper	Resource allocation strategy			Flexiblitly (Transceiver's Degree)					
	ILP	Heuristic (Decomposition)	Objective	PSD	MF	FEC (TDHMF)	Spectrum		
							Bandwidth (Baud-rate)	Channel spacing (Center frequency)	Channel order
[32]	yes	yes	min-RSA		yes		yes	Flex grid	
[124]	yes	yes	min-RSA		yes	FEC	yes	Fixed vs. Flex grid	
[111]		yes	min-RSA			FEC	yes	Flex grid	
[37]		yes(MF first)	min-RSA		yes			Flex grid	
[39]	yes	yes	max-RWA		yes	TDHMF		Fixed grid	

[1] The routing in these studies is unicast.

rather than the discrete coarse granularity of MF. Like the combination of MF and FEC, the scheme of TDHM also enables the continuous adaptation of spectral efficiency and transmission reach. Thus, the achievable capacity of each lightpath is determined by the interpolated value of different MFs, which has a finer granularity. An ILP model that maximizes the acceptable transmission capacity and a fast heuristic algorithm were proposed to investigate the benefit of TDHM. Through simulations, the increasing capacity and accepted demands are validated. However, it is uncertain whether their method is suitable for FONs with heterogeneous bandwidths and flexible grids. Moreover, it cannot directly solve the PLI-aware routing and resource allocation problem in FONs due to the lack of NLI calculation for each lightpath.

In [23], Cantono et al. proposed a statistical approach to evaluate the throughput of an optical network. The approach unloads all requests initially, then progressively loads the traffic from a given demand set. When the network reaches saturation or at a particular state, several desired metrics are evaluated based on Monte Carlo simulation, including blocking probability, average bit-rate per lightpath, link saturation status, and network throughput. Through simulations in a network with 49 nodes and 68 bidirectional links, they showed that the average bit-rate per lightpath follows the Gaussian distribution.

Similar to the study in [23], Ives et al. in [63] also used a sequential loading algorithm to investigate the maximal throughput with adaptive MF and adaptive FEC. Through the simulations in UK 20+2 network with small diameters, they obtained some interesting observations from an economic view. Given the same network throughput, (1) the price of adaptive MF must cost more than 20% than fixed MF transceiver with the only PM-16QAM. (2) Adaptive FEC must cost no more than 6% FEC to the price of adaptive MFs. The results in their study could be further improved and demonstrated in FON with heterogeneous bandwidths rather than a DWDM network.

The above studies show that the utilization of adaptive MFs outperforms the fixed MF. The performance gain will increase when using advanced MF (FEC in[110] and TDHMF in[23, 39]). Besides, as the number of available options increases, the performance gain also rises ([87]). Due to these benefits, the heterogeneous applications in virtual network[77, 124] and inter datacenter networks are regarding the FON as an important infrastructure[80]. The potential capability of FON motivates us to think about how to utilize the various flexibilities to maximize the overall network performance. In addition, there also exists a scalability issue.

1.4.2 PLI-aware flexibility design

In [149], Zhao et al. investigated the routing, spectrum assignment incorporating the flexibility of MF. The objective is to minimize the spectrum resources by solving the routing, MF, and spectrum assignment problem while considering the NLI. They developed an ILP model and several heuristic algorithms that dealt with the ordered demands one by one. Simulation results showed that spectrum saving is 22% in the high bit-rate scenario, while it is 31% in the low bit-rate scenario. In addition, the optimal PSD will increase with the network diameter and the bit-rates. However, due to the

Table 1.2: *Related studies on PLI-aware resource allocation in FON*

Paper	Resource allocation strategy			Flexibility (Transceiver's Degree)						PLIs	
	ILP	Heuristic	Objective	PSD	MF	FEC (TDHMF)	Spectrum			NLI	Node crosstalk
							Bandwidth (Baud-rate)	Channel spacing (Center frequency)	Channel order		
[149]	yes	yes	min-RSA	yes	yes		yes	Flex grid		yes	
[52]	yes	yes	min-RSA	yes	yes		yes	yes	yes	yes	
[139, 140]	yes	yes	min-RSA	opti-mized	yes		yes	yes	yes, empirically	yes	
[133]	yes	yes	min-RSA	yes	yes		yes			yes	
[13, 14]	yes	yes	min-RSA	yes	yes		yes	Fixed guard band		yes	slot-based
[62, 63]	yes	yes	max-RWA	opti-mized	yes	FEC		Fixed grid	Random selection	yes	
[23]		yes	max-RWA	yes	yes	TDHMF				yes	
Study 1	yes	yes	max-RSA	yes	yes	FEC	yes	yes	yes	yes	**channel-based**
Study 2	yes	yes	max-RSA	yes	yes	FEC	yes	**Optimized (low-complexity)**		yes	
Study 3	yes	yes	max-RSA	yes	yes	FEC	yes			yes	

complexity of that problem, processing one request may cost about 10 min. Thus, the algorithm may only suit the static network design with limited requests.

In [133], Wang et al. investigated the lightpath provisioning for the incremental loads. The complex NLI calculation is simplified by a simple NLI estimation model that can roughly estimate the complex NLI according to the current network loads. Another study that focuses on the estimation of NLI can refer to [137]. A lightpath provisioning with a higher spectrum efficiency can be realized with a PLI model with enough accuracy. Through the simulations, Wang et al. in [133] validated that the blocking performance of the hybrid NLI model is lower than the benchmark of the worst-case assumption. This result is validated by their sequential loading algorithm and the reconfiguration module. Specifically, the new request is sequentially added to the network as usual. When the blocking occurs, three reconfiguration schemes are used in an effort to accommodate the pending request. The first scheme is based on a complex MILP model, the second scheme still uses the same MILP model while partitioning the pending requests into several groups, and the third one uses a heuristic algorithm to rescue the blocked requests. In addition, similar to the previous study in [149], they also found that the optimal PSD will increase as the network load increases.

In [13, 14], Behera et al. developed an MILP model incorporating the effect of ASE noise, NLI, and node crosstalk into resource allocation with MF. The lightpaths that pass through the same node will experience in-band node crosstalk. The amount of node crosstalk depends on their overlapping spectrum resource. The impact of node crosstalk on resource allocation is validated by comparing the blocking performance of different crosstalk levels. However, the crosstalk component is evaluated only through the slot, which still seems insufficient. For example, the node crosstalk on provisioned bandwidth of 12.5 GHz slot is larger than the actual value of the sub-channel bandwidth with 6.25 GHz[85, 118, 125]. To reduce the PLIs, one may use a guard band (*e.g.*, at least 12.5 GHz), but incurring inefficient usage of spectrum resources (real guard band could be larger than 12.5 GHz). The model based on channel bandwidth ensures that the PLIs are suitably estimated. Therefore, the PLI model that we propose evaluates the node crosstalk by using the channel bandwidth.

In [140], Yan et al. investigated the relationship between spectrum usage and the transceiver's parameters, including MF, center frequency, and PSD. Using the proposed method (an ILP with a weighted objective of spectrum usage and other parameters), they obtained three observations: (1) the spectrum usage can be significantly reduced using the continuous channel spacing rather than the fixed-grid. The main reason is that the unnecessary guard band between channels can be removed without degrading the QoT. (2) Generally, the metric of spectrum usage could be sensitive to the channel order of the lightpaths, in which the solution space is the permutation of all lightpaths. However, they found that most of the orderings (over 90%) can achieve near-to-optimal performance with an optimal gap of less than 6%. (3) A great deal of time is required for the joint optimization of bandwidth, PSD, and center frequency, even in ring networks with fixed routes. In other words, the last observation also poses a question of whether this model can solve the optimization in a typical mesh network.

In [17], Bhar et al. investigated the problem of channel order assignment. For the lightpaths that share the same link, only the interference between the nearest channel is considered, while the other neighborhood interferences on the distant spectrum are neglected (the impact of this assumption is also discussed in their study). Thus, the interference between lightpaths is represented by a digraph, where each node denotes the lightpath and each directed link denotes the interference between two lightpaths. The weight on the link denotes the strength of the interference. The objective of the channel ordering assignment problem is to find the minimum interference for all involved lightpaths. Each channel order solution of this problem corresponds to a Hamiltonian path that only traversed each node at once while minimizing the maximum interference on each node. When solving the problem, they used a bottleneck traversing salesman algorithm that restricts the maximum interference per lightpath. Through simulations under different PSD settings, they observed that the channel order optimization outperforms the random order in the scenario of large PSD.

In [102], Rabbani et al. developed a PLI-aware resource allocation strategy for the joint optimization of wavelength and power. When a random demand comes, the algorithm will optimize the PSD for all existing lightpaths. In their algorithm, they used a gradient-based method to obtain a local convex optimization result. Compared to the optimization using ILP, the gradient-based method provides a fast solution. However, this study aims to improve the network physical layer performance (SNR margin and achievable information rate) rather than enhancing the potential network capacity.

Meanwhile, the max-RSA was also investigated in the study[62]. In [62], Ives et al. studied the maximum throughput through optimizing the physical layer parameters. Given a network with a determined network configuration, such as a set of given MFs and a given spectrum resources, they proposed a gradient descent procedure to optimize the PSD and an iterative algorithm to reduce the rest SNR margin of network. Through numerical simulations, the throughput improvement of adaptive MFs is demonstrated. Besides, after optimizing the launch PSD and adjusting the SNR margin in NSF network, they found that about 50% throughput improvement can be achieved compared to the fixed PSD with fixed MF. However, it still remains a practical question that how much throughput can be obtained in the non-full-load scenario. Moreover, the impact of heterogeneous traffic demands in FONs has not been investigated.

1.5 Conclusion

In this chapter, we presented the trends of current Internet traffic and revenue. By describing the flexible transceivers, flexible optical switch, and flexible grid, we obtain an overview of the FONs. Then, we present the studied routing and resource allocation problem of this thesis, including the objectives and constraints. The related studies on the flexibility design and PLI-aware design are also presented, respectively.

Chapter 2

Physical-Layer-Impairment Model

Contents

This chapter will present the PLIs and the QoT metric. The PLIs are classified into linear and nonlinear impairments, which will be briefly discussed. Besides, a review of the modeling technique to calculate the QoT is also presented. As severe PLIs influences the QoT and the selection of different MFs, it could impair the transmission capacity of the lightpath. Thus, we associate the achievable bit-rate, and required QoT threshold of different MFs and different FECs for the network design.

The organization of this chapter is as follows.

- In Sec. 2.1, we briefly review the related PLIs of optical transmission systems;
- In Sec. 2.2, we describe the QoT metric in this thesis;
- In Sec. 2.3, we measure the maximum transmission capacity of a certain combination of MF and FEC as well as the required SNR threshold. By doing so, we can incorporate the physical layer parameters (PSD, MF, FEC, channel spacing, and bandwidth) into the network design.

2.1 The PLI in optical transmission systems

It is well understood that the PLIs come from the optical equipment. Fig 2.1 shows a typical optical transmission system that includes the basic components, such as transceivers that convert the data to optical signal, WSSs that multiplex / demultiplex the optical signals onto a single optical fibre, erbium-doped fibre amplifiers (EDFAs) that compensate the power loss, and the ROADMs that switch the optical signal to another route. Each optical signal will be degraded by the impairments of the Amplified Spontaneous Emission (ASE) noise of optical amplifiers as well as the linear and nonlinear signal distortions on these devices. For these devices, we use different colors to illustrate the different PLIs.

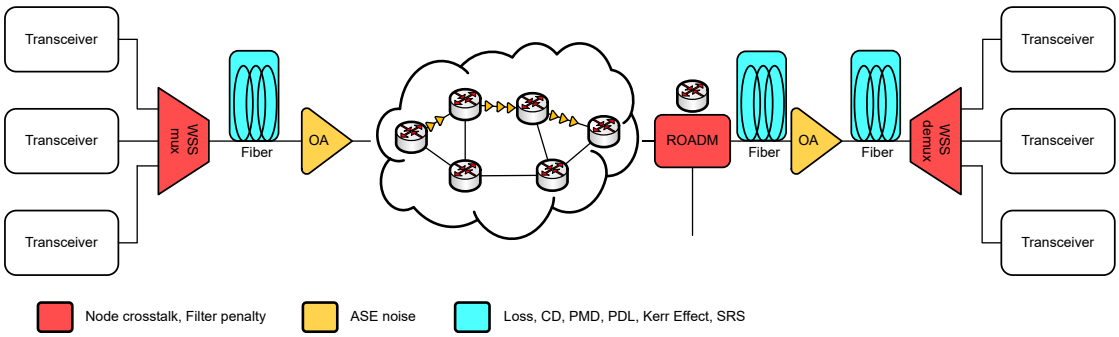

Figure 2.1: *Different impairments along a lightpath[22].*

We denote the linear impairments as those propagation effects that depend linearly on the signal power. Linear impairments at least include the following five factors[9]: (i) signal power loss, (ii) chromatic dispersion (CD), (iii) polarization mode dispersion (PMD), (iv) polarization-dependent loss (PDL), and (v) filtering effect and node crosstalk of ROADM at node[9]. The signal power loss is caused by the absorption of

the fiber optic cable itself. The CD is caused by different velocities of the signal on different frequencies. The PMD is caused by asymmetric fiber, which leads to different velocities at two different polarizations. The PDL leads to different power losses at two polarizations. The filtering effect is caused by the non-ideal rectangular shape of the filters inside the ROADM and WSS mux. The node crosstalk leads to signal leakage from one output port to another output port due to the imperfect isolation. As part of the impairments (CD, PMD, and PDL) can be mitigated by using efficient DSP algorithms at the receiver[81, 113, 116, 127], we neglect them for the PLI model.

The nonlinear impairments are those propagation effects that are not linear to the signal power, which can be caused by the Kerr effect and scattering phenomenon[4]. Due to the Kerr effect, the signal phase is distorted by the refractive index that depends on the intensity of the incident optical signal. Then, the phase distortion will be converted to amplitude distortion due to the fibre dispersion[4]. Except for the Kerr effect, the stimulated Raman scattering (SRS) and stimulated Brillouin scattering (SBS) are other two nonlinear effects that impair the signal quality. When the incident signal power exceeds a certain level, the scattering effect of the fiber can amplify the signal at another frequency[4].

When evaluating the QoT, this thesis chooses one typical PLI from the link and node, respectively, including *ASE noise*, *the nonlinear effect on links*, and *node crosstalk at optical switches*. Thus, we can numerically evaluate the PLIs as the lightpath configuration changes, which cannot be easily completed by the previous studies that set a constant penalty value[136]. Next, we will present how to evaluate the QoT.

2.2 QoT metric based on SNR

For a long time, there are several typical metrics to measure the QoT of an optical signal[47], including optical signal-to-noise ratio (OSNR), Q-factor, error vector magnitude. One of the widely used metrics is based on Q-factor[5, 47, 95], which has been used in the past few decades[9, 47, 103]. In this method, the key parameter, Q, is measured by observing the eye diagram. For example, with the On-Off Key (OOK) signal, Q is related to the eye amplitude level of the symbols 0 and 1, as well as the sum of their standard derivations[47]. Thus, the ultimate QoT performance, namely bit-error-ratio (BER), is obtained by the following equation,

$$BER = \frac{1}{2}\,\mathrm{erfc}\left(\frac{Q}{\sqrt{2}}\right) \tag{2.1}$$

With the advance of flexible transceivers, the QoT metric based on Q-factor is not convenient anymore, which needs to analyze both the in-phase signal and quadrature signal of a high-order MF. Moreover, the eye diagram lacks the consideration of FEC that is implemented in the digital domain. Consequently, the QoT metric based on the numerical calculation of SNR is suggested in the studies[66, 129]. In addition, the performance of different QoT is expressed by a ratio of SNR to SNR threshold, namely *SNR margin* [62, 100].

Different from the Q-factor, the QoT based on SNR needs to quantitatively evaluate various physical layer impairments. As stated before, these impairments include the ASE noise, NLI, node crosstalk, filtering effect, transceiver's back-to-back penalty, etc. The classical evaluation metric, optical SNR (OSNR, or OSNR^{ASE}), merely denotes one of the components, ASE[53, 129]. Recently, a more general metric, *generalized SNR* (GSNR) is proposed to include other line-related impairments, e.g. the NLI and node crosstalk[45, 143]. In the definition of GSNR, the impairments (NLI and node crosstalk) are assumed as additive noise[53, 54]. For NLI, this hypothesis has been validated using the GN model both theoretically and experimentally[96, 99, 129]. While for node crosstalk, we assume it is additive too[13], so that we can combine the two impairments easily,

$$\frac{1}{GSNR_i} = \frac{P_i^{NLI}}{P_i^{sig}} + \frac{P_i^{AD}}{P_i^{sig}} + \frac{1}{OSNR_i^{ASE}} \tag{2.2}$$

where $OSNR_i^{ASE}$ is the optical signal to ASE noise ratio measured before the receiver, P_i^{NLI} is NLI power, and P_i^{AD} is AD node crosstalk power. Depending on the reference bandwidth B_{ref}, the OSNR could be scaled with a factor R/B_{ref}, where R is the baud-rate. A typical assumption is to use B_{ref}=0.1 nm (≈12.5 GHz at 1550 nm). In this thesis, we consider the reference bandwidth B_{ref} equal to the baud-rate in order to remove the dependency of reference bandwidth, i.e. a constant scaling factor of 1.

Finally, combining the GSNR and transceiver's penalty, we can evaluate the total received SNR (SNR_i^{tot})[53, 129],

$$\frac{1}{SNR_i^{tot}} = \frac{1}{GSNR_i} + K_{TRX} \tag{2.3}$$

where K_{TRX} is a fixed constant depending on the particular implementation of the transceivers[48]. The SNR metric in this thesis is only evaluated by the ASE, NLI, and node crosstalk, i.e. ideal case with zero penalty on transceivers ($K_{TRX} = 0$). In other words, we adopt $GSNR$ to denote the signal quality, which is expressed as follows[45],

$$SNR_i = \frac{G_i}{G_i^{\text{ASE}} + G_i^{\text{NLI}} + G_i^{\text{AD}}} \tag{2.4}$$

where G_i^{ASE} is the PSD of ASE noise from optical amplifiers, G_i^{NLI} is the PSD of NLI, and G_i^{AD} is the PSD of node crosstalk. Next, we will explain in detail the computation of various impairments. Table 2.1 shows the PLI related parameters that will be used in the following.

2.2.1 Model of ASE noise

ASE noise is a white noise, whose intensity is proportional to the number of optical amplifiers and channel bandwidth. We use the ASE PSD G_i^{ASE} to denote the strength, which is expressed by

$$G_i^{\text{ASE}} = N_{\text{span}}(10^{\alpha L_{\text{span}}} - 1) n_{\text{sp}} \cdot h \cdot \nu \tag{2.5}$$

where N_{span} is the number of optical amplifiers and L_{span} (unit: km) is the distance between two optical amplifiers[62].

Table 2.1: *Parameters for PLIs*

Parameters and description	
α	Power attenuation ratio of fiber, 0.2 dB/km.
β_2	Second order dispersion of 1550nm wavelength, -21.7 ps^2/km.
γ	Non-linear coefficient, 1.3 $(W{\cdot}Km)^{-1}$.
h	Planck's constant.
ν	Frequency of optical signal, 192.5 THz.
μ	$\frac{3\gamma^2}{2\pi\alpha\beta_2}$.
ρ	$\pi^2\beta_2/\alpha$.
ϵ_{X}	Port leakage ratio of WSS and OXC, -25 dB.
n_{sp}	Noise factor of optical amplifier, 7 dB.
G_i	Launch PSD of request i.
G_i^{ASE}	PSD of ASE.
G_i^{SCI}	PSD of SCI.
G_i^{XCI}	PSD of XCI.
G_{ijv}^{AD}	PSD of AD node crosstalk from j to i at node v.
G_i^{AD}	PSD of AD, $G_i^{\mathrm{AD}} = \sum_{jv} G_{ijv}^{\mathrm{AD}}$.
L_{span}	Span length, 100 km/span.

2.2.2 Model of NLI

This thesis considers the GN model in [66], which assumes that the NLI maintains a simple and linear relationship to the number of spans. In particular, the NLI PSD on a single span is expressed as follows,

$$G_{span}^{NLI}(f) = \int\int \frac{3\gamma^2 G(\nu)G(\nu')G(\nu+\nu'-f)}{\alpha^2 + 16\pi^4\beta_2^2(\nu-f)^2(\nu'-f)^2} d\nu d\nu' \tag{2.6}$$

where $G(\nu)$ is the signal PSD. An example that illustrates the signal PSD $G(f)$ and NLI PSD $G^{NLI}(f)$ in Eq. (2.6) can refer to Fig. 2.2, where we have assumed that these three Nyquist WDM channels are with the following parameters: a bandwidth of 28 GHz, a roll factor of 0.2, and power of 20 mW (PSD = 0.714 mW/GHz).

We see that the calculation of NLI needs the complex numerical integration, which makes it difficult for network designer. To tackle this challenge, a common approach is to separate the NLI by self-channel interference (SCI) and cross-channel interference (XCI) separately[62, 66, 96, 122, 139] and neglects other weak residual NLI (e.g., multi-channel interference). The studies in [122, Table 2.1] and [60, Chapter 4] also summarized and compared the existing approaches to calculate SCI and XCI. Considering the ease of use, in this thesis, we continue to adopt the dilog method in [66, Eq. (11)] to calculate the NLI, even though it is conservative.

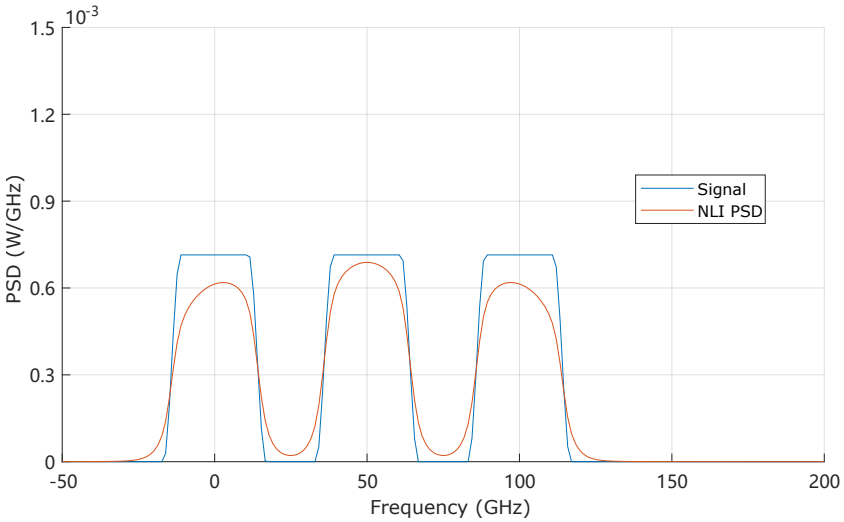

Figure 2.2: *An example NLI PSD for three channels based on [66, Eq. (3)].*

$$G_{span}^{NLI} = G_{span}^{SCI} + G_{span}^{XCI} \tag{2.7}$$

$$= \eta_{ch}^{SCI} \cdot {G_{ch}}^3 + G_{ch} \cdot \sum_{ch'} \eta_{ch,ch'}^{XCI} \cdot {G_{ch'}}^2 \tag{2.8}$$

$$G_i^{NLI} = N_{span,i} \cdot \eta_{ch}^{SCI} \cdot {G_{ch}}^3 + G_{ch} \cdot \sum_{ch'} \eta_{ch,ch'}^{XCI} \cdot N_{span,i,j} \cdot {G_{ch'}}^2 \tag{2.9}$$

where G_{span}^{NLI} represents the NLI PSD of one channel, ch and ch' are the occupied channels of lightpaths i and j, $N_{span,i,j}$ is the number of common spans for lightpath i and j, η_{ch}^{SCI} and $\eta_{ch,ch'}^{XCI}$ are the SCI efficiency and XCI efficiency of a single span, respectively. Here, we provide an expression to calculate the NLI when signal bandwidth $R_i \geq 28\ GHz$[66, 139].

$$G_i^{\text{SCI}} = N_{\text{span}} \mu G_i^3 \text{arcsinh}(\rho R_i^2) \tag{2.10}$$

$$G_i^{\text{XCI}} = \sum_j N_{\text{span},ij} \mu G_i G_j^2 \ln\left(\frac{|f_i - f_j| + R_j/2}{|f_i - f_j| - R_j/2}\right) \tag{2.11}$$

where f_i is the relative carrier centre frequency to 192.5 THz (unit: GHz).

2.2.3 Model of node crosstalk

Impairments at OXCs come from filtering effects and node crosstalk. Only in-band crosstalk is considered in this thesis, *i.e.*, the lightpath experiences node crosstalk if it is exposed to the other lightpaths with the overlapping bandwidth. As an example, we use 9-node network in Fig. 2.3(a) to illustrate the different node crosstalk components. The primary signal P1 is added at node C1, passes through node C2, and is dropped at node C3. Other three crosstalk signals I1, I2, and I3, are also depicted. At each of

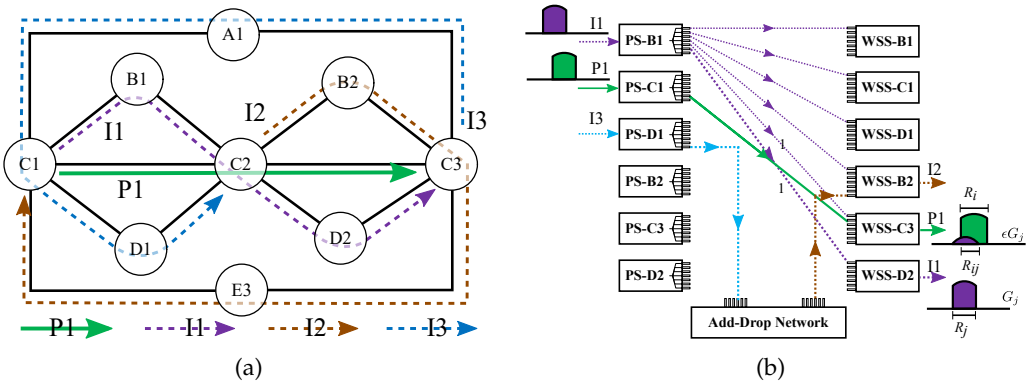

Figure 2.3: *(a) A 9-node network for illustrating different forms of AD node crosstalk, (b) Illustration of node crosstalk at node C2 considering a B&S architecture[145]. PS: power splitter.*

its nodes(C1, C2 and C3), P1 will experience all forms of crosstalk, *i.e.*, adding, passing through, and dropping.

To analyze the node crosstalk, we assume a broadcast-and-select (B&S) OXC architecture for intermediate node C2[145], as illustrated in Fig. 2.3(b). It consists of passive optical splitters (PSs) with 1×N ports that broadcast signal copies to the common port at local add/drop side, and wavelength selective switches (WSSs) facing different output ports and collecting the signals from add ports. A node crosstalk from signal I1 to P1 arises on WSS-C3 because the broadcast signal I1 is leaked into WSS-C3. We can also observe that the crosstalk signal I3 can leak into P1 on WSS-C3 due to the broadcast function of PS-D1. In addition, we also observe other forms of interference at nodes C1 and C3, which are not shown in Fig. 2.3(b). When primary signal P1 is added at node C1, it experiences the dropping crosstalk of I2 and the passing-through crosstalk of I3. When the primary signal is dropped at node C3, there is no crosstalk, because P1 is dropped locally. In short, the add and drop (AD) node crosstalk exists if the two conditions are satisfied: (i) primary signal is added at or passing through the node, and (ii) crosstalk signal is passing through or dropped at that node.

Different from the approach of [13] that only supports the node crosstalk by fixed FS, we propose to improve it by adopting the channel bandwidth, which supports arbitrary channel bandwidth. Thus, assuming the overlapping bandwidth between the primary signal R_i and the interfering signal R_j is R_{ij}, we give the amount of node crosstalk as follows,

$$G_{ijv}^{\mathrm{AD}} = \epsilon_X R_{ij} G_j \tag{2.12}$$

where G_j is the PSD of other interfering signal (j = I1 in the example), v is the node (C2 in the example), and $R_{ij} = \left| \frac{R_i + R_j}{2} - |f_i - f_j| \right|$. All node crosstalks are linearly summed together when considering the AD node crosstalk of one lightpath.

2.3 The physical layer model in a network context

With the considered PLIs including ASE noise, NLI, and AD node crosstalk, we can evaluate the QoT of each ligthpath. According to this metric, we can select an efficient MF to satisfy the required bi-rate of each request. Meanwhile, the chosen MF should satisfy the physical layer constraint, i.e., SNR is no smaller than the SNR threshold.

This part will describe the QoT model for the lightpaths in a network as well as their available transmission rates. We denote an FON by a graph $G(V, E)$. Each node $v \in V$ represents an OXC. A link $e \in E$ represents two fibers uv and vu ($u, v \in V$) that carry traffic in opposite directions. Each request i is characterized by its source node s_i, destination node d_i, required bit-rate r_i (Gbps), PSD G_i ($G_i = G$). The consumed spectrum resource Δf_i (=R_i) should guarantee that $\Delta f_i \cdot \mathrm{SE}(c_i) \geq r_i$, where $\mathrm{SE}(c_i)$ is the spectral efficiency of MF c_i and Δf_i is the subcarrier bandwidth.

2.3.1 QoT model for a lightpath

We denote by c_i the MF of lightpath i, $SNR_{c_i}^{\mathrm{th}}$ the SNR threshold of c_i. A lightpath i can be served if it satisfies the QoT constraint as depicted in Eq. (2.13).

$$SNR_i = \frac{G_i}{G_i^{\mathrm{ASE}} + G_i^{\mathrm{NLI}} + G_i^{\mathrm{AD}}} \geq SNR_{c_i}^{\mathrm{th}} \tag{2.13}$$

For ease of the MILP modeling, we express Eq. (2.13) in its reciprocal form,

$$\begin{cases} \dfrac{1}{\mathrm{SNR}_i} = t_i^{\mathrm{ASE}} + t_i^{\mathrm{NLI}} + t_i^{\mathrm{AD}} \leq \dfrac{1}{\mathrm{SNR}_{c_i}^{\mathrm{th}}} \\ t_i^{\mathrm{ASE}} = G_i^{\mathrm{ASE}} / G_i \\ t_i^{\mathrm{NLI}} = G_i^{\mathrm{NLI}} / G_i = (G_i^{\mathrm{SCI}} + G_i^{\mathrm{XCI}}) / G_i \\ t_i^{\mathrm{AD}} = G_i^{\mathrm{AD}} / G_i \end{cases} \tag{2.14}$$

where NLI is decomposed into SCI and XCI, t_i^{ASE}, t_i^{SCI}, t_i^{XCI}, and t_i^{AD} are the noise to signal ratios of ASE, SCI, XCI, and AD node crosstalk, respectively.

The parameters to be optimized can include center frequency, PSD, and bandwidth. However, from a network designer's view, the nonlinear relationship between NLI and these physical parameters will greatly increase the problem complexity of the network design, as shown in Eqs. (2.10) and (2.11). In order to accelerate the calculation of NLI and make it suitable for linear programming, we precalculate the XCI efficiency, and fit the specified related physical parameters using the piecewise linear fitting tool.

Taking the channel spacing ($f_i - f_j$, center frequency difference) as an example, the expression of piecewise-linear fitting function in Eq. (2.9) is written as follows,

$$\eta^{XCI}(f) \approx \bar{\eta}^{XCI}(f) = \max_{1 \leq q \leq Q_{PWL}} \left(a_q f + b_q\right) \tag{2.15}$$

where Q_{PWL} is the number of segments for piecewise linear fitting, a_q and b_q are the coefficients calculated by piece-wise nonlinear fitting term[83, 139]. For a specific value f, only one of these linear segments that yields the maximal value $\bar{\eta}^{XCI}$ is satisfied. The remaining segments will be deactivated. That is to say, Eq. (2.15) guarantees a linear relationship between $\bar{\eta}^{XCI}$ and f. A simple version of the algorithm that calculates the fitting parameters is shown in the Appendix A. As an example, we show the fitting results in Fig. 2.4 when center frequency distance $|f_i - f_j|$ varies. The data in Fig. 2.4 is obtained by repeating different channels in Eq. (2.15), i.e., (R_i=16 GBaud, R_j=16 GBaud), (R_i=16 GBaud, R_j=32 GBaud), and (R_i=16 GBaud, R_j=64 GBaud). The maximum fitting error is less than 2% when Q=20, which exhibits modest performance.

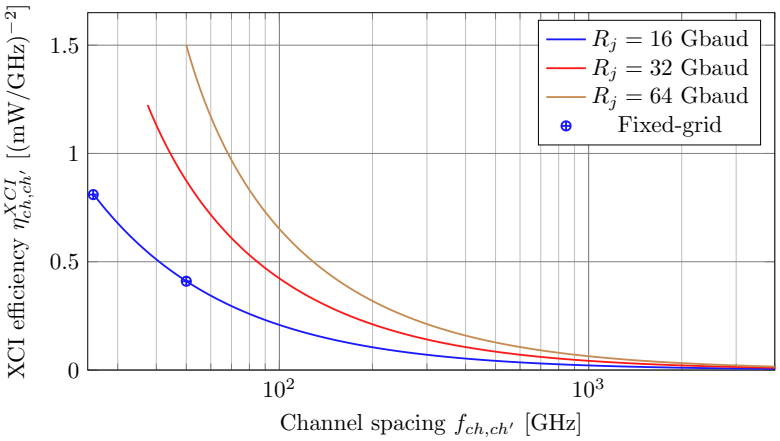

(a) XCI efficiency

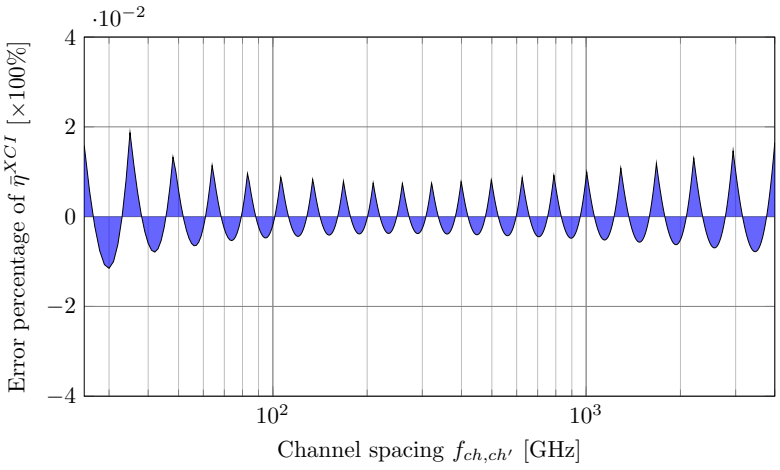

(b) Fitting error (R_i = 16 GBaud, R_j = 16 GBaud)

Figure 2.4: *XCI efficiency η^{XCI} versus channel spacing [66, Eq. (11)]. The channel under test uses the transceiver with bandwidth of 16 GHz. We also mark the XCI efficiency of fixed channel spacing of 25 GHz and 50 GHz, which will be used in the Chapter 3.*

Note that the PLIs of XCI and AD depend on the lightpaths that have a common

link or a common node. Taking the network in Fig. 2.5 as an example, we illustrate the interference by using a graph. Three requests R1, R2, and R3 are labeled with source, destination, bit-rate, and revenue, which are shown on the right part of Fig. 2.5(a). Besides, we fix their routes on 0-1-3, 0-1-3-4, and 3-4. Their spectrum usages are illustrated in Fig. 2.5(b).

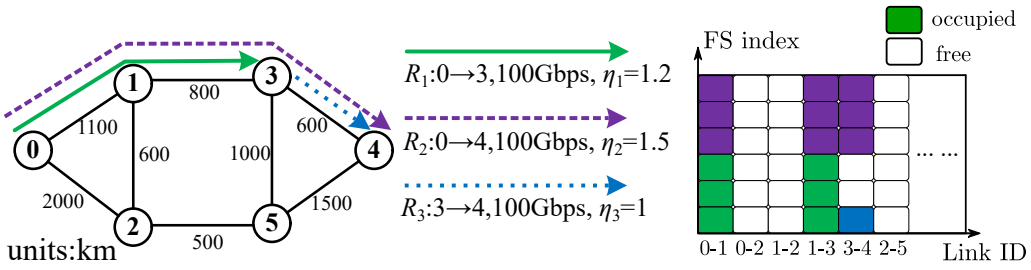

(a) Network (b) Link spectrum status

Figure 2.5: *A 6-node network and the link status.*

The Fig. 2.6 uses an interference graph to illustrate the NLI and AD node crosstalk between R1, R2, and R3. Each node represents a lightpath. The directed arc connecting two nodes represents that the interference is from the source to the sink. For example, R2 will generate NLI to R3, because they traverse a common link 3-4, and vice versa. As the crosstalk signal of R2 will leak to R3 on node 3, there is an AD node crosstalk from R2 to R3. However, R2 will not receive the node crosstalk from R3, because R2 has dropped at node 4 and there is no adding interference from node 3. Through this example, we find that the interference graph of NLI and node crosstalk is generally not the same, which poses a challenge to the network design.

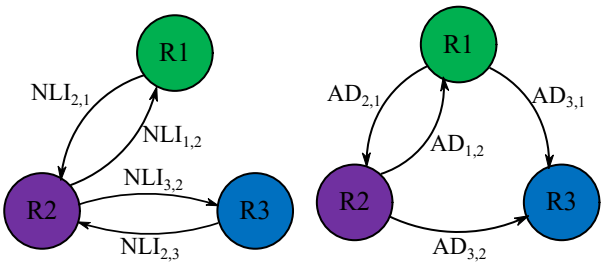

(a) NLI (b) AD node crosstalk

Figure 2.6: *Interference graph PLIs for three requests.*

2.3.2 Transmission capacity of a transmission mode

After obtaining the SNR, each lightpath will choose the MF as high as possible while satisfying QoT constraints. Today's flexible transceivers can use the standard polarization-multiplexed MFs, e.g., PM-BPSK, PM-QPSK, PM-8QAM, and PM-16QAM. However, there are two drawbacks for the current MFs[18]: (i) a gap to Shannon limit, and (ii) a coarse granularity of spectral efficiency. For example, the ideal spectral efficiency of

these MFs are assumed to be 2, 4, 6, and 8 bps/Hz, respectively [68, 139]. To overcome such drawbacks, variable DSP techniques have been proposed[6, 21, 51, 69] to increase the bit-rates of a given SNR. In this thesis, we incorporate the standard MFs with different FECs. Such a combination is named as a *transmission mode* in this thesis. It is anticipated that larger capacity can be realized by more flexible transmission modes. Next, we calculate the provisioned bit-rates by reviewing the basic communication theory. Finally, a list is presented that determines the bit-rate and the required SNR threshold for each transmission mode.

Assuming an obtained SNR from Eq. 2.13, its bit-error-ratio (BER) with PM-mQAM can be calculated by using the analytical expressions of [28, Eq. (23)],

$$P_{BER} \approx \frac{1}{\log_2(I \cdot J)} \left[\frac{I-1}{I} \operatorname{erfc}\left(\sqrt{\frac{3\log_2(I \cdot J) \cdot \gamma}{I^2 + J^2 - 2}} \right) + \frac{J-1}{J} \operatorname{erfc}\left(\sqrt{\frac{3\log_2(I \cdot J) \cdot \gamma}{I^2 + J^2 - 2}} \right) \right] \tag{2.16}$$

where $I \times J$ is the rectangular constellation diagram of mQAM, $\gamma = SNR/\log_2(m)$ denotes the SNR per bit (not per symbol). Assuming we use the simple hard-decision and binary symmetrical channel for optical channel, the required maximum code rate r_c to recover the original signal is given as follows[42, 115],

$$r_c = 1 + P_{BER} \cdot \log_2(P_{BER}) + (1 - P_{BER}) \cdot \log_2(1 - P_{BER}) \tag{2.17}$$

Thus, the required overhead (OH) as well as the spectral efficiency are stated as follows[63],

$$OH = (1/r_c - 1) \times 100\% \tag{2.18}$$

$$SE = 2 \cdot r_c \cdot r_{OTU} \cdot \log_2(m) \tag{2.19}$$

$$= 2 \cdot \frac{1}{1 + OH} \cdot r_{OTU} \cdot \log_2(m) \tag{2.20}$$

where r_{OTU} is a fixed ratio of the data and other necessary information in one optical transponder unit (OTU) frame, e.g., typically 5% or 7% as indicated in [1, 63]. Therefore, the maximum bit-rate of that transmission mode is $SE \cdot \Delta f_i$, where Δf_i is the signal bandwidth (or the baud rate).

As a summary, we show the network parameters of different transmission modes in Table 2.2 and Fig. 2.7 [1]. Table 2.2 shows the required MFs, the corresponding SNR threshold, and the code rate, for a bit-rate step of 25 Gbps[2]. Also, the maximum trans-

[1] To keep up with the reference in [63], we assume that the fixed overhead for the OTU is 5% , i.e., $r_{OTU} = 1/(1 + 0.05)$ and the signal bandwidth is 32 GHz (or 32 Gbaud).

[2] The data in this table is calculated in the following way, *step 1*: precalculate the spectral efficiency, bit-rate, and code rate for all MFs under a given SNR range, *step 2*: given a bit-rate, we find the MF that requires the minimum SNR among the candidate MFs, then the corresponding code rate is determined by the minimum SNR with Eqs. (2.16) and (2.17); *step 3*: the reach is determined by finding the maximum N that satisfies the equation $SNR_1 - \log_{10}(N) \geq SNR^{threshold}$, where SNR_1 is the SNR after one span assuming that the total spectrum resources is fully occupied.

mission reach is illustrated, which has assumed the worst-case scenario that total available spectrum of 4,000 GHz is fully occupied. Figure 2.7 illustrates the corresponding SNR and spectral efficiency.

Table 2.2: *Bit-rates and SNR thresholds of different transmission modes [63, Table I]*

Transmission mode	MF	FEC code rate	Bit-rate (Gbps)	SNR threshold (dB)	Reach[†] (×100km)
QPSK1	PM-QPSK	0.41	50	0.59	158
QPSK2	PM-QPSK	0.62	75	3.16	87
QPSK3	PM-QPSK	0.82	100	5.69	49
16QAM1	PM-16QAM	0.49	125	7.63	31
16QAM2	PM-16QAM	0.62	150	9.14	22
16QAM3	PM-16QAM	0.72	175	10.58	15
16QAM4	PM-16QAM	0.82	200	12.08	11
16QAM5	PM-16QAM	0.92	225	13.99*	7
64QAM1	PM-64QAM	0.68	250	15.45	5
64QAM2	PM-64QAM	0.75	275	16.57	4
64QAM3	PM-64QAM	0.82	300	17.73	3
64QAM4	PM-64QAM	0.89	325	19.07	2
64QAM5	PM-64QAM	0.96	350	20.85	1

[*] We have revised the small difference in the reference.
[†] When calculating the PLIs and evaluating the QoT, we have assumed the worst-case scenario that total spectrum resources are fully occupied and also neglect the node crosstalk.

In addition, we use Table 2.3, to show the bit-rate, signal bandwidth, occupied FSs, as well as net spectral efficiency when the reference channel bandwidth is larger than the signal bandwidth. This table also compares the spectral efficiency of BVT and S-BVT. For the conventional sliceable multi-flow transceiver, the bit-rate of each subflow is proportional to the number of slices. Unlike that, the bit-rate of BVT depends on the exact baud-rate rather than merely the used spectrum resource[56], i.e., FSs. This is because the wasted spectrum resources between the subflows have been used for transmission by BVTs. The benefits of a high baud rate transceiver will be discussed in Chapter 4.

Table 2.3: *Bandwidths and bit-rates of six transceivers (three single baud-rate transceivers and three sliceable transceivers)*

Transceiver type (Baud)	Channel bandwidth R_t (GHz)	FS B_t (GHz)	Bit-rate (Gbps) [§]	Net spectral efficiency (bps/Hz)
16G	17.6	25 (= 2 slots)	50	2
32G	35	50 (= 4 slots)	100	2
64G	70	75 (= 6 slots)	200	2.67
16G, 1 slice	17.6	25 (= 2×1 slots)	50×1	2
16G, 2 slices	-	50 (= 2×2 slots)	50×2	2
16G, 3 slices	-	75 (= 2×3 slots)	50×3	2

Data source: `https://www.oiforum.com/wp-content/uploads/2019/01/OIF-Tech-Options-400G-01.0.pdf`
[§] Assume PM-QPSK with FEC code rate 0.82.

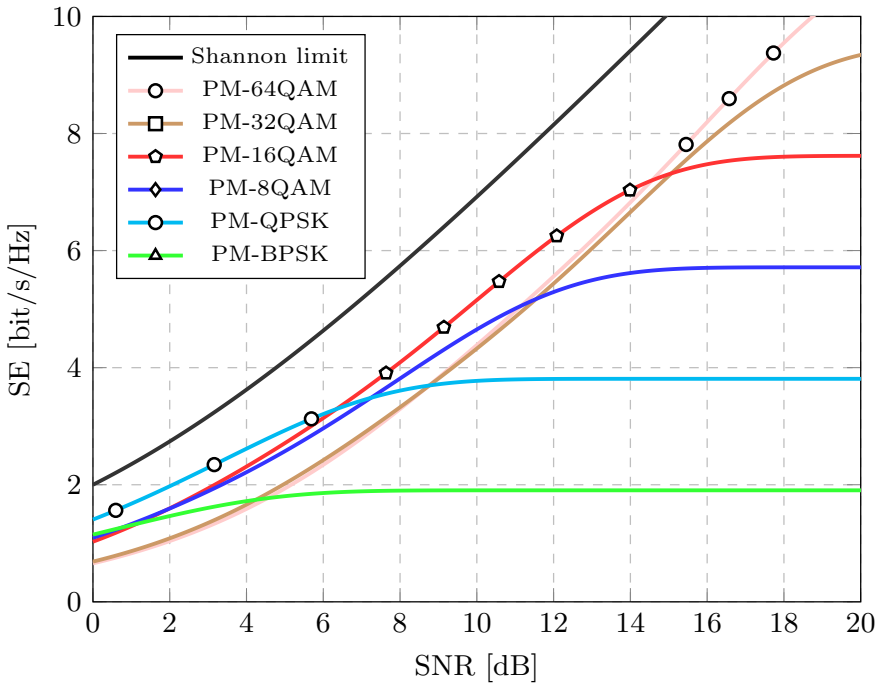

Figure 2.7: *SE vs. SNR. Each point is separately by a unit step of spectral efficiency of 0.78 bps/Hz[63].*

2.4 Conclusion

In this part, we have briefly presented the PLIs in the optical transmission system. Among the PLIs, we choose ASE noise, NLI, and node crosstalk for QoT evaluation. Finally, we present the QoT of a lightpath in FONs as well as the transmission modes that can obtain a larger bit-rate than existing standard MFs. Through the physical layer modeling, we can associate the different physical layer parameters with the network design.

Chapter 3

Revenue Maximization Problem with Adaptive MF and Multiple FEC

Contents

3.1 Introduction

According to recent traffic reports, network traffic (fueled by successful network services like video on demand, file sharing, online gaming, and video conferencing) is still growing exponentially in today's Internet[36]. This constant traffic growth can be accommodated by novel FONs which can support large transmission capacity. As busy hour traffic peaks are expected to increase almost 5 times between 2017 and 2022 (average Internet traffic will increase only 3.7 times), the problem of coping with sudden resource crunches will become even more a matter of concern in next years, especially during peak usage periods[36, 75, 79, 150]. During resource crunch, given the limited spectrum resources in FONs, not all traffic requests can be fully satisfied, and some traffic must be blocked. As carried traffic brings revenue to operators, resource crunch events can lead to significant revenue losses for operators. Hence, efficient provisioning strategies in optical networks are required to reduce blocking and maximize operators' revenue.

In FONs, an adequate amount of spectrum resources to establish a lightpath is required for each request. Since FONs can support variable routes, bandwidth, and MFs, the routing and wavelength assignment problem has evolved into the routing and spectrum assignment[71, 84, 108, 139]. However, since the spectral efficiency granularity of mQAM is coarse, the conventional resource provisioning cannot give full play to its advantages in collecting the services' revenue. Hence, to achieve even higher resource-allocation flexibility that granted by multiple MFs, tunability of FEC has been introduced to adjust the spectral efficiency[7, 18, 69, 111]. It can be typically observed that overhead ratios range values from 7% to 20%. The combination of MF and FEC, referred to as *transmission mode* in this study, can provide more candidate choices in terms of spectral efficiency and transmission reach. Compared to the traditional approaches aiming at revenue improvement, such as using backup lightpaths for living traffic [131] or upgrading to multi-core fibers[74], using MF and FEC is more efficient and faster. The traffic provisioning with multiple MFs and FECs maps into a problem of RMFSA[124]. Although some researchers have proposed heuristic algorithms[69, 84, 111], like *congestion-aware sequential loading* algorithm[114], and *adaptive FEC selection*[76], there is no complete mathematical model for the lightpath provisioning in FONs with both MF and FEC, which also accounts for PLIs modeling. While the optimal combination of MF and FEC has been investigated at the transmission layer in, *e.g.*, [73], in this study we investigate how the combination of MF and FEC can be used to maximize revenues through appropriate traffic provisioning strategies.

To support multiple MFs and FECs in FONs, traffic provisioning strategies must be cross-layer[29], *i.e.*, they must be capable of taking in account physical layer aspects, to achieve efficient spectrum usage. The PLIs of a lightpath are influenced by the bandwidth, by PSDs, by the route length, and by the number of crossed nodes. Due to the impact of all the parameters just mentioned, the QoT (expressed by lightpath's SNR) may degrade and fall below acceptable threshold for correct signal reception after a long distance. Recent studies on the node crosstalk have considered the wavelength-related and FS-related crosstalk component[13, 30]. However, current

studies overestimate the PLIs with the assumption of full wavelength or full consecutive FSs for each lightpath. For example, the node crosstalk on provisioned bandwidth of 12.5 GHz slot is larger than the actual value of the sub-channel bandwidth with 6.25 GHz[85, 118, 125]. To reduce the PLIs, a guard band (*e.g*, 12.5 GHz) may be used, but incurring in inefficient usage of spectrum resources. Therefore, the PLI model that we propose is based on channel bandwidth, which means that the impairments of node crosstalk and fiber nonlinear interference are evaluated by the bandwidth rather than a wavelength or slot, which ensures that the PLIs are properly estimated and spectrum resource is effectively utilized.

The main novelty and contributions of this study can be summarized as follows:

1. We devise novel traffic provisioning strategies to maximize the total revenue using different MF and FEC configurations. The lightpaths can adopt transmission mode with either higher spectral efficiency or longer transmission reach to guarantee the bit-rate under resource crunch. Compared to single MF or single FEC, the combination can provide just-enough spectral efficiency and transmission reach thus improve the traffic provisioning. By using a piece-wise linear fitting function to model the nonlinear interference and calculating the crosstalk of intermediate nodes, we linearize the PLIs then model the studied problem as a MILP. Our MILP model is based on flow rather than pre-calculated route. Without using the candidate route, our method can get the optimal solution irrespective of the number of routes.

2. We propose a novel lightpath's PLI evaluation model based on the channel bandwidth that incorporates the impact of different PSDs, FECs, and MFs. By tracing the relationship between the PSD and SNR, we observe that using MFs enables to increase revenues with high SNR, while using multiple FECs is preferred for the scenarios of low SNR. Besides, compared to the wavelength-related or FS-related method, the bandwidth-related method evaluates the PLIs by using channel bandwidth. To this end, the spectrum resources of fiber are assumed to be continuous rather than discrete FS.

3. A fast and near-optimal heuristic algorithm is also proposed to solve the revenue maximization problem.

The rest of this study is organized as follows. We describe our proposed PLI model in Sec. 3.2. The problem of traffic provisioning with adaptive MFs and multiple FECs is stated in Sec. 3.3. To solve it, we present an MILP model in Sec. 3.4 and a heuristic algorithm in Sec. 3.5. Illustrative numerical results are presented in Sec. 3.6. Finally, Sec. 3.7 concludes this study.

3.2 Physical Layer Model

In this section, we discuss our proposed PLI evaluation model. We also include a brief description of the signal impairments and of the optical transmission.

3.2.1 MF and FEC

We denote as transmission mode $\mathcal{C}$ the combination set of MF and FEC, $\mathcal{C}$=($\mathcal{M}$,$\mathcal{F}$). For an arbitrary transmission mode $c \in \mathcal{C}$, its spectral efficiency is

$$SE(c) = SE(m, f) = m/(1 + OH_f) \tag{3.1}$$

where m is the theoretically maximum spectral efficiency of the MF, and OH_f is the FEC overhead ($\times$100%)[7, 73]. The spectral efficiency and SNR threshold of several transmission modes are shown in Fig. 3.1. In particular, we assume four available polarization-multiplexing MFs (PM-BPSK, PM-QPSK, PM-8QAM, and PM-16QAM) and six FEC OHs (1%, 7%, 10%, 20%, 30%, and 50%). For example, the spectral efficiency of PM-16QAM with FEC OHs 10% is 4/(1+10%)=3.63 bit/s/Hz, while the SNR threshold is 15.7 dB. To satisfy QoT, the SNR should be over the threshold for each transmission mode. Next, we present the PLI model that impacts SNR.

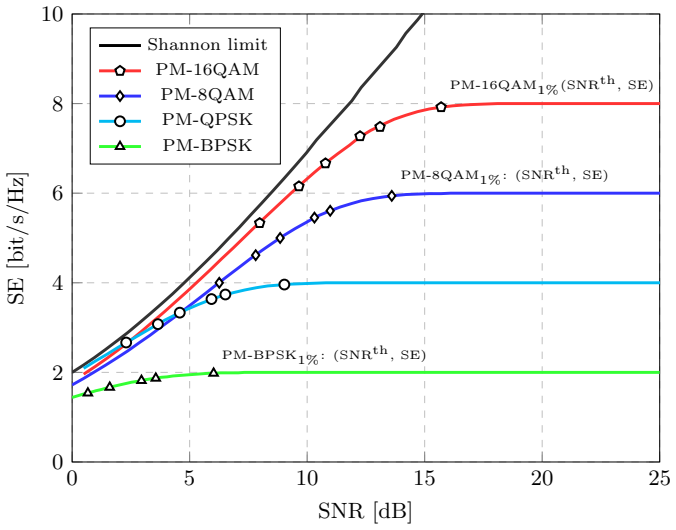

MF	m	FEC					
		OH=1%	OH=7%	OH=10%	OH=20%	OH=30%	OH=50%
PM-BPSK	2	6.02	3.56	2.95	1.6	0.67	-
PM-QPSK	4	9.03	6.52	5.93	4.58	3.65	2.3
PM-8QAM	6	13.6	10.98	10.31	8.85	7.81	6.26
PM-16QAM	8	15.7	13.1	12.25	10.78	9.65	7.98

Figure 3.1: *The maximum achievable spectral efficiency of different transmission modes with different SNRs[7, 142]. With a target pre-FEC BER of 10^{-4}, the SNR threshold for each marker is illustrated in the table below.*

3.2.2 PLIs model

When an optical signal propagates, it suffers diverse forms of PLIs, including white Gaussian noise ASE, SCI, and XCI [66, 96, 139]. Both SCI and XCI interference are caused by the Kerr effect of fiber, which can be estimated as additive white Gaussian

noise by the GN model[96]. When a signal traverses an OXC, the node crosstalk from signal AD at node must be also considered[13, 29].

The PLI related parameters are given in Table 3.1. We note c_i as the transmission mode used by request i. SNR_i denotes its received SNR, and $\mathrm{SNR}^{\mathrm{th}}_{c_i}$ is the SNR threshold for c_i. By summing up all noise contributions due to PLIs, a request i can be served if it satisfies the QoT constraint as in Eq. (3.2).

$$\mathrm{SNR}_i = \frac{G_i}{G_i^{\mathrm{ASE}} + G_i^{\mathrm{SCI}} + G_i^{\mathrm{XCI}} + G_i^{\mathrm{AD}}} \geq \mathrm{SNR}^{\mathrm{th}}_{c_i} \tag{3.2}$$

For ease of the MILP modeling, we can also express Eq. (3.2) in its reciprocal form,

$$\begin{cases} \dfrac{1}{\mathrm{SNR}_i} = t_i^{\mathrm{ASE}} + t_i^{\mathrm{SCI}} + t_i^{\mathrm{XCI}} + t_i^{\mathrm{AD}} \leq \dfrac{1}{\mathrm{SNR}^{\mathrm{th}}_{c_i}} \\ t_i^{\mathrm{ASE}} = G_i^{\mathrm{ASE}} / G_i \\ t_i^{\mathrm{SCI}} = G_i^{\mathrm{SCI}} / G_i \\ t_i^{\mathrm{XCI}} = G_i^{\mathrm{XCI}} / G_i \\ t_i^{\mathrm{AD}} = G_i^{\mathrm{AD}} / G_i \end{cases} \tag{3.3}$$

where t_i^{ASE}, t_i^{SCI}, t_i^{XCI}, and t_i^{AD} are the noise to signal ratios of ASE, SCI, XCI, and AD node crosstalk, respectively. The noise to signal ratios can be regarded as the amount of PLIs of ASE, SCI, XCI, and node crosstalk. In the following, we will explain in detail the computation of various impairments.

Table 3.1: *Parameters for PLIs*

Parameters and description	
α	Power attenuation ratio of fiber, 0.2 dB/km.
β_2	Second order dispersion of 1550nm wavelength, -21.7 ps^2/km.
γ	Non-linear coefficient, 1.3 $(\mathrm{W{\cdot}Km})^{-1}$.
h	Planck's constant.
ν	Frequency of optical signal, 192.5 THz.
μ	$\dfrac{3\gamma^2}{2\pi\alpha\beta_2}$.
ρ	$\pi^2\beta_2/\alpha$.
ϵ_{X}	OXC port leakage ratio, -25 dB.
n_{sp}	Noise factor of optical ampilier, 7dB.
G_i	Launch PSD of request i.
G_i^{ASE}	PSD of ASE.
G_i^{SCI}	PSD of SCI.
G_i^{XCI}	PSD of XCI.
G_{ijv}^{AD}	PSD of AD node crosstalk from j to i at node v.
G_i^{AD}	PSD of AD, $G_i^{\mathrm{AD}} = \sum_{jv} G_{ijv}^{\mathrm{AD}}$.
$\mathrm{SNR}_c^{\mathrm{th}}$	SNR threshold of transmission mode c.
L_{span}	Span length, 100 km/span.

Impairments along fibers (ASE, SCI, and XCI)

ASE noise is a white noise, whose intensity is proportional to the number of fiber spans and channel bandwidth. Its PSD can be expressed by

$$G_i^{\text{ASE}} = N_{\text{span}}(e^{\alpha L_{\text{span}}} - 1)n_{\text{sp}}h\nu \tag{3.4}$$

where N_{span} is the number of spans (see Table 3.1 for the other parameters).

In GN model[96], both SCI and XCI are regarded as white noise, whose PSD is related to the light power, bandwidth and center frequency. Eqs. (3.5) and (3.6) can be used to calculate the PSD of SCI and XCI[66, 98] (note that the calculation has been validated for bandwidth Δf_i bigger than 28 GHz[66].

$$G_i^{\text{SCI}} = N_{\text{span}}\mu G_i^3 \text{arcsinh}(\rho \Delta f_i^2) \tag{3.5}$$

$$G_i^{\text{XCI}} = \sum_j N_{\text{span},ij}\mu G_i G_j^2 \ln\left(\frac{|f_i - f_j| + \Delta f_j/2}{|f_i - f_j| - \Delta f_j/2}\right) \tag{3.6}$$

where Δf_i is the bandwidth of request i (unit: GHz), and f_i is the relative carrier center frequency (unit: GHz).

Impairments at nodes

Impairments at nodes come from filtering effects and node crosstalk. In-band crosstalk is considered in this study, *i.e.*, the lightpath experiences node crosstalk if it is exposed to the other lightpaths with the overlapping bandwidth. As an example, we use 9-node network in Fig. 3.2(a) to illustrate the different node crosstalk components. The primary signal P1 is added at node C1, passes through node C2, and is dropped at node C3. Other three crosstalk signals I1, I2, and I3, are also depicted. At each of its nodes(C1, C2 and C3), P1 will experience all forms of crosstalk, the primary signal will experience all forms of crosstalk, *i.e.*, adding, passing through, and dropping.

To analyze the node crosstalk, we assume a broadcast-and-select (B&S) OXC architecture for intermediate node C2[145], as illustrated in Fig. 3.2(b). It consists of passive optical splitters (PSs) with 1×N ports that broadcast signal copies to the common port at local add/drop side and wavelength selective switches (WSSs) facing different output ports and collecting the signals from add ports. A node crosstalk from signal I1 to P1 arises on WSS-C3 because the broadcast signal I1 is leaked into WSS-C3. We can also observe that the crosstalk signal I3 can leak into P1 on WSS-C3 due to the broadcast function of PS-D1. In addition, we also observe other forms of interference at nodes C1 and C3, which are not shown in Fig. 3.2(b). When primary signal P1 is added at node C1, it experiences the dropping crosstalk of I2 and the passing-through crosstalk of I3. When the primary signal is dropped at node C3, there is no crosstalk, because P1 is dropped locally. In short, the AD node crosstalk exists if primary signal is added at or passing through the node, and crosstalk signal is passing through or dropped at that node.

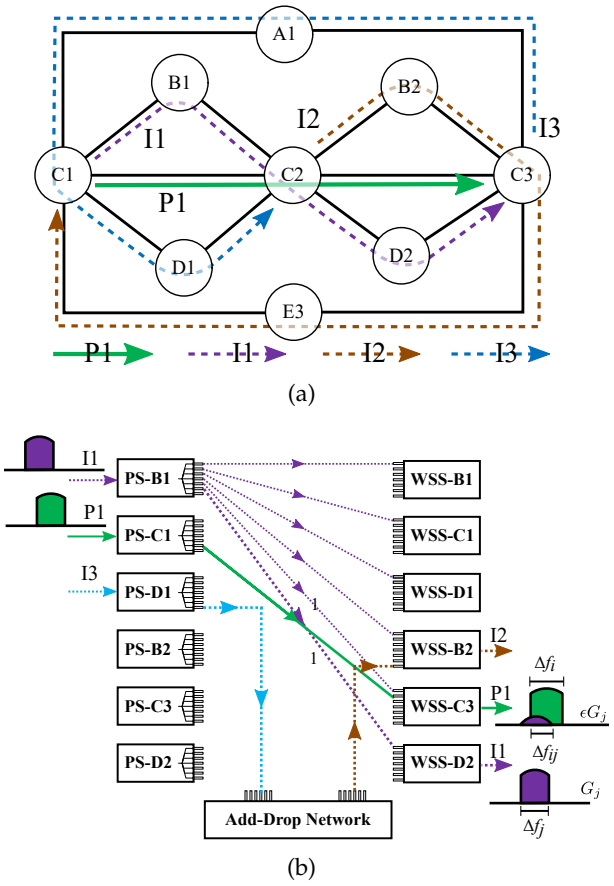

Figure 3.2: *(a) The 9-node network used to illustrate different forms of AD node crosstalk, (b) Illustration of node crosstalk at node C2 considering a B&S architecture[145]. PS: power splitter (PS).*

Different from the approach of [13] that only supports the node crosstalk by fixed FS, we propose to improve it by adopting the channel bandwidth, which supports arbitrary bandwidth. Thus, assuming the overlapping bandwidth between the primary signal Δf_i and the interfering signal Δf_j is Δf_{ij}, we give the amount of node crosstalk as follows,

$$G_{ijv}^{\mathrm{AD}} = \epsilon_X \Delta f_{ij} G_j \tag{3.7}$$

where G_j is the PSD of other interfering signal (j = I1 in the example), v is the node C2, and $\Delta f_{ij} = \left| \frac{\Delta f_i + \Delta f_j}{2} - |f_i - f_j| \right|$. In addition, P1 also experiences the crosstalk of I2 at node C1 and the crosstalk of I3 at node C2.

3.3 Problem statement

We denote a FON by a graph $G(V, E)$. Each node $v \in V$ represents an OXC. A link $e \in E$ represents two fibers uv and vu ($u, v \in V$) that carry traffic in opposite direc-

tions. Each request i is characterized by its source node s_i, destination node d_i, bit-rate r_i (Gbps), PSD G_i ($G_i = G$), and revenue level η_i. The consumed spectrum bandwidth counts $\Delta f_i = r_i/\mathrm{SE}(c_i)$, where $\mathrm{SE}(c_i)$ is the spectral efficiency of transmission mode c_i. Normally, the revenue η_i is determined by the operator's preference or the importance, such as (*i*) time of day, (*ii*) duration, (*iii*) location, (*iv*) distance, (*v*) connection speed, and (*vi*) service type [79]. A random service type parameter is adopted in this study. Assuming a set of requests in demand D, the total network revenue is the sum of accepted requests' revenue. Available spectrum resource of each fiber is limited to F ($F \in \mathbb{R}^+$).

To serve a request, a lightpath should be established on a continuous and contiguous spectrum interval. We indicate the continuous spectrum interval as $[b_i, e_i]$, where b_i and e_i are the beginning and end of the spectrum interval of request i, respectively. To satisfy the spectrum continuity and contiguity constraints, the spectrum interval $[b_i, e_i]$ must be the same on all traversed links, and can not overlap with other lightpath. Due to limited spectrum resources, not all lightpaths can be provisioned. Therefore, our objective is to maximize the total revenue by optimizing spectrum resource allocation. We use variable B_i to indicate whether request i is served ($B_i = 1$ if it is accepted, 0 otherwise), then the objective function can be expressed by

$$\sum_{i \in D} \eta_i B_i \tag{3.8}$$

We give an example of revenue difference for different traffic provisioning using transmission mode configurations, *i.e.*, single-FEC and multiple-FEC in Fig. 3.3. Each link has limited spectrum of 100 GHz. The number near each link denotes the length. Three requests R1, R2, and R3 are labeled with source, destination, bit-rate, and revenue. The PSDs for all lightpaths are -11 dBm/GHz.

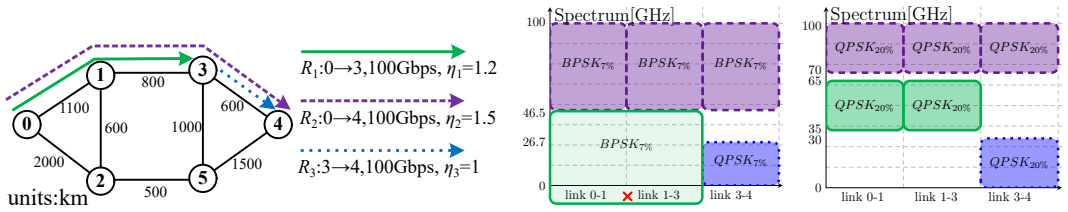

(a) 6-node network (b) Single-FEC (c) Multiple-FEC

Request	Single-FEC	Multiple-FEC
R1: 0-1-3	blocked	$\mathrm{QPSK}_{20\%}$
R2: 0-1-3-4	$\mathrm{BPSK}_{7\%}$	$\mathrm{QPSK}_{20\%}$
R3: 3-4	$\mathrm{QPSK}_{7\%}$	$\mathrm{QPSK}_{20\%}$
Revenue	2.5	3.7

[i] Single-FEC $\mathcal{C}$: {$\mathrm{BPSK}_{7\%}$,$\mathrm{QPSK}_{7\%}$}
[ii] Multiple-FEC $\mathcal{C}$: {$\mathrm{QPSK}_{7\%}$,$\mathrm{QPSK}_{20\%}$}

Figure 3.3: *Traffic provisioning example with single-FEC and multiple-FEC configurations in 6-node network.*

In single-FEC configuration, FEC OH is fixed at 7%, hence R2 uses $\text{BPSK}_{7\%}$ on the channel [46.5, 100], and R3 uses $\text{QPSK}_{7\%}$ on channel [0, 26.7]. However, the remaining spectrum [0, 46.5] on link 0-1 is not enough to support R1 with $\text{BPSK}_{7\%}$. Otherwise, if $\text{QPSK}_{7\%}$ had been chosen, the QoT of R1 would not have been satisfied because of the fiber nonlinear interference from R2 to R1. Therefore, only two requests can be accepted with single-FEC configuration, leading to a revenue of 2.5.

In multiple-FEC configuration, two FEC OHs can be used. The requests R1, R2, and R3 are served with $\text{QPSK}_{20\%}$, as the SNRs with $\text{QPSK}_{20\%}$ are 6.0 dB, 4.78 dB, and 10.8 dB, respectively, according to Eqs. (3.2), (3.4), (3.5), and (3.6), which are all over the threshold 4.58 dB. Hence, for multiple-FEC configuration, the revenue is 3.7.

From the example, we see that the revenues can be improved by using multiple-FEC configuration. The traffic provisioning is composed by routing, MF, FEC, and spectrum assignment.

3.4 MILP formulation

In this section, we formulate the revenue maximization problem as a MILP, named as RMAX. The parameters and variables of the MILP are summarized in Table 3.2.

To provision the lightpaths, both *network flow constraints* and *spectrum assignment constraints* must be taken into account. Besides, *SNR constraints* are also considered to ensure lightpaths' QoT. Thus, the problem is modeled as follows,

$$\max \quad \sum_{i \in D} (\eta_i B_i - \epsilon_1 t_i^{\text{PLI}}) \quad \textbf{(RMAX)}$$

s.t. Constraints (3.9)-(3.11).

The main objective of this MILP is to maximize the total revenue and the second objective is to minimize the total PLIs for all requests. The second objective can reduce the PLIs and improve the SNR margin of network, which is regarded as an indirect way that can be used to guarantee the revenue performance[100]. The weighted factor ϵ_1 is used to balance the importance between revenue and PLIs. For the sake of readability, we use $\forall i, \forall v, \forall uv, \forall c$ to denote $\forall i \in D, \forall v \in V, \forall uv \in E, \forall c \in \mathcal{C}$ in the following text.

Network flow constraints

$$q_v^i = \sum_{u \in N(v)} x_{uv}^i \qquad \forall i, \forall v \qquad (3.9a)$$

$$p_v^i = \sum_{u \in N(v)} x_{vu}^i \qquad \forall i, \forall v \qquad (3.9b)$$

$$p_v^i - q_v^i = \begin{cases} B_i, & v = s_i \\ -B_i, & v = d_i \\ 0, & \text{others.} \end{cases} \qquad \forall i, \forall v \qquad (3.9c)$$

Table 3.2: *Parameters And Variables in RMAX*

Network Sets and Parameters	
V, E	Node set and link set of the FON G.
$uv \in E$	A link from node u to v.
$s_i, d_i \in V$	Source and destination node of request i.
L_{uv}	Number of spans on link uv.
$F \in \mathbb{R}_{\geq 0}$	Available spectrum resources of an optical fiber.
$N(v)$	Adjacent node set of v in G.
D	Traffic demand matrix.
$i, j \in D$	Any two requests i and j in traffic demand matrix D.
r_i	Required bit-rate (Gbps) of request i.
η_i	Revenue of request i.
$c \in \mathcal{C}$	Transmission mode in candidate transmission mode set $\mathcal{C}$.
θ	A large constant.
ϵ_1	A factor balancing the importance between revenue and PLIs.
o_k^1, o_k^0	Coefficients of piece-wise linear fitting function for fitting the XCI, $k \in \{1, 2, ..., Q\}$, where Q is the number of segments.
Variables in RMAX	
$B_i \in \{0, 1\}$	Equals 1 if request i is accepted, 0 otherwise.
$q_v^i \in \{0, 1\}$	Equals 1 if request i goes into node v, 0 otherwise.
$p_v^i \in \{0, 1\}$	Equals 1 if request i goes out of node v, 0 otherwise.
$x_{uv}^i \in \{0, 1\}$	Equals 1 if request i uses link uv, 0 otherwise.
$x_{uv,c}^i \in \{0, 1\}$	Equals 1 if request i uses link uv and transmission mode c, 0 otherwise.
$m_c^i \in \{0, 1\}$	Equals 1 if request i uses transmission mode c, 0 otherwise.
$f_i \in [0, F]$	Center frequency of request i.
$f_{ij} \in [0, F]$	Center frequency difference between requests i and j.
$\Delta f_i \in [0, F]$	Bandwidth of request i.
$\Delta f_{ij} \in [0, F]$	Overlapping bandwidth between i and j.
$f_{ij}^X \in [0, F]$	Auxiliary variable of overlapping bandwidth Δf_{ij}.
$w_{ij} \in \{0, 1\}$	Equals 1 if f_i is greater than f_j, 0 otherwise.
$t_i^{\text{ASE}} \in \mathbb{R}_{\geq 0}$	PLI of ASE noise of request i, G_i^{ASE}/G_i.
$t_i^{\text{SCI}} \in \mathbb{R}_{\geq 0}$	PLI of SCI of request i, G_i^{SCI}/G_i.
$t_{ij,u}^{\text{XCI}} \in \mathbb{R}_{\geq 0}$	Accumulated PLI of XCI of request i from source node s_i to u that is generated by request j.
$t_{ij,v}^{\text{AD}} \in \mathbb{R}_{\geq 0}$	Accumulated PLI of AD node crosstalk of request i from source node s_i to node v that is generated by request j.
h_c^{ij}	Piece-wise linear fitting term for XCI from j to i if j takes transmission mode c.
$t_i^{\text{PLI}} \in \mathbb{R}_{\geq 0}$	Total PLIs of request i.

Constraints (3.9a) and (3.9b) determine the incoming and outgoing flow of request i at node v. For any request i, the incoming degree q_v^i counts 1 if request i passes through or drops at node v. Also, for any request i, the outgoing degree p_v^i counts 1 if request i is added at or passes through node v. We will see that, with the help of q_v^i and p_v^i, we can calculate the node crosstalk and other PLIs node-by-node. Constraints (3.9c) are the flow conservation constraints. If a request i gets accepted (B_i=1), there exists a lightpath from the source node s_i to the destination node d_i.

Spectrum assignment constraints

$$\sum_{c\in\mathcal{C}} m_c^i = B_i \qquad \forall i \qquad \text{(3.10a)}$$

$$\Delta f_i \geq \sum_{c\in\mathcal{C}} \frac{r_i}{\mathrm{SE}(c)} m_c^i \qquad \forall i \qquad \text{(3.10b)}$$

$$w_{ij} + w_{ji} = 1 \qquad \forall i < j \qquad \text{(3.10c)}$$

$$\left.\begin{array}{l} f_i + \Delta f_i/2 \leq F \\ 0 \leq f_i - \Delta f_i/2 \end{array}\right\} \qquad \forall i \qquad \text{(3.10d)}$$

$$\left.\begin{array}{l} f_{ij} \leq f_i - f_j + 2F(1-w_{ij}) \\ f_i - f_j \leq f_{ij} \end{array}\right\} \qquad \forall i < j \qquad \text{(3.10e)}$$

$$\Delta f_{ij} \geq \min\left(\Delta f_i, \Delta f_j, f_{ij}^X\right) \qquad \forall i < j \qquad \text{(3.10f)}$$

$$\Delta f_{ij} \leq F(2 - x_{uv}^i - x_{uv}^j) \qquad \forall uv, \forall i < j \qquad \text{(3.10g)}$$

$$\left.\begin{array}{l} \Delta f_{ij} = \Delta f_{ji} \\ f_{ij} = f_{ji} \end{array}\right\} \qquad \forall i < j \qquad \text{(3.10h)}$$

Constraints (3.10a) select one transmission mode for non-blocked request i (if $B_i = 1$). Constraints (3.10b) define the bandwidth of request i by its bit-rate and the adopted transmission mode. Constraints (3.10c) assure that either w_{ij} or w_{ji} should be equal to 1. Constraints (3.10d) limit the fiber spectrum within $[0, F]$. Constraints (3.10e) calculate the frequency difference f_{ij} between i and j. Constraints (3.10f) calculate the overlapping bandwidth Δf_{ij}. As it is not linear, we replace it by the following equations,

$$\Delta f_{ij} \geq \min\left(\Delta f_i, \Delta f_j, f_{ij}^X\right)$$

$$\Leftarrow \begin{cases} \Delta f_i - F a_{ij}^1 \leq \Delta f_{ij} \\ \Delta f_j - F a_{ij}^2 \leq \Delta f_{ij} \\ f_{ij}^X - F a_{ij}^3 \leq \Delta f_{ij} \\ 0 \leq f_{ij}^X \\ \dfrac{\Delta f_i + \Delta f_j}{2} - f_{ij} \leq f_{ij}^X \\ f_{ij}^X = f_{ji}^X \\ a_{ij}^1 + a_{ij}^2 + a_{ij}^3 = 2 \\ a_{ij}^1, a_{ij}^2, a_{ij}^3 \in \{0,1\} \end{cases} \qquad \forall i < j$$

Constraints (3.10g) are spectrum non-overlapping constraints, indicating that when i and j share a common link, the overlapping bandwidth Δf_{ij} on that link must be 0. Constraints (3.10h) guarantee that both variables Δf_{ij} and f_{ij} are symmetric.

SNR constraints

$$t_i^{\mathrm{ASE}} = \sum_{uv} \frac{G_i^{\mathrm{ASE}}}{G_i} L_{uv} x_{uv}^i \qquad \forall i \tag{3.11a}$$

$$t_i^{\mathrm{SCI}} = \sum_{uv} \sum_{c} \mu G_i^2 L_{uv} \mathrm{arcsinh}\left(\rho \left(\frac{r_i}{\mathrm{SE}(c)}\right)^2\right) x_{uv,c}^i \quad \forall i \tag{3.11b}$$

$$x_{uv,c}^i + 1 \geq x_{uv}^i + m_c^i \qquad \forall i, \forall c, \forall uv \tag{3.11c}$$

$$t_{ij,v}^{\mathrm{XCI}} - t_{ij,u}^{\mathrm{XCI}} + \theta(2 - x_{uv}^i - x_{uv,c}^j) \geq \mu G_j^2 h_c^{ij} L_{uv} \qquad \forall uv, \forall i \neq j, \forall c \tag{3.11d}$$

$$t_{ij,v}^{\mathrm{XCI}} - t_{ij,u}^{\mathrm{XCI}} + \theta(1 - x_{uv}^i) \geq 0 \qquad \forall uv, \forall i \neq j \tag{3.11e}$$

$$t_{ij,v}^{\mathrm{AD}} + \theta(3 - p_v^i - q_v^j - m_c^j) \geq \epsilon_X (\Delta f_{ij} G_j) / (r_i / \mathrm{SE}(c) G_i) \qquad \forall c, \forall i \neq j, \forall v \tag{3.11f}$$

$$t_i^{\mathrm{PLI}} \geq t_i^{\mathrm{ASE}} + t_i^{\mathrm{SCI}} + \sum_{j \neq i} t_{ij,d_i}^{\mathrm{XCI}} + \sum_{j \neq i} t_{ij,d_i}^{\mathrm{AD}} \qquad \forall i \tag{3.11g}$$

$$t_i^{\mathrm{PLI}} \leq \sum_{c \in \mathcal{C}} \frac{m_c^i}{\mathrm{SNR}_c^{\mathrm{th}}}, \qquad \forall i. \tag{3.11h}$$

Constraints (3.11a) calculate PLI of ASE noise on the lightpath. Also, it is applied on the SCI calculation in constraints (3.11b). Whether request i uses link uv and transmission mode c is assured by the constraints (3.11c).

Since XCI is caused by two lightpaths, it will increase along with their sharing links, and non-decrease along with the other links. The nonlinear interference XCI, here, is the interaction between two lightpaths. The multi-channel interference (MCI, sometimes called as Four-wave Mixing or FWM) caused by multiple lightpaths is neglected for its minor impact on NLI (less than 1% reported in [66, 96]) but additional difficulty in modelling. Therefore, we only consider the XCI and exclude the MCI here. Constraints (3.11d) and (3.11e) implement the XCI calculation, respectively. But the nonlinear expression between XCI and f_i in Eq. (3.6) makes a nonlinear calculation term h_c^{ij}. To address this issue, we replace the nonlinear term h_c^{ij} by the following linear approximation $\hat{h}_c^{ij}$,

$$\begin{aligned} & h_c^{ij}\left(2\frac{|f_i - f_j|}{\Delta f_j}\right) \geq \ln\left(\frac{2|f_i - f_j|/\Delta f_j + 1}{2|f_i - f_j|/\Delta f_j - 1}\right) \\ \Leftarrow & \hat{h}_c^{ij}(x) \geq \max_{1 \leq k \leq Q} \left(o_1^1 x + o_1^0, \cdots, o_k^1 x + o_k^0, \cdots, o_Q^1 x + o_Q^0\right) \\ \Leftarrow & \hat{h}_c^{ij} \geq o_k^1 (2\mathrm{SE}(c) f_{ij} / r_j) + o_k^0 \qquad \forall i \neq j, \forall c, 1 \leq k \leq Q \end{aligned} \tag{3.12}$$

where o_k^1 and o_k^0 are the coefficients solved by piece-wise linear fitting (see Appendix A). We use the least-square algorithm in [83] to fit the convex function $\ln\left(\frac{x+1}{x-1}\right)$ in the domain $x \in [x_1, x_2]$, where we set x_1=1.001, x_2=200, and Q=20. The fitting error $(\hat{h}_c^{ij} - h_c^{ij})/h_c^{ij}$ can be minimized by increasing the number of segments Q. As shown in Fig. 3.4, the maximum fitting error is less than 5%.

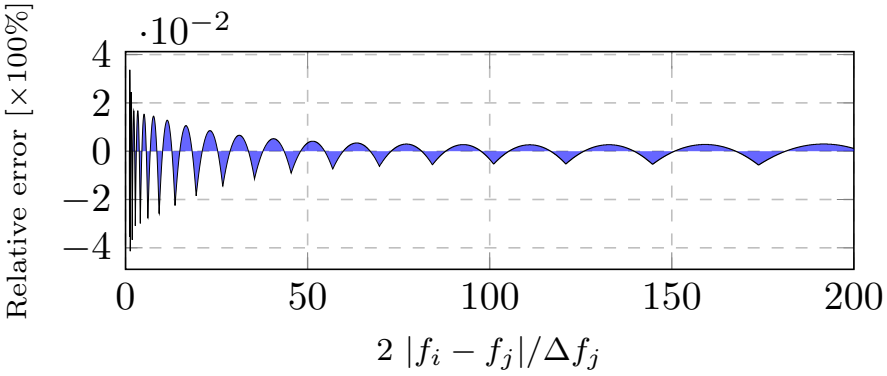

Figure 3.4: *Illustration for the piece-wise linear fitting performance,* $(\hat{h}_c^{ij} - h_c^{ij})/h_c^{ij}$ *versus* $2|f_i - f_j|/\Delta f_j$*, Q=20.*

Constraints (3.11f) calculate the node crosstalk along the lightpath, which is implemented by emphasizing the incoming degree q_v^j of crosstalk signal j and the outgoing degree p_v^i of primary signal i. Constraints (3.11g) calculate the total PLIs of all traversed links and nodes. Constraints (3.11h) represent the QoT formulation. The MILP is NP hard and time-consuming[30]. Considering the scalability limitations of MILP, we also design a heuristic algorithm to solve the revenue maximization problem with lower complexity.

3.5 Heuristic algorithm

In this section, we design a decomposition algorithm (DEC-ALG) to solve (a) the problem of routing, MF, and FEC assignment, and (b) the problem of spectrum assignment, separately. In addition, we also present a heuristic as benchmark, which is adapted from existing literature.

3.5.1 DEC-ALG

DEC-ALG algorithm consists of two phases: (a) Routing and transmission mode assignment (RTMA); (b) Spectrum assignment (SA). The related parameters and variables are explained in Table 3.3.

Table 3.3: *Parameters & Variables in algorithm DEC-ALG*

Network sets & Parameters	
$\phi \in [0,1]$	A ratio on SNR threshold considering ASE+SCI. $1-\phi$ represents the part considering XCI+AD.
P_i	Route and transmission mode pairs set (ξ, c) of request i.
P_{ie}	Route and transmission mode pairs set (ξ, c) of request i that traverses link e.
$V_{i\xi}$	Node set on the ξ-th route of request i.
ϵ_2	Factors adjusting the weight of rest SNR margin.
b_i, e_i	Spectrum beginning and end of request i.
$\phi_{i\xi c} \in \mathbb{R}$	SNR margin of request ξ using transmission mode c and ξ-th route after RTMA.
Δf_{ic}	Bandwidth of request i using transmission mode c.
N_{RTMA}	Number of RTMA_{opt} solutions.
N_{round}	Number of attempts in the spectrum assignment.
Variables	
$B_i \in \{0,1\}$	Equals 1 if request i is accepted, 0 otherwise.
$g_{i\xi c} \in \{0,1\}$	Equals 1 if request i uses the ξ-th route and transmission mode c, 0 otherwise.
ϕ_{avg}	Average SNR margin of all requests.

Step 1: Pre-calculation process

We pre-calculate route and transmission mode pairs for each request. Candidate routes are obtained by the K shortest path algorithm[141], while transmission modes are from $\mathcal{C}$.

For any request i, the tuple (ξ_i, c_i) denotes a route and transmission mode pair. The ASE and SCI are the known impairments for a given (ξ_i, c_i), which are obtained by Eqs. (3.4) and (3.5). However, the node crosstalk and XCI can not be determined because they are related with the exact spectrum channel of all lightpaths. Thus, some route and transmission mode pairs may experience strong PLIs, thus the QoT cannot be satisfied in the subsequent process. Therefore, we choose the route and transmission mode pair (ξ, c) based on the residual SNR margin $\phi_{i\xi c}$ as follows,

$$\phi_{i\xi c} = \frac{\phi}{\text{SNR}_c^{\text{th}}} - t_i^{\text{ASE}} - t_i^{\text{SCI}} - \epsilon_{\text{X}} \sum_{v \in V_{i\xi}} \frac{N(v)+1}{2} \tag{3.13}$$

where ϕ is an estimated ratio considering the ASE and SCI.

Step 2: RTMA

In RTMA, each request can choose one route and transmission mode pair (ξ, c). For all requests, one assignment of the route and transmission mode pair, named as RTMA_{opt},

is solved by the following RTMA model,

$$\max \quad \sum_{i \in D} \eta_i B_i + \epsilon_2 \phi_{\text{avg}} \quad \textbf{(RTMA)}$$

$$\textbf{s.t.} \sum_{(\xi,c) \in P_i} g_{i\xi c} = B_i \qquad \forall i \tag{3.14a}$$

$$\sum_{i \in D} \sum_{(\xi,c) \in P_{ie}} \Delta f_{ic} g_{i\xi c} \leq F \qquad \forall e \tag{3.14b}$$

$$0 \leq \sum_{(\xi,c) \in P_i} g_{i\xi c} \phi_{i\xi c}, \qquad \forall i \tag{3.14c}$$

$$\phi_{\text{avg}} = \frac{1}{|D|} \sum_{i \in D} \sum_{(\xi,c) \in P_i} g_{i\xi c} \phi_{i\xi c} \tag{3.14d}$$

The main objective of RTMA is to maximize the accepted revenue and the second one is to maximize average SNR margin. The multi-objective function can be adjusted by a weighting factor ϵ_2. Constraints (3.14a) make sure that a route and transmission mode pair (ξ, c) is chosen for request i if B_i=1. Constraints (3.14b) restrict the spectrum usage of each link. Bandwidth requirement of i with the transmission mode c has been pre-calculated and denoted by Δf_{ic}. Constraints (3.14c) make sure that the minimum SNR margin is non-negative. Constraint (3.14d) defines the average SNR margin of all requests.

In RTMA, only one RTMA_{opt} solution is obtained. However, this solution may not bring the maximum revenue after spectrum assignment. To this end, we intend to generate N_{RTMA} solutions. The n-th solution is generated by adding constraints (3.15) to RTMA, which is used for excluding the previous RTMA_{opt}. In constraints (3.15), both B_i^{n-1} and $g_{i\xi c}^{n-1}$ are the results from $(n-1)$-th solution.

$$\begin{aligned} &\sum_{\substack{i \in D \\ B_i^{n-1}=1}} \sum_{\substack{(\xi,c) \in P_i \\ g_{i\xi c}^{n-1}=1}} g_{i\xi c} + \frac{1}{K * |\mathcal{C}|} \sum_{\substack{i \in D \\ B_i^{n-1}=0}} \sum_{\substack{(\xi,c) \in P_i \\ g_{i\xi c}^{n-1}=0}} (1 - g_{i\xi c}) \\ &\leq |D| - \frac{1}{K * |\mathcal{C}|}, n \in \{1, 2, 3, \cdots, N_{RTMA}\} \end{aligned} \tag{3.15}$$

Explanation of excluding constraints (3.15) : In the n-th loop, we suppose that $\forall i, (\xi, c)$, the variable $g_{i\xi c} = g_{i\xi c}^{n-1}$, then the value of the left side in constraints (3.15) becomes $|D|$, which is larger than the right. Therefore, we can say that constraints (3.15) hold if $\exists i, (\xi, c), g_{i\xi c} \neq g_{i\xi c}^{n-1}$. Let us focus on the request i that satisfies $g_{i\xi c} \neq g_{i\xi c}^{n-1}$. Since constraints (3.14a) require $\sum_{(\xi,c)} g_{i\xi c}^{n-1} = B_i^{n-1} \leq 1$, we discuss the case $B_i^{n-1} = 1$ and $B_i^{n-1} = 0$, respectively.

- If $B_i^{n-1} = \sum_{(\xi,c)} g_{i\xi c}^{n-1} = 1$ holds,

$$\left.\begin{aligned} B_i^{n-1} = \sum_{(\xi,c)} g_{i\xi c}^{n-1} = 1 \\ \exists(\xi,c), g_{i\xi c} \neq g_{i\xi c}^{n-1} \\ \sum_{(\xi,c)} g_{i\xi c} \leq 1 \end{aligned}\right\} \Rightarrow \sum_{\substack{(\xi,c)\in P_i \\ g_{i\xi c}^{n-1}=1}} g_{i\xi c} = 0 \tag{3.16}$$

- Otherwise $B_i^{n-1} = \sum_{(\xi,c)} g_{i\xi c}^{n-1} = 0$ holds, then we can get the result $\frac{1}{K*|\mathcal{C}|} \sum_{\substack{(\xi,c)\in P_i \\ g_{i\xi c}^{n-1}=0}} (1 - g_{i\xi c}) = \frac{K*|\mathcal{C}|-1}{K*|\mathcal{C}|} < 1$ with the following proof,

$$\left.\begin{aligned} B_i^{n-1} = \sum_{(\xi,c)} g_{i\xi c}^{n-1} = 0 \\ \exists(\xi,c), g_{i\xi c} \neq g_{i\xi c}^{n-1} \\ \sum_{(\xi,c)} g_{i\xi c} \leq 1 \end{aligned}\right\} \Rightarrow \begin{cases} \sum_{\substack{(\xi,c)\in P_i \\ g_{i\xi c}^{n-1}=0}} g_{i\xi c} = 1 \\ \sum_{\substack{(\xi,c)\in P_i \\ g_{i\xi c}^{n-1}=0}} (1 - g_{i\xi c}) = K*|\mathcal{C}| - 1 \end{cases} \tag{3.17}$$

In addition, for the request i that satisfies $\forall(\xi,c), g_{i\xi c} = g_{i\xi c}^{n-1}$, the first item of left sides still equals 1. The number is denoted by n_1, $n_1 \leq |D| - 1$. Thus, we can get $0 \cdot n_{(3.16)} + 1 \cdot n_1 + (1 - 1/K/|\mathcal{C}|) \cdot n_{(3.17)} \leq |D| - 1/K/|\mathcal{C}|$, where $n_{(3.16)}$ and $n_{(3.17)}$ are the number of requests satisfying (3.16) and (3.17), respectively, and $n_{(3.16)} + n_1 + n_{(3.17)} = |D|$. Therefore, the left side of constraints (3.15) must be no bigger than $|D| - \frac{1}{K \cdot |\mathcal{C}|}$.

The pseudocode in Algorithm 3.1 illustrates the procedure of generating N_{RTMA} solutions by RTMA. In line 1, the model is initialized with the constraints (3.14) and the input parameters $G(V,E)$, D, N_{RTMA}, and $\mathcal{C}$. In line 2, RTMA_{opt} solution with $g_{i\xi c} = 0$ is initialized. Then, from lines 3 to 5, the RTMA model is repeated to get N_{RTMA} solutions.

Step 3: SA

Once the RTMA problem is solved, from the solution RTMA_{opt}, we can obtain the pair index of route and transmission mode used for each request i, *i.e.*, $(\bar{\xi}_i, \bar{c}_i) = \{(\xi,c) | g_{i\xi c} = 1, i \in D\}$.

When assigning the spectrum interval on the determined route for each request, SA needs to take into account both spectrum continuity and spectrum contiguity constraints. To reduce the impact of XCI, we also set a guard band Δ=12.5 GHz. If the request is accepted, a specific lightpath with its spectrum interval will be allocated. Otherwise, it will move the spectrum interval when necessary until it is out of the fiber

Algorithm 3.1: RTMA: generating N_{RTMA} solutions

Input : G(V, E), D, N_{RTMA}, $\mathcal{C}$
Output: $\boldsymbol{g}^{N_{RTMA}}$

1 Create the RTMA model with the constraints in (3.14) and the input parameters G(V,E), D, N, and $\mathcal{C}$;
2 $g^0_{i\xi c} \leftarrow 0, \forall i, (\xi, c)$ // $g^0_{i\xi c} \in \boldsymbol{g^0}$
3 **for** $n \in \{1, 2, ..., N_{RTMA}\}$ **do**
4 Update the RTMA model with excluding constraints (3.15) and previous solution $\boldsymbol{g^{n-1}}$;
5 Get the RTMA_{opt} solution $\boldsymbol{g^n}$ by solving RTMA model;
6 **end**

spectrum. An new incoming request can be blocked if it affects the QoT of other requests. To ensure the blocked requests can be accepted again, we repeat the assignment process N_{round} times. For the request in each round, the SNR threshold is designed to decrease gradually, and equals to the SNR threshold of transmission mode c in the final round.

The SA procedure is illustrated in Algorithm 3.2. In line 1, we sort the requests in D by function ARRANGE, which will be explained later. Then, in lines 5 and 6, the required spectrum bandwidth and route can be both found from the RTMA result RTMA_{opt}. In line 7, we merge the available spectrum of the ξ-th route and assign it to $MERGED_{\text{space}}$, where both spectrum continuity and spectrum contiguity constraint are satisfied. Then, from lines 8 to 16, the algorithm SA tries to search a spectrum interval $[b_i, b_i + \Delta f_i]$ from $MERGED_{\text{space}}$ that satisfies the QoT.

In the ARRANGE function of Algorithm 3.2, we sort the requests in D by four different assignment polices, *random order* Δf_i (SA), descending order of *bandwidth* Δf_i (SA-B), *revenue* η_i (SA-R), and *revenue to bandwidth ratio* $\eta_i / \Delta f_i$ (SA-RA), respectively. The performances of these four arrangement policies are compared in simulations.

Summaries : DEC-ALG

It is worth mentioning that the size of RTMA_{opt} solution space can reach $(K \cdot |\mathcal{C}| + 1)^{|D|}$. With small N_{RTMA}, *i.e.*, $N_{RTMA} \ll (K \cdot |\mathcal{C}| + 1)^{|D|}$, the potential RTMA_{opt} solution that provides the maximum revenue may not be included. In addition, the solution space of RTMA is determined by the number of routes K, the size of candidate transmission mode $\mathcal{C}$ and demand D. It may happen that we get the identical result even with different configurations $\mathcal{C}'$ or different demand matrix D'.

To solve the problem caused by different transmission mode configurations $\mathcal{C}$, we use a perturbation strategy to extend RTMA_{opt} solutions by its subset, $\mathcal{C}_l^{sub}$, $1 \leq l \leq |\mathcal{C}|$. Each subset takes l elements from $\mathcal{C}$. For the l-th subset $\mathcal{C}_l^{sub}$, the l-th transmission mode of $\mathcal{C}$ is added compared to the previous $l-1$ subsets. Constraints (3.18) are used to generate RTMA_{opt} for the subset $\mathcal{C}_l^{sub}$ that forces the use of transmission mode c^l but

Algorithm 3.2: SA : Spectrum Assignment

Input : $\boldsymbol{g}$
Output: $\boldsymbol{alloc}$

$D_{\text{arr}} \leftarrow$ **ARRANGE**(D);
$\boldsymbol{alloc} \leftarrow \mathbf{0}$ // $alloc_i \in \boldsymbol{alloc}$;
for $n_{round} \in [0, 1, ..., N_{ROUND}]$ **do**
  for $i \in D_{arr}$ & $alloc_i$==0 **do**
    $(\bar{\xi}_i, \bar{c}_i) \leftarrow \{(\xi, c) | g_{i\xi c} = 1\}$ // $g_{i\xi c} \in \boldsymbol{g}$;
    $\Delta f_i \leftarrow r_i / \text{SE}(\bar{c}_i)$;
    $\text{MERGED}_{\text{space}} \leftarrow$ available spectrum space on $\bar{\xi}_i$-th route;
    for the spectrum beginning b_i: 0→F, with step Δ=12.5 GHz & $alloc_i$==0 **do**
      if $[b_i, b_i + \Delta f_i] \in \text{MERGED}_{\text{space}}$ **then**
        try :
          Assign $[b_i, b_i + \Delta f_i]$ on $\bar{\xi}_i$-th route;
          Check QoT of assigned requests by Eq. (3.3);
          Check QoT of current request i by Eq. (3.3);
          $alloc_i \leftarrow 1$;
        catch *Check failed*:
          $alloc_i \leftarrow 0$;
        end
      end
    end
  end
end

excludes the use of the other transmission modes c^r.

$$\sum_{i \in D, 1 \le \xi \le K} g_{i\xi c^l} \ge 1 \tag{3.18a}$$

$$\sum_{i \in D, 1 \le \xi \le K} g_{i\xi c^r} = 0, \forall c^r \in \mathcal{C} \backslash \mathcal{C}_l^{sub} \tag{3.18b}$$

We give the pseudocode of DEC-ALG as illustrated in Algorithm 3.3. In line 2, we initialize the candidate transmission sets $\mathcal{C}_l^{sub}$. From lines 3 to 7, we conduct the algorithm RTMA and SA to obtain the optimal result. Finally, the maximum revenue MAXOBJ is saved.

3.5.2 Benchmark algorithm

To efficiently utilize the spectrum resource of fiber, a large number of algorithms on traffic provisioning have been proposed[139, 149]. To make a fair comparison, we take the algorithm in [139] that also adopts the continuous spectrum allocation. The benchmark algorithm, called as REF-A in this study, is implemented by using the same objective function of RTMA in Eq. (3.14) and restricting the fiber spectrum resources. It should

Algorithm 3.3: DEC-ALG

Input : $G(V, E), D, N_{RTMA}, \mathcal{C}$
Output: MAXOBJ

MAXOBJ $\leftarrow 0$;
for $c^l \in \mathcal{C}$ **do**
  Initialize the current transmission mode set $\mathcal{C}_l^{sub}$;
  Use RTMA model to generate $\text{RTMA}_{\text{opt}}(G, D, N_{RTMA}, \mathcal{C})$ solutions, with constraints (3.18) emphasizing the lock transmission mode c^l;
  for $n \in \{0, 1, ..., N_{RTMA}\}$ **do**
    $\boldsymbol{alloc} \leftarrow \text{SA}(\boldsymbol{g}^n)$ // $\text{alloc}_i \in \boldsymbol{alloc}$
    $\text{Obj} \leftarrow \sum_i \text{alloc}_i{}^*\eta_i$;
    MAXOBJ$\leftarrow$max(Obj, MAXOBJ);
  end
end

be also noted that, the spectrum assignment of REF-A is implemented by passing the solution of RTMA to RMAX.

3.6 Illustrative numerical results

In this section, we present the numerical experiment results. First, we compare the efficiency of our proposed heuristic and the MILP model. Then, we investigate revenues in scenarios with different PSDs and different transmission modes. Finally, we consider the experiments for severe resource crunch, which is simulated by increasing bit-rate and number of requests.

The MILP, heuristic algorithm DEC-ALG, and REF-A run on an Intel Core PC with 4.0 GHz CPU and 16 GB RAM. Specifically, we solved the MILP model by CPLEX 12.6 and implemented the two heuristic algorithms using an ad-hoc code developed in C++. Maximum computing time for the MILP was fixed to one hour. All illustration results have been averaged over 10 independent simulation runs to guarantee statistical accuracy.

The 6-node network in Fig. 3.3, NSFNET (14 nodes, 44 links) [68], and US Backbone network (28 nodes, 90 links)[68] are used as case study topologies (note that, since the path length of NSF network and US Backbone network cannot support high-order MF, we divide the length of link by 6 in the simulations). The spectrum resource of each fiber F is assumed with 1,000 GHz to increase the simulation speed for large networks. The fiber parameters α, β_2, and γ are from Table 3.1. The algorithm parameter ϵ_1=0.01 and ϵ_2=0.001 are adjusted to be small to emphasize the revenue rather than the other parameters for simulation. The parameters N_{RTMA}=40, N_{round}=2, and K=4 are adjusted to guarantee stable good simulation results in a reasonable time. The bit-rates r_i are randomly chosen from the set {250, 500, ... , 250+n*250, ... 250+2n*250} Gbps. For

the lowest bit-rate, the channel can be guaranteed with bandwidth over than 28 GHz with PM-16QAM[139], which is acceptable for the GN model in [66]. The large bit-rate request is assumed by super-channel with large baud rates. The initial launch power PSD for all lightpaths is simplified with -16 dBm/GHz by using the LOGON strategy [97] for one span with the heaviest spectral loads. The definition of revenue and other used notations for simulation are given as follows,

1. *Revenue*: $\eta_i = u_i$, where u_i is the service type parameter. In this study, we consider the service type parameter u_i follows the Zipf distribution Zipf(1,5)[152]. The revenue of a network is sum of all accepted lightpaths' revenue.
2. *Adaptive MFs* : $\mathcal{C} = (\hat{\mathcal{M}}_m, \mathcal{F}_f)$. Notation $\mathcal{F}_f$ represents one f-th level FEC, and $\hat{\mathcal{M}}_m$ represents all the MFs not beyond the m-th order.
3. *Multiple FECs*: $\mathcal{C} = (\mathcal{M}_m, \hat{\mathcal{F}}_f)$. Notation $\mathcal{M}_m$ represents the m-th order MF, and $\hat{\mathcal{F}}_f$ represents the FEC OHs not beyond the f-th one.

3.6.1 Validation using MILP

We validate the MILP on the 6-node network. The bit-rate per request is fixed at 1,000 Gbps. Figure 3.5 illustrates the revenue and computational time of three algorithms as the number of request increases.

In Fig. 3.5, we can observe that the computational time of MILP reaches the preset maximum computing time one hour, when the number of requests increases to 33. It means that MILP is intractable even in the case with either small networks or small number of requests. But the heuristic algorithm REF-A and DEC-ALG can solve it in a few minutes and a few seconds, respectively. Besides, we observe that both DEC-ALG and REF-A are able to obtain an approximate optimal value of MILP. Therefore, the proposed algorithm DEC-ALG is not only time-efficient but also near-optimal.

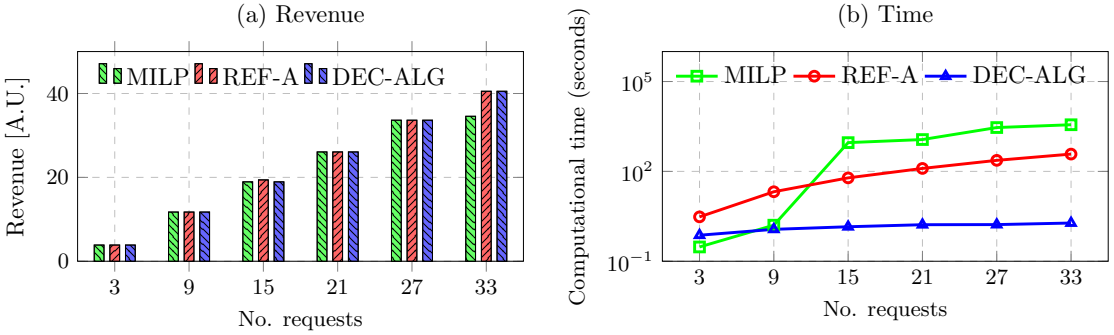

Figure 3.5: *Comparison of revenue and computational time in 6-node network.*

In the SA of DEC-ALG algorithm, we have mentioned four different sorting policies in the ARRANGE function. In order to find the best sorting policy, we compared their results in Fig. 3.6. The simulation is carried out in NSF network. As we see in Fig. 3.6, the revenue with different sorting policies increases with the number of requests. It can be also seen that SA-RA, which sorts the requests by the descending order of

revenue/bandwidth ratio, gets the largest revenue. Therefore, we confirm to use SA-RA for heuristic algorithm DEC-ALG.

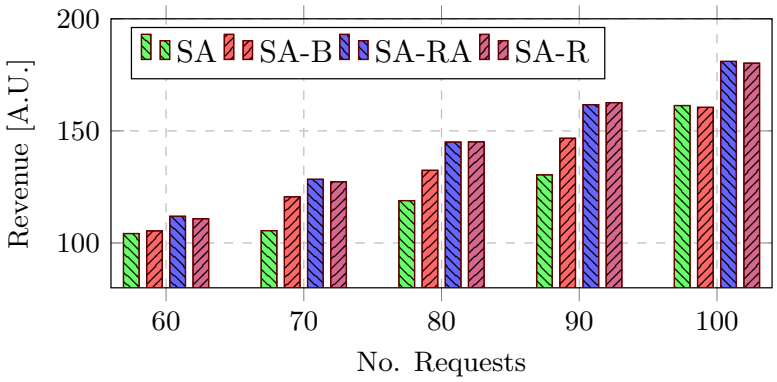

Figure 3.6: *Revenue comparison with four different sorting policies of ARRANGE function.*

3.6.2 Impacts of PSD, MF and FEC

As we have seen in the example of Fig. 3.3, revenues can be influenced by SNR requirements of different transmission mode configurations. In Eqs. (3.3), (3.4) and (3.5), when PSD G_i increases, the noise to signal ratio of ASE, t_i^{ASE} will decrease inversely, while the t_i^{SCI} and t_i^{XCI} will increase quadratically. The PSD of ASE noise, SCI, and XCI, as well as the SNR for a 250 Gbps request with PM-QPSK$_{7\%}$ in the middle of a fully occupied fiber span are illustrated in Fig. 3.7. According to the SNR and PSD, we briefly distinguish three different scenarios, namely scenario 1: *low SNR with low PSD*, scenario 2: *high SNR with median PSD*, and scenario 3: *low SNR with high PSD*. By adjusting PSDs, we can investigate the revenue impact of MF and FEC in different SNR scenarios.

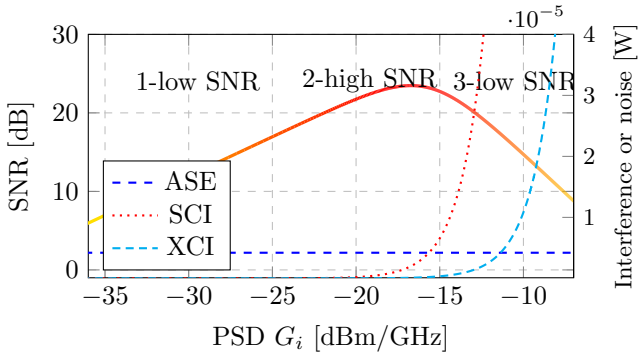

Figure 3.7: *SNR vs. PSD G_i.*

First, we fix FEC OH at 7% and compare different MFs as PSD varies. The simulation results of NSF network using 100 requests and 1,000 Gbps per request are illustrated in Fig. 3.8. It is observed in Fig. 3.8.(a) that the revenue of different MFs increases as PSD changes from scenario 1 to 2, but then decreases from scenario 2 to 3. Both adaptive MF $\hat{\mathcal{M}}_3$ and $\hat{\mathcal{M}}_4$ that contain MFs {BPSK,QPSK,8QAM} get the largest revenue in scenario

2, with 118% improvement compared to $\hat{\mathcal{M}}_1$. It can be explained by the SNR threshold and spectral efficiency of different MFs. Only in the scenario with high SNR, high-order MFs can be adopted, which reduces the spectrum usage and spares more spectrum resources for other requests. However, in the scenario with low SNR, the adaptive method with four MFs has no difference with either one MF or two MFs, because the high-order MF cannot be adopted.

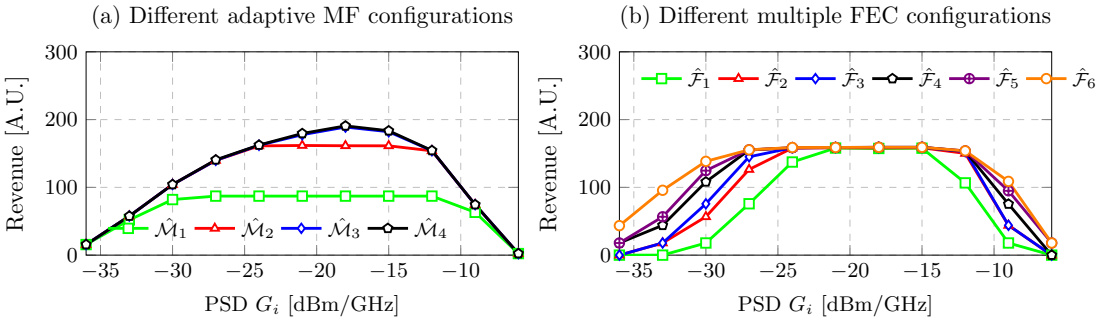

Figure 3.8: *Impact of PSD.*

Then, we fix MF at QPSK and compare multiple FECs. The results are illustrated in Fig. 3.8.(b), where we can see that, also in this case, as PSD changes from scenario 1 to 2, the revenue of different FEC increases, while from scenario 2 to 3, the revenue decreases. Different from the adaptive MF, having multiple FEC choices has a tiny impact on revenue difference on scenario 2, while a bigger difference is only observed for both scenarios 1 and 3, which is a different result with respect to adaptive MF. In low SNR scenario, most lightpaths with small FEC OHs are blocked, while the redundant FEC with large FEC OHs can lower the SNR requirement and provide more SNR margins to overcome the PLIs. But in high SNR scenario, many requests have adopted the transmission mode f_1 with the highest spectral efficiency. Therefore, no revenue improvement can be observed in this scenario.

Figures 3.8.(a) and 3.8.(b) indicate that adaptive MF brings more revenue in high SNR with median PSD, while multiple FECs configuration brings more revenue in low SNR scenarios. As we introduce more MFs and FEC, the high-order MF will mitigate the resource crunch and the low-spectral efficiency FEC with large OH can mitigate the PLIs.

Given suitable PSD scenario of multiple FECs and adaptive MF, we further investigate the impact of joint MF and FEC schemes in NSF and US Backbone network. The revenues of 100 requests with average bit-rate 1,000 Gbps are illustrated in Fig. 3.9. In high SNR scenario with median PSD (G_i =-18 dBm/GHz), we find that the adaptive MFs enable to improve the revenue, while the configuration of multiple FECs has weak impact on the revenue. In low SNR scenario with high PSD (G_i =-9 dBm/GHz), both adaptive MFs and multiple FECs enable to improve the revenue, which means that the combination of MF and FEC is preferred in high PSD scenario rather than median PSD scenario. We also find that the revenue of adaptive MF configuration $\hat{\mathcal{M}}_3$ and multiple FEC configuration $\hat{\mathcal{F}}_5$ can reach the almost maximum value for both high and low SNR

scenarios. It means that the usage of MF with PM-16QAM and FEC OH with 50% can be saved.

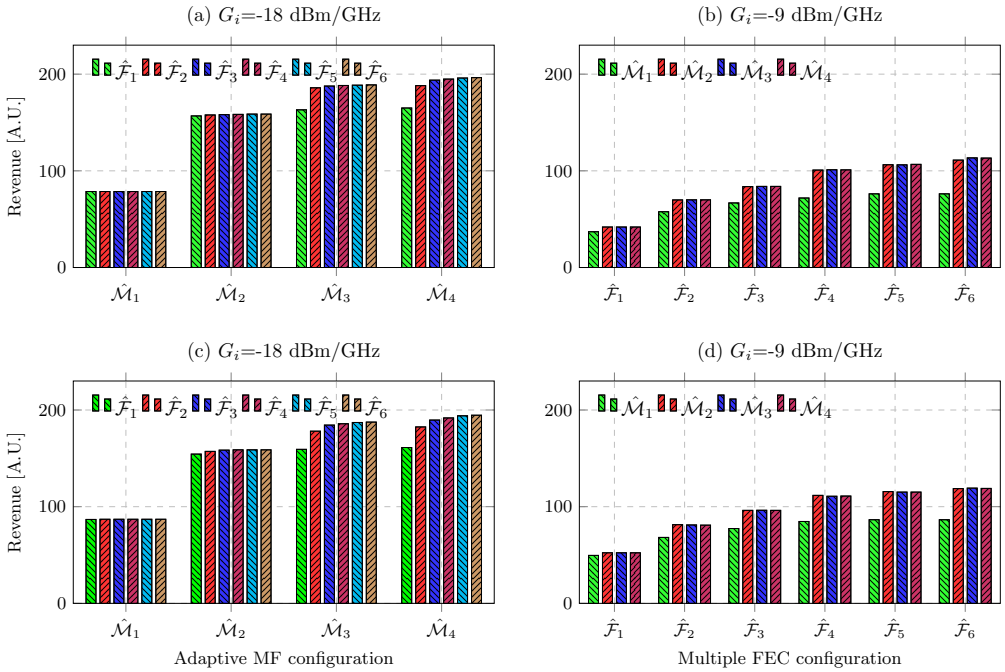

Figure 3.9: *Revenue impact of joint MF and FEC. (a) and (b) are in NSF network; (c) and (d) are in US Backbone network.*

3.6.3 Different traffic loads

Let us now study the impact of different numbers of requests. The simulations assume all requests with identical 1,000 Gbps[139]. The PSD is either -18 dBm/GHz or -9 dBm/GHz, such that we operate in scenarios that benefit of adaptive MFs and multiple FECs, respectively. The results of different adaptive MFs and different FECs are shown in Fig. 3.10(a) and 3.10(b). In Fig. 3.10(a), the four adaptive MFs obtain the same result with 20 requests, but, as the number of requests increases, the gain achieved by using four different adaptive MFs also increases. The maximum improvement of adaptive MFs (186% higher compared to $\hat{\mathcal{M}}_1$) is obtained with 200 requests. In Fig. 3.10(b), multiple FECs' revenue also increases with the number of requests. Configuration $\hat{\mathcal{F}}_6$ gets the largest revenue, which is 3.6 times higher than $\hat{\mathcal{F}}_1$.

We report the simulation results with different average bit-rates in Fig. 3.11. For a given average bit rate of 250+n*250, each request can randomly chose the bit-rate from the set {250, ..., 250+2n*250}. 160 requests are assumed in the simulation. The results of different MFs and FECs are shown in Figs. 3.11(a) and 3.11(b). We observe that the revenue decreases with the average bit-rate. The larger the bit-rate, the more spectral resources' consumption of fiber, which leads to blocked requests. For the case with more transmission modes, such as $\hat{\mathcal{M}}_4$ or $\hat{\mathcal{F}}_6$, it can also gain more revenue compared to the other configuration with fewer transmission modes, $\hat{\mathcal{M}}_1$ or $\hat{\mathcal{F}}_1$. When the average

bit-rate increases to 1,500 Gbps, the revenue improvement ratio of $\hat{\mathcal{M}}_4$ and $\hat{\mathcal{F}}_6$ reaches about 98% and 362% compared to $\hat{\mathcal{M}}_1$ and $\hat{\mathcal{F}}_1$, respectively.

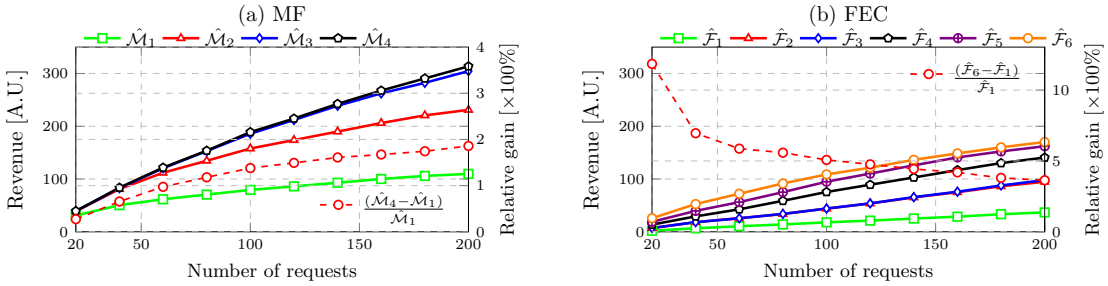

Figure 3.10: *Revenue impact with the number of requests in NSF network. Bit rate per request is 1,000 Gbps.*

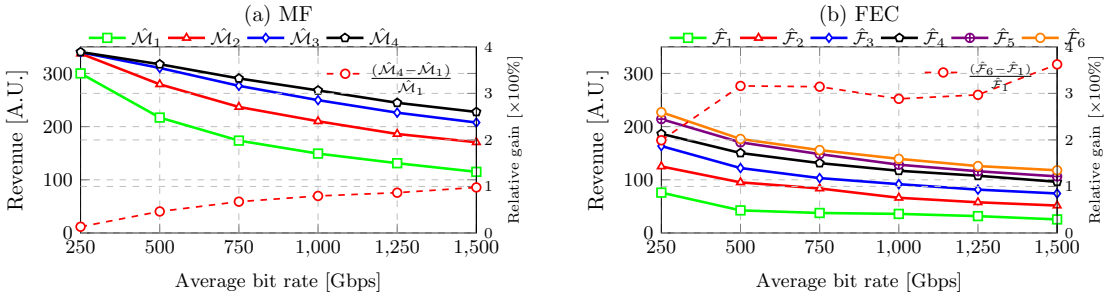

Figure 3.11: *Revenue impact with different traffic rates in NSF network. The simulations use 160 requests.*

3.7 Conclusion

In this chapter, we studied the problem of using adaptive MFs and multiple FECs to improve the traffic provisioning in FONs. The objective is to maximize the total network revenue. To this end, we develop a MILP model and a fast two-phase heuristic algorithm, which is shown to be near-optimal for revenue maximization. Although the revenue loss is inevitable under different resource crunch scenarios, it can be improved by properly choosing the transmission mode configurations and physical parameters.

Through simulations, we demonstrate that using adaptive MF enables to increase the revenue more than 100% in the scenario of high SNR while using adaptive FEC is profitable for scenarios with low SNR. While guaranteeing the revenue performance, the usage of adaptive MF configuration with PM-16QAM and multiple FEC configuration with OH 50% can be saved. We also carry out experiments to demonstrate the case of severe resource crunch, which is simulated by increasing bit-rate and number of requests. It shows that for the case of high traffic load (large number of requests or big average bit-rate), adaptive MF takes more advantage than single MF with PM-BPSK, because it can offer more spectrum-efficient transmission modes.

Chapter 4

Throughput Maximization Leveraging Just-enough SNR Margin and Channel Spacing Optimization

Contents

4.1 Introduction

According to recent traffic reports, network traffic (fueled by network services like video on demand, file sharing, online gaming, video conferencing, etc.) are still growing exponentially in today's Internet[36]. The constant traffic growth relies on optical networks. In optical networks, the resource allocation consists of finding a proper lightpath with adequate spectrum resources. Traditionally, each channel in WDM networks has to follow a rigid fixed-sized grid, e.g., 50 GHz. Recently, in the new paradigm of FONs, each channel can choose multiple contiguous FSs with the size of 12.5 GHz, and freely adjust the center frequency. More recently, with the advance of coherent detection technology and commercially available DACs, a large number of transceiver's parameters are possible to be optimized to further improve the spectral efficiency, such as baud-rate, MF, FEC, probabilistic shaping, etc[18, 123]. The development of optical networks enables us to reduce the spectrum resource waste, increase spectral efficiency, and obtain a higher cost-effective capacity. However, it is not easy to jointly optimize these parameters.

In addition, the selection of these flexible parameters must satisfy the QoT requirement. Each lightpath experiences not only the ASE noise of optical amplifiers, but also the NLI from the lightpaths that share a common fiber link. To avoid the complex calculation of the physical layer while guaranteeing uninterrupted communication, the selection criteria are generally constrained by a high SNR margin in the physical layer, i.e., assuming that each lightpath experiences the most interference under resource underprovisioning scenario. This potentially decreases the capacity or restricts the transmission reach. To this end, PLI-aware resource allocation techniques have been proposed to reduce the overestimation of NLI in order to exploit the stranded capacity[16, 133, 138, 139, 149]. This mode is also named as *low margin network* [33, 100, 117] or *just-enough SNR margin* in this study. Nevertheless, the transmission capacity of the lightpath in these studies mostly depends on the occupied FSs instead of the baud-rate, thus only needs to solve the RMSA. Limited by the frequency grid, single or the combinational baud-rates can be both used for the same channel once the allocated spectrum resource is sufficient[56]. These transceivers will also experience different filter penalties[24, 88]. Thus, the problem of routing, MF, baud-rate, and spectrum assignment was investigated in[107, 124]. As far as we know, there are no studies on the optimization of route, MF, FEC, baud-rate, spectrum assignment (RMFBSA) while considering the NLI. As the joint optimization of these parameters is already complex, it becomes more complex when introducing the NLI.

Optimizing the physical layer parameter is also important to mitigate the NLI and improve network capacity[8, 92, 117]. According to the description of the GN model on the Nyquist WDM channel[66, 96], the NLI between channels relates to the signal bandwidth, power, and channel spacing. We have seen a large number of studies on the power optimization [17, 62, 106, 139] and the channel order optimization (the different relative orders of channels) [17, 140]. The last factor—channel spacing—is generally implemented by setting a guard band. Throughout this study, we use the terms "guard band" and "channel spacing" interchangeably. Fixed and candidate guard band meth-

ods are the widely used strategies for determining the proper channel spacing. The former one has the lowest complexity but easily causes spectrum resource waste, while the latter one increases the robustness but also incurs a large number of combinations and consequently increases the complexity. To overcome the complexity of the existing methods, the study in [140] proposed to reduce the NLI by individually optimizing the center frequency using an MILP model. The nonlinearity was then solved by using a piecewise linear fitting method [139]. However, the issue of complexity still exists when facing a large number of lightpaths in mesh optical networks. Another issue in the current studies[133, 139, 149] is the evaluation metric, *minimizing the maximum spectral usage*, which potentially encourages the use of narrow channel spacing and neglects the benefit of large channel spacing on mitigating the filter narrowing effect and NLI. Thus, an efficient channel spacing optimization strategy and a proper metric for evaluating its advantage are still required.

Motivated by the above, we aim at maximizing the network throughput in a static FON by leveraging just-enough SNR margin and channel spacing optimization. As shown in Fig. 4.1, only the lowest and fixed transmission capacity can be used for the lightpath between (s, d) when considering the excessive SNR margin and fixed channel spacing, namely 100 Gbps in the traditional operation mode. The transmission capacity can increase up to 150 Gbps or larger when leveraging the just-enough SNR margin provisioning and channel spacing optimization. To implement this function in large networks, we propose an iterative feedback tuning algorithm to provide a just-enough SNR margin for each lightpath. Specifically, our algorithm is implemented in *three* steps. First, starting from a high SNR margin, we establish an ILP model and a heuristic algorithm that maximizes the network throughput. Unlike the existing lightpath provisioning that only addresses routing and spectrum assignment, the transceivers' parameters are also optimized, including MF, FEC, and baud-rate. Second, we provide a low-complexity channel spacing optimization model to mitigate the NLI, which is implemented by using the nearest neighbor channel. This model also extends the application case from a ring network into a mesh network compared to our previous study[27]. Finally, we iteratively reduce the SNR margin of each lightpath to the just-enough level to increase the throughput. The main contributions are summarized as follows,

- We propose to *maximize the throughput by leveraging just-enough SNR margin and channel spacing optimization*. Different from the conventional lightpath provisioning constrained by the stringent QoT through preserving an excessive SNR margin, leveraging the just-enough SNR margin permits to increase the network throughput by using the stranded transmission capacity of flexible transceivers. Through analyzing and evaluating the impact of different lightpath's parameters, we determine the value of just-enough SNR margin accordingly. As far as we know, this is the first time that the flexible parameters (route, MF, FEC, baud-rate, spectrum assignment) are jointly optimized while considering the NLI.
- We introduce a nearest neighbor channel method in optimizing the channel spacing, resulting in a low-complexity method that applies to a large number of lightpaths in both ring and mesh optical networks. The performance improvement

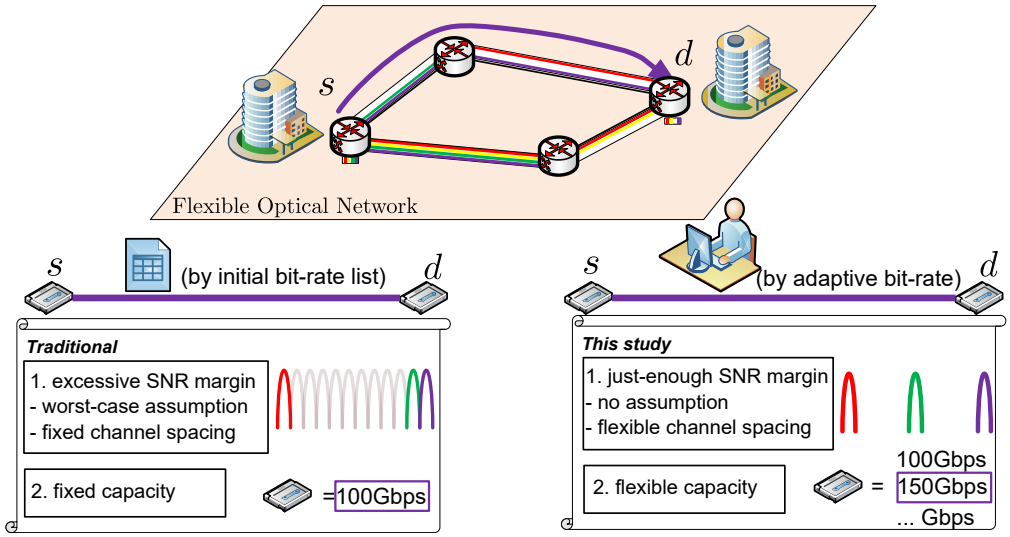

Figure 4.1: *Illustration of two operation modes in FON.*

(SNR performance and the throughput) is validated by comparing with the widely used channel spacing strategies (fixed and candidate channel spacing).

- Next, for a given resource over-provisioning scenario, we devise an iterative feedback tuning algorithm that can efficiently solve the *throughput maximization leveraging just-enough SNR margin and channel spacing optimization problem*. Specifically, we reduce the SNR margin by adjusting a slack parameter iteratively so that we can obtain the just-enough SNR margin.
- Finally, through extensive simulations in different network topologies and with different baud-rates, we confirm the throughput improvement with the help of the just-enough SNR margin and channel spacing optimization. Specifically, we observe that the relative throughput gain ratio (no smaller than 20% in our case) is more evident in resource over-provisioning scenarios, while the absolute throughput gain is more evident when network traffic load is medium.

The rest of this study is organized as follows. In Sec. 4.2, we present the preliminary information of the lightpath provisioning in FONs and the *throughput maximization leveraging just-enough SNR margin and the channel spacing optimization problem*. Next, we propose an iterative feedback tuning algorithm to solve this problem in Sec. 4.3. To reduce the complexity of the lightpath provisioning, we also present an efficient heuristic in Sec. 4.4. Illustrative numerical results are presented in Sec. 4.5. Finally, Sec. 4.6 concludes this study.

4.2 Problem statement

In this section, we present the studied *throughput maximization leveraging just-enough SNR margin and channel spacing optimization problem*. First, we provide the necessary information about the lightpath provisioning of FONs and explain how we calculate the

SNR. Then, we describe the throughput maximization problem and present a benchmark method that utilizes the fixed baud-rate. Next, we present the key problem to be solved in this study. Finally, a case study is used to illustrate the throughput improvement with the help of channel spacing optimization and just-enough SNR margin.

4.2.1 Network model

We use $G = (V, E)$ to denote an FON, where V and E are the node and link set, respectively. A link $l \in E$ represents a fiber uv ($u, v \in V$). On that fiber, the available spectrum resource is F (unit: GHz), while the number of available FSs is W (F=$f_{grid} \cdot W$, f_{grid} is 12.5 GHz bandwidth). A bit-mask $b[1...W]$ of size W is introduced to represent the occupied FS status of a fiber link, where $b[w]$=1 means the w-th FS is occupied. We also use $b_*[w]$ to represent whether the entity '*' uses w-th FS, where '*' could be either a lightpath p, or a link l, or a channel ch.

We assume that each lightpath p connecting a node pair (s, d) can adopt a transceiver t operating at a baud-rate R_t, which needs to occupy a certain number of FSs denoted by B_t (refer to [104, Table 3]). The adopted transceiver is assumed with the rectangular Nyquist spectrum and has a unique channel ch. Note that the different baud-rates R_t could use the same amount of FS(s) B_t or the same baud-rate could use the different amount of FS(s) only if $B_t \cdot f_{grid} \geq R_t$[56], we determine the available bit-rate by using baud-rate rather than occupied B_t. Also, the bit-rate depends on the spectral efficiency of adopted MF and FEC (an example table that shows the SNR threshold and bit-rate of transceiver at 32 Gbaud can refer to [63]). For ease of expression, we introduce the term *transmission mode* to refer to a combination of MF and FEC. Such a transmission mode can be adopted by the lightpath if the SNR is no less than SNR threshold of joint MF and FEC, i.e., QoT is satisfied. Next, we describe how we calculate the SNR of each lightpath.

For each lightpath, the SNR will be degraded by the ASE noise and NLI. Supposing the transceiver of lightpath p uses a launch PSD G_p, its SNR is stated as follows[63, 66],

$$SNR_p = \frac{R_t \cdot G_p}{f_{grid} \cdot B_t \cdot (G_p^{ASE} + G_p^{NLI})} \tag{4.1a}$$

$$= \frac{R_t \cdot G_p}{f_{grid} \cdot B_t \cdot G_p^{ASE}} \cdot \frac{1}{1 + \frac{G_p^{NLI}}{G_p^{ASE}}} \tag{4.1b}$$

$$= SNR_p^{best} \cdot \frac{1}{1 + \frac{G_p^{NLI}}{G_p^{ASE}}} = SNR_p^{best} \frac{1}{\mathcal{X}_p} \tag{4.1c}$$

where G_p^{ASE} is the accumulated PSD of ASE noise in optical amplifiers, G_p^{NLI} is the accumulated PSD of NLI on fibers, $SNR_p^{best} = \frac{R_t \cdot G_p}{f_{grid} \cdot B_t \cdot G_p^{ASE}}$ is the received best-case

SNR without NLI, $\mathcal{X}_p = 1 + \frac{G_p^{NLI}}{G_p^{ASE}}$ is the strength of NLI. By assuming a coherent receiver with adaptive DSP and a matched receiver filter, the noise equivalent bandwidth $f_{grid} \cdot B_t$ is equal to the baud-rate R_t. Thus, we can ignore the impact of bandwidth and baud-rate on the SNR evaluation in the following. We also assume a uniform launch PSD for all transceivers.

The factor $\mathcal{X}_p$ in Eq. (4.1c) depends on the occupied channels of lightpath. For ease of discussion, we present the log form of SNR as follows,

$$SNR_{p,[\text{dB}]} = SNR^{best}_{p,[\text{dB}]} - \mathcal{X}_{p,[\text{dB}]} \tag{4.2}$$

where $\mathcal{X}_{p,[\text{dB}]} = 10\log_{10}\left(1 + \frac{G_p^{NLI}}{G_p^{ASE}}\right)$. Next, we explain the calculation of ASE noise and NLI.

- **ASE**. We use the following equation to calculate the ASE noise of optical amplifiers,

$$G_p^{ASE} = N_p \left(10^{\alpha L_{span}} - 1\right) n_{sp} h\nu \tag{4.3}$$

  where N_p is the number of spans, L_{span} (unit: km) is the length of one span between two optical amplifiers, α is the fiber attenuation factor, n_{sp} is the noise figure of optical amplifiers, h is the Planck constant, and ν is the absolute frequency of optical signal at 1,550 nm.

- **NLI**. We adopt the dilog method of [66, Eq. (11)] that calculates the NLI based on channel,

$$G_p^{NLI} = N_p \eta_{ch}^{SCI} {G_p}^3 + G_p \sum_{ch'} \eta_{ch,ch'}^{XCI}(f_{ch,ch'}) N_{p,p'} {G_{p'}}^2 \tag{4.4}$$

  where ch and ch' are the occupied channel of lightpath p and p' respectively, $N_{p,p'}$ is the number of common spans of lightpath p and p', η_{ch}^{SCI} and $\eta_{ch,ch'}^{XCI}$ are the SCI efficiency and XCI efficiency respectively, $f_{ch,ch'}$ is the *channel spacing* of the center frequency of two lightpaths. An example curve of the XCI efficiency at different channel spacing can refer to [61, Fig. 1]. Meanwhile, we ignore the impact of SCI, as it can be compensated by digital back propagation [58] and has a weak impact on the parameter of channel spacing[66].

4.2.2 Throughput maximization problem

Let us now look at the throughput of an FON. We first define a traffic demand matrix $\boldsymbol{D}$, where each item $D_{s,d}$ denotes the bit-rate demand between each node pair (s, d). We also define another network provisioning capacity matrix $\boldsymbol{T}$, where each item $T_{s,d}$ is the transmission capacity of the lightpaths between node pair (s, d). To ensure that the traffic demand could be fully accommodated, the bit-rate demand should be no greater

than the transmission capacity, i.e., $D_{s,d} \leq T_{s,d}$. The network throughput TH in this study is the sum of all bit-rate demands, i.e., $TH = \sum_{(s,d)} D_{s,d}$.

As this study considers a static lightpath provisioning, we begin by assuming a constant traffic distribution, namely the normalized traffic demand matrix $\hat{\boldsymbol{D}}$ is constant, where $\hat{D}_{s,d} = \dfrac{D_{s,d}}{\sum_{(s,d)} D_{s,d}}$. Thus, we have $TH \cdot \hat{D}_{s,d} = D_{s,d} \leq T_{s,d}$.

Given a normalized traffic demand matrix $\hat{\boldsymbol{D}}$ and a transmission mode set $\mathcal{M}$, the objective function is expressed as follows,

$$\max \left\{ \sum_{(s,d)} D_{s,d} \right\} \tag{4.5}$$

In this problem, we need to individually design the number of lightpaths to implement the network provisioning capacity $T_{s,d}$ for each node pair. Besides, we also need to optimize the parameters of each lightpath, such as route, MF, FEC, baud-rate, and spectrum position. Meanwhile, the following constraints should be satisfied for two arbitrary lightpaths p and p' in an FON.

- **C1 - QoT constraint**: Each lightpath should guarantee that the QoT is satisfied. The QoT constraint can be expressed by using the QoT metric $\mathcal{Q}_p = \dfrac{SNR_p}{SNR_p^{threshold}} \geq 1$, or the log form by using Eq. (4.2),

$$SNR_{p,[\mathrm{dB}]}^{best} - \mathcal{X}_{p,[\mathrm{dB}]} - SNR_{m,[\mathrm{dB}]}^{threshold} \geq 0, \tag{4.6}$$

  where $SNR_m^{threshold}$ is the SNR threshold of the adopted transmission mode m. Recall that the second term $\mathcal{X}_p$ in Eq. (4.6) depends on the route and spectrum positioning of other undetermined lightpaths, which could dramatically increase the difficulty of lightpath provisioning. A simple way to eliminate $\mathcal{X}_p$ in Eq. (4.6) is using a high SNR margin M_p. Such a margin needs to compensate all possible NLI for lightpath p. Thus, we give another alternative constraint, *SNR margin requirement*.

- **C1* - SNR margin requirement**:

$$SNR_{p,[\mathrm{dB}]}^{best} - M_{p,[\mathrm{dB}]} - SNR_{m,[\mathrm{dB}]}^{threshold} \geq 0, \tag{4.7}$$

  where M_p is the *SNR margin* used for compensating the unknown NLI. Generally, the SNR margin $M_p \geq \mathcal{X}_p^{worst}$, where $\mathcal{X}_p^{worst}$ is calculated by the worst-case assumption under which other spectrum resources of the links along lightpath are fully occupied by different channels. With the SNR margin requirement constraint, we can neglect the complex physical layer calculation in QoT constraint and focus on the lightpath provisioning.

- **C2 - one baud-rate and one transmission mode constraint**: Each lightpath can adopt one and only one baud-rate and one transmission mode.

- **C3 - spectrum contiguity constraint**: For each used baud-rate R_t, we need to allocate B_t contiguous FSs, namely $b_{ch}[1...W] = [\underbrace{0\cdots0\overbrace{11\cdots11}^{B_t}0\cdots0}_{W}]$. It needs to ensure the size of spectrum allocated is sufficient, that is $f_{grid} \cdot B_t \geq R_t$.
- **C4 - spectrum continuity constraint**: The occupied FSs of the channel for a lightpath should be identical on each link.
- **C5 - spectrum non-overlapping constraint**: The occupied FSs of two lightpaths should not overlap. Alternatively, each FS of a link can be used at most once.

Let us discuss the constraints (**C1**) and (**C1***). Traditional method takes constraint (**C1***) rather than (**C1**). The benefit is that lightpath provisioning can be greatly simplified by splitting the physical layer calculation and lightpath provisioning when the SNR margin is enough for compensating the NLI. The limitation is that the improper SNR margin M_p requires each lightpath to adopt the low order transmission mode with a low SNR threshold. As a result, the transmission bit-rate or transmission reach of each lightpath is strictly constrained, especially under the resource over-provisioning scenario where the actual NLI may be far less than the worst-case NLI.

Here, to make it clear, we present a benchmark method that preserves excessive SNR margin[62]. It mainly includes two parts, a lightpath precalculation based on constraint (**C1***) and an ILP model based on constraints (**C2**)-(**C5**). The ILP model uses the pre-calculated lightpaths and obtains the maximal throughput by solving the routing, transmission mode, and spectrum assignment problem. Except for the above five constraints, we also introduce another constraint to define the mentioned scenario of resource over-provisioning where the actual NLI is much lower than the preserved SNR margin. This constraint limits the current maximum FS index of ILP model by W_{cur}, $W_{cur} \leq W$. It should be noted that this benchmark method only allows the fixed baud-rate.

Lightpath precalculation

This part calculates and stores all possible lightpaths that satisfy (**C1***) for each node pair. We use the link length as the metric to generate the K-shortest routes[141]. We also initialize the channel index set of different contiguous FSs[130] that records both the bandwidth B_t and spectrum position. The lightpaths that satisfy Eq. (4.7) are stored into the lightpath set $\mathcal{P}$, where $M_p = \mathcal{X}_p^{worst}$. Since one baud-rate is assumed in this method, the bit-rate of each lightpath only depends on the transmission mode.

Maximize throughput

This part maximizes the network throughput based on (**C2**)-(**C5**).

Parameters

- $\hat{D}_{s,d}$, normalized traffic demand ratio of node pair (s, d).

- $ch \in CH$, channel index of different contiguous FSs. For example, for the transceiver using two contiguous FSs, $CH = \{[110\cdots], [0110\cdots], \cdots, [\cdots 011]\}$.
- $b_{ch}[w]$, equals 1 if the channel ch uses the w-th FS, 0 otherwise.
- $p_{s,d,k}^{ch,m} \in \mathcal{P}$, lightpath ID of the k-th route of (s,d) if it uses channel ch and transmission mode m.
- $C_{s,d,k}^{ch,m}$, transmission bit-rate of the lightpath $p_{s,d,k}^{ch,m}$ if it satisfies Eq. (4.7), 0 otherwise.
- $\beta_{s,d,k,l}$, equals 1 if the k-th route of node pair (s,d) uses link l, 0 otherwise.

Variables

- $D_{s,d}$, bit-rate demand of node pair (s,d).
- $T_{s,d}$, provisioning capacity of node pair (s,d).
- $\delta_{s,d,k}^{ch,m}$, equals 1 if the lightpath $p_{s,d,k}^{ch,m}$ is adopted, 0 otherwise.
- TH, network throughput.

Objective

$$\max_{\delta_{s,d,k}^{ch,m}, \boldsymbol{TH}} \quad TH \quad \texttt{(Max TH)}$$

$$\textbf{\textit{s.t.}} \quad D_{s,d} = TH \cdot \hat{D}_{s,d}, \qquad \forall s,d \neq s \tag{4.8a}$$

$$T_{s,d} = \sum_{k,ch,m} \delta_{s,d,k}^{ch,m} \cdot C_{s,d,k}^{ch,m}, \quad \forall s,d \neq s \tag{4.8b}$$

$$D_{s,d} \leq T_{s,d}, \qquad \forall s,d \neq s \tag{4.8c}$$

$$\sum_{s,d \neq s,k,ch,m} \delta_{s,d,k}^{ch,m} \cdot \beta_{s,d,k,l} \cdot b_{ch}[w] \leq 1, \quad \forall l,w \tag{4.8d}$$

$$\delta_{s,d,k}^{ch,m} \cdot b_{ch}[w] = 0. \quad \forall s,d,k,ch, W_{cur} < w \leq W, m \tag{4.8e}$$

The objective is to maximize the network throughput. Constraints (4.8a) ensure that the bit-rate demand follows the distribution of the given normalized traffic demand matrix $\hat{\boldsymbol{D}}$ for each node pair. Constraints (4.8b) obtains the transmission capacity between (s,d). Constraints (4.8c) ensure that the traffic demand could be fully accommodated by the network provisioning capacity. Constraints (4.8d) ensure that each FS of a link can be used at most once, which also guarantees only one transmission mode. Constraints (4.8e) are used to simulate the resource over-provisioning scenario by the FS index W_{cur}. In addition, we see that the benchmark method has ignored the constraints (**C3**) and (**C4**) because we use utilize the pre-calculated lightpaths.

4.2.3 Throughput maximization leveraging just-enough SNR margin provisioning and channel spacing optimization

As we see in the benchmark method, only one fixed baud-rate is permitted for each lightpath. The low baud-rate transceiver with fine-grained bandwidth can reduce the blocking probability[114], but probably result in a low spectral efficiency for the large

frequency grid. The high baud-rate transceiver is promising to reduce the spectrum resource waste and consequently increase the net spectral efficiency[56]. Future FONs are considering the coexistence of flexible baud-rate transceivers[94]. Thus, the benchmark with only fixed baud-rate allocation is insufficient to adapt to future needs. The first question is that i) *how to efficiently use the flexible baud-rate transceiver for lightpath provisioning*?

In addition, the ILP model in the benchmark method may inevitably generate redundant lightpaths. For example, the lightpath between some node pair (s, d) with a short distance has a high capacity, easily satisfies the bit-rate demand, and probably leaves idle spectrum resources on the connected links. It is inevitable to generate additional lightpaths that still connect the same node pair using these idle spectrum resources. Nevertheless, the capacity improvement of several node pairs may not improve the scaling factor TH. Meanwhile, these lightpaths will however introduce extra network cost and NLI. Thus, the second question is that ii) *how to remove these lightpaths while guaranteeing the maximal network throughput*?

Through Eq. (4.6), we see that the lower NLI allows the lightpath to choose a higher-order transmission mode, which further improves the network throughput. Optimizing the channel spacing can reduce the interference by using the large number of idle spectrum resources in the resource over-provisioning scenario. Therefore, the third question is that iii) *how to minimize the NLI to allow each lightpath to adopt a higher-order transmission mode*?

Furthermore, as stated before, setting the high and excessive SNR margin M_p restricts the transmission mode of each lightpath in the lightpath precalculation part. We find that each lightpath is permitted to adopt the high-order transmission mode with a high SNR threshold by reducing the high preserved SNR margin in Eq. (4.7). Now, the fourth question is that iv) *how to find a proper preserved SNR margin to allow each lightpath to adopt a higher-order transmission mode*? Meanwhile, the QoT constraint should be also satisfied.

Question i) is solved by incorporating the baud-rate into the lightpath pre-calculation. Question ii) is solved by adding a posterior optimization similar to `Max TH` but using a modified objective function that minimizes the total lightpaths. The exact technique for these two questions will be presented in Sec. 4.3. Different from the previous two questions, questions iii) and iv) involve the physical layer optimization. Note that it is not easy to simultaneously optimize the channel spacing and implement and just-enough provisioning. Here, we present the two problems sequentially.

Channel spacing optimization

Given a lightpath set $\mathcal{P}_{adopt}$ with determined route, determined baud-rate, and determined transmission mode, we want to enhance the SNR by minimizing the NLI for each lightpath. The QoT metric $\mathcal{Q}_p$ of different lightpaths is considered while minimizing the NLI. Thus, we leverage the left terms in Eq. (4.6) as the objective. With these three terms, the objective function that minimizes the NLI is expressed as follows,

$$\min_{f_{ch}} \left\{ \max_{p \in \mathcal{P}_{adopt}} \left\{ \mathcal{X}_{p,[\mathrm{dB}]} + SNR^{threshold}_{m,[\mathrm{dB}]} - SNR^{best}_{p,[\mathrm{dB}]} \right\} \right\}$$
$$\textit{s.t.} \quad \textbf{(C1), (C5)}$$

Just-enough SNR margin provisioning

Given a normalized traffic demand matrix, an available transmission mode set $\mathcal{M}$, and an available baud-rate set $\mathcal{T}$, the objective function is expressed as follows,

$$\max_{\delta^{ch,m,R}_{s,d,k}, f_{ch}, M_p} \quad TH$$
$$\textit{s.t.} \quad \textbf{(C1), (C2)} - \textbf{(C5)}$$

Our aim is to improve the network throughput by determining a proper SNR margin M_p for each lightpath compared to the benchmark. Besides, the route (s, d, k), channel ch, transmission mode m, and baud-rate R, as well as a proper channel location f_{ch} for each lightpath are to be optimized.

A small instance

We illustrate how to optimize the throughput for provisioning 30 lightpaths in a point-to-point network with available spectrum resources of 4,000 GHz (F=4,000 GHz, W = 320 FSs). In Fig. 4.2, we plot the SNR distribution of 30 lightpaths provisioned by using three different techniques: traditional provisioning with an excessive SNR margin, provisioning with channel spacing optimization, and provisioning with just-enough SNR margin. Each red circle denotes a lightpath that uses two contiguous FSs at 16 Gbaud, where x-axis is the spectrum position and y-axis is the lightpath's actual SNR. They can adopt either the transmission mode (16QAM, FEC = 0.92) or (64QAM, FEC = 0.68)[63] without any SNR penalty. The bit-rates are set with 112.5 and 125 Gbps to match the 16 Gbaud transceiver in our assumption[63]. Other detailed parameters (fiber type, EDFA noise figure, and span length) can refer to Sec. 4.5. The PSD G_{opt} (15.03μW/GHz) is calculated by using the LOGON strategy[97, Eq. (6)] among 4,000 GHz.

In Fig. 4.2(a), 30 lightpaths all adopt 16QAM and provide the bit-rate of 112.5 Gbps. The QoT is satisfied because all SNRs are over the SNR threshold. Next, if we apply the channel spacing optimization, as shown in Fig. 4.2(b), the SNRs of these lightpaths rise because of the less NLI. In Fig. 4.2(c), by using a lower SNR margin, we can upgrade the transmission mode to 64QAM which provides a larger bit-rate of 125 Gbps while guaranteeing the QoT for all lightpaths. Therefore, we can increase the network throughput from 30×112.5 Gbps in Fig. 4.2(a) to 30×125 Gbps in Fig. 4.2(c).

It should be also mentioned that the maximum SNR margin improvement of the traditional fixed channel spacing is achieved by 125 GHz in this case, which obtains

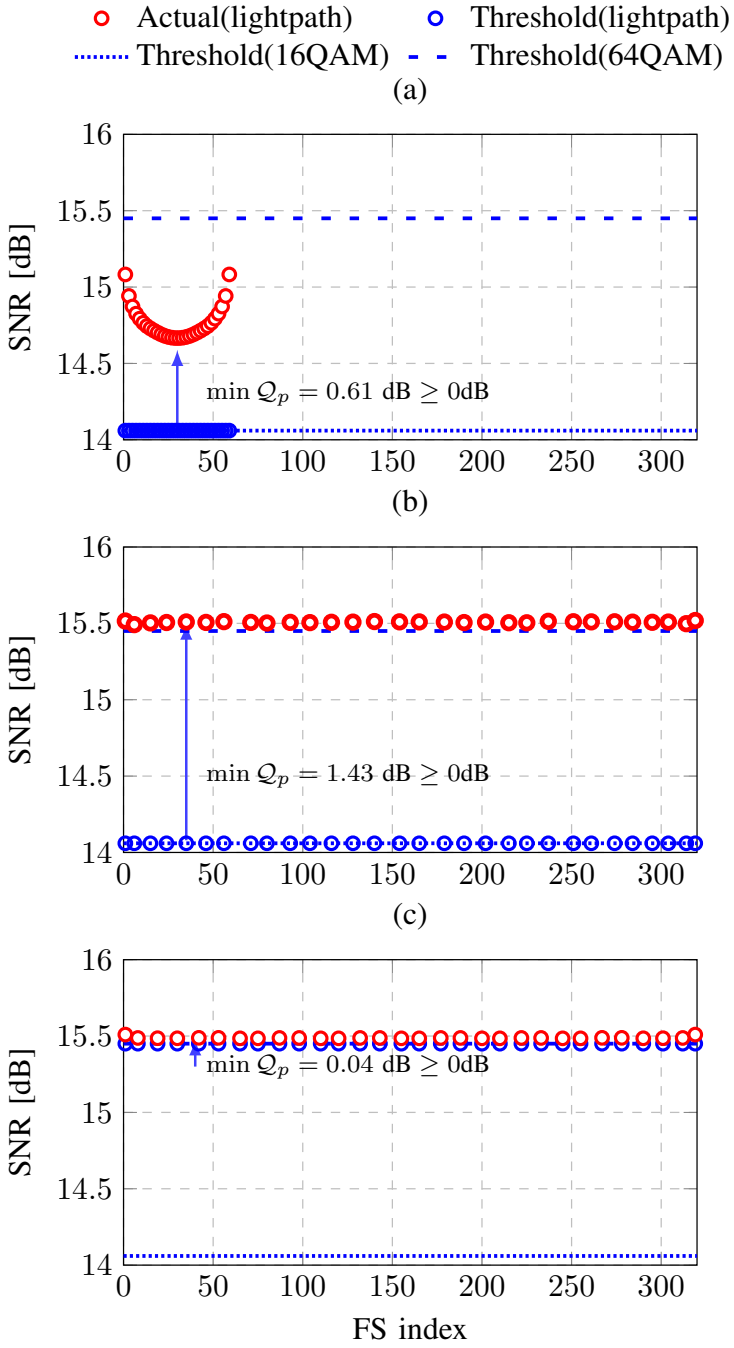

Figure 4.2: *An example of lightpath provisioning leveraging just-enough SNR margin and channel spacing optimization in a point-to-point network with 600 km (W_{cur}=60 FSs, W=320 FSs, PSD=15 μW/GHz in this example). The lightpaths need to satisfy the QoT, i.e., Eq. (4.6) holds. (a) Traditional provisioning through preserving an excessive SNR margin (throughput is 30×112.5 Gbps); (b) Provisioning with channel spacing optimization; (c) Provisioning with just-enough SNR margin (throughput is 30×125 Gbps).*

only 0.02 dB QoT metric (min $\mathcal{Q}_p$) in Fig. 4.2(c) (not shown in the figure for the sake of clarity). This is still less than the 0.04 dB of flexible channel spacing. It shows the advantage of flexible channel spacing compared to the fixed channel spacing in terms of mitigating the NLI and improving the SNR performance.

Through the example in Fig. 4.2, we can upgrade the transmission mode and increase the bit-rate by properly setting the channel spacing and carefully adjusting the SNR margin. However, it is not easy to simutanesouly adjust the channel spacing and SNR margin, especially for a large number of lightpaths. To tackle this challenge, we design an iterative feedback tuning algorithm to gradually and sequentially adjust these parameters until the just-enough SNR margin is found.

4.3 Iterative feedback tuning algorithm

In this section, we present the algorithm that solves the *throughput maximization leveraging just-enough SNR margin and channel spacing optimization problem*. The flowchart is illustrated in Fig. 4.3. The first two phases mainly follow the benchmark method in Sec. 4.2.2. The difference lies in that the flexible baud-rates are incorporated. Then, we use the `Phase 3` to remove the redundant lightpaths of `Phase 2`. Next, in `Phase 4`, we optimize the channel spacing through an LP model. Motivated by [62], we try to determine the just-enough SNR margin M_p with a unit gradient step of Δ_M. Compared to last iteration, the higher-order transmission mode is permitted for each lightpath, which can provide a larger bit-rate. By doing so, we can take the lightpaths with upgraded higher-order transmission mode to increase the network throughput in `Phase 2`. Finally, the algorithm terminates once a lightpath violates the QoT constraint.

4.3.1 Lightpath precalculation with flexible baud-rate

- **Input**: topology $G(V, E)$, maximal FS index W_{cur}, transceiver set $\mathcal{T}$, transmission mode set $\mathcal{M}$, SNR margin M_p (initialized by $\mathcal{X}_p^{worst}$).
- **Output**: lightpath set $p_{s,d,k}^{ch,m,R} \in \mathcal{P}$, capacity set $\mathcal{C}_{s,d,k}^{ch,m,R} \in \mathcal{C}$, boolean indicator $\beta_{s,d,k,l}$.
- **Process**: it stores the lightpath p that satisfies the SNR margin requirement in Eq. (4.7), where M_p acts as a slack variable for each iteration. The results are stored into the candidate lightpath set $\mathcal{P}$ and the capacity set $\mathcal{C}$. Different from the lightpath precalculation in Sec. 4.2.2, here, we use $p_{s,d,k}^{ch,m,R}$ to denote the lightpath ID rather than $p_{s,d,k}^{ch,m}$. Besides, the channel index set CH is also extended considering the occupied FS of different baud-rates.

4.3.2 Throughput maximization with flexible baud-rate

Phase 2

- **Input**: candidate lightpath set $\mathcal{P}$, capacity set $\mathcal{C}$, boolean indicator $\beta_{s,d,k,l}$, normalized traffic demand matrix $\hat{\boldsymbol{D}}$.

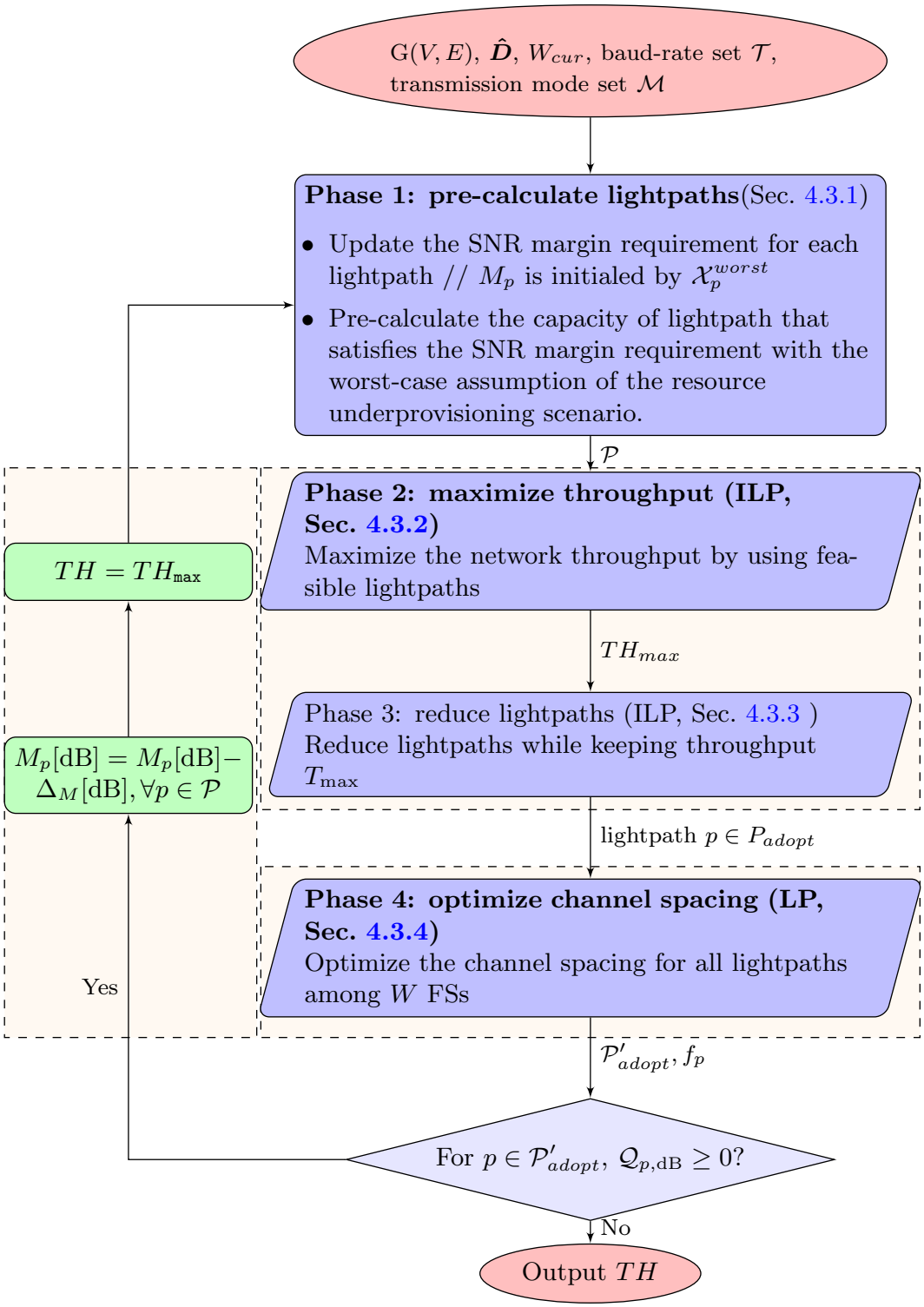

Figure 4.3: *Flowchart of our iterative feedback tuning algorithm.*

- **Output**: network throughput $TH_{\texttt{max}}$.
- **Process**: this phase calculates the maximal network throughput through the following model,

$$\max_{\delta_{s,d,k}^{ch,m,R},\boldsymbol{TH}} \quad TH \quad \texttt{(Max TH with FB)}$$

$$\begin{aligned}
\textbf{\textit{s.t.}}\quad & D_{s,d} = TH \cdot \hat{D}_{s,d}, \qquad \forall s,d \neq s && \text{(4.10a)}\\
& T_{s,d} = \sum_{k,ch,m,R} \delta_{s,d,k}^{ch,m,R} \cdot C_{s,d,k}^{ch,m,R}, \quad \forall s,d \neq s && \text{(4.10b)}\\
& D_{s,d} \leq T_{s,d}, \qquad \forall s,d \neq s && \text{(4.10c)}\\
& \sum_{s,d\neq s,k,ch,m,R} \delta_{s,d,k}^{ch,m,R} \cdot \beta_{s,d,k,l} \cdot b_{ch}[w] \leq 1, \quad \forall l,w && \text{(4.10d)}\\
& \delta_{s,d,k}^{ch,m,R} \cdot b_{ch}[w] = 0. \quad \forall s,d,k,ch,R, W_{cur} < w \leq W, m && \text{(4.10e)}
\end{aligned}$$

The description of these constraints can refer to the benchmark method in Sec. 4.2.2. Different from that, we have replaced the variable $\delta_{s,d,k}^{ch,m}$ with $\delta_{s,d,k}^{ch,m,R}$ in order to optimize the baud-rate. Thus, the route (s,d,k), spectrum position ch, transmission mode m, and baud-rate R in `Max TH with FB` are jointly optimized.

Phase 3

- **Input**: candidate lightpath set $\mathcal{P}$, capacity set $\mathcal{C}$, boolean indicator $\beta_{s,d,k,l}$, normalized traffic demand matrix $\hat{\boldsymbol{D}}$, network throughput $TH_{\texttt{max}}$.
- **Output**: adopted lightpath set $\mathcal{P}_{adopt}$.
- **Process**: this phase removes the redundant lightpaths of previous model. Based on the model `Max TH with FB`, we minimize the total number of lightpaths. The network throughput is also maintained in this model.

$$\min_{\delta_{s,d,k}^{ch,m,R}} \sum_{s,d\neq s,k,ch,m,R} \delta_{s,d,k}^{ch,m,R} \quad \texttt{(Remove Redundant)}$$

$$\begin{aligned}
\textbf{\textit{s.t.}}\quad & (4.10a) - (4.10e)\\
& TH \geq TH_{\texttt{max}} && \text{(4.11a)}
\end{aligned}$$

The objective is to minimize the total number of lightpaths in the network. Constraint (4.11a) maintains the throughput $TH_{\texttt{max}}$ that is obtained from previous model. The redundant lightpaths can be removed through this model.

4.3.3 Channel spacing optimization

- **Input**: adopted lightpath set $\mathcal{P}_{adopt}$.
- **Output**: optimal center frequency f_p.

- **Process**: $\min\limits_{f_p} \left\{ \max\limits_{p \in \mathcal{P}_{adopt}} (\mathcal{X}_p + SNR^{threshold}_{m,[\mathrm{dB}]} - SNR^{best}_{p,[\mathrm{dB}]}) \right\}$.

The linear form of this objective function is $\min \left\{ \max \left\{ \frac{SNR^{threshold}_m}{SNR^{best}_p} \mathcal{X}_p \right\} \right\}$. We take the center frequency as a continuous variable among the available spectrum resources $[0, F]$. Thus, the center frequency of each lightpath can be individually optimized by an LP model. Meanwhile, we have to resolve the issue that the relationship between XCI efficiency and channel spacing in Eq. (4.4) is nonlinear. To this end, we use a piecewise-linear fitting function[139]. Finally, the continuous variable f_p is rounded to fit the frequency grid of f_{grid} (unit: GHz). The frequency mapping process in the final step is decomposed into two-step to accelerate the optimization.

The linear approximation function for fitting the XCI efficiency is expressed as follows [139],

$$\bar{\eta}^{XCI}_{B_p,B_{p'}}(f_{ch,ch'}) = \max_{1 \le q \le Q} \left(a_q^{B_p,B_{p'}} f_{ch,ch'} + b_q^{B_p,B_{p'}} \right) \tag{4.12}$$

where Q is the number of fitting segments ($Q = 5$), $a_q^{B_p,B_{p'}}$ and $b_q^{B_p,B_{p'}}$ are the coefficients calculated by the algorithm in [83] based on the XCI efficiency of the channels from p' to p.

Parameters

- f_{grid}, bandwidth of an FS (12.5 GHz).
- $x_{p,l}$, equals 1 if lightpath p uses link l, 0 otherwise.
- $y_{p,p'}$, equals 1 if lightpath p and p' share a common fiber link, 0 otherwise.
- γ_p, spectrum position of a lightpath p. Here, we take the starting FS index.
- $u_{p,p'}$, equals 1 if γ_p is bigger than $\gamma_{p'}$, 0 otherwise.
- B_p, number of occupied FSs of a lightpath p.
- m_p, transmission mode of p.
- $a_q^{B_p,B_{p'}}$, $b_q^{B_p,B_{p'}}$, coefficients of piecewise linear fitting function.
- G^{ASE}_{span}, PSD of ASE between two optical amplifiers, i.e., per one span.

Variables

- f_p, center frequency of lightpath p that is relative to the optical signal frequency ν.
- $\bar{\eta}^{XCI}_{p,p'}$, linear approximation of the XCI efficiency from lightpath p' to p.
- $\mathcal{X}_{p,l}$, the strength of NLI of lightpath p on link l.
- $\mathcal{X}^{network}$, the maximum NLI strength in a network considering the QoT metric.

Objective function

$$\min_{f_p, \eta^{XCI}_{p,p'}} \quad \mathcal{X}^{network} \quad \texttt{(Phase 4)}$$

$$\textbf{s.t.} \quad \frac{SNR^{threshold}_{m_p}}{SNR^{best}_{p}} \cdot \sum_{l} \mathcal{X}_{p,l} \leq \mathcal{X}^{network}, \quad \forall p \tag{4.13a}$$

$$x_{p,l} \left\{ 1 + \frac{\sum_{p' \neq p} x_{p',l} \cdot {G_p}^3 \cdot \bar{\eta}^{XCI}_{p,p'}}{G^{ASE}_{span}} \right\} \leq \mathcal{X}_{p,l}, \forall p, l \tag{4.13b}$$

$$y_{p,p'} \left\{ \begin{bmatrix} a_q^{B_p,B_{p'}} \left(f_p - f_{p'}\right) + b_q^{B_p,B_{p'}} \end{bmatrix} \cdot u_{p,p'} - \bar{\eta}^{XCI}_{p,p'} \right\} \leq 0, \quad \forall p, p' \neq p, q \tag{4.13c}$$

$$y_{p,p'} \left\{ \begin{bmatrix} a_q^{B_p,B_{p'}} \left(f_{p'} - f_p\right) + b_q^{B_p,B_{p'}} \end{bmatrix} \cdot (1 - u_{p,p'}) - \bar{\eta}^{XCI}_{p,p'} \right\} \leq 0, \quad \forall p, p' \neq p, q \tag{4.13d}$$

$$0 \leq \left[\left(\frac{f_p}{f_{grid}} - \frac{B_p}{2} \right) - \left(\frac{f_{p'}}{f_{grid}} + \frac{B_{p'}}{2} \right) \right] y_{p,p'} \cdot u_{p,p'}, \forall p, p' \neq p \tag{4.13e}$$

$$\frac{f_p}{f_{grid}} + \frac{B_p}{2} \leq W, 0 \leq \frac{f_p}{f_{grid}} - \frac{B_p}{2}. \quad \forall p \tag{4.13f}$$

The objective is to minimize the maximum fair ratio of NLI strength for all lightpaths. Such a ratio, denoted by $\mathcal{X}^{network}$, is calculated by constraints (4.13a). Constraints (4.13b) calculate the NLI strength for the lightpath p on link l. Constraints (4.13c) and (4.13d) calculate the XCI efficiency $\bar{\eta}^{XCI}_{p,p'}$ between lightpath p and p' using $|f_p - f_{p'}|$. Constraints (4.13e) guarantee that the occupied spectrum resources of two lightpaths are non-overlapping if they use a common link. Constraints (4.13f) restrict the spectrum resources among the spectrum interval $[0, F]$. Note that the QoT constraint in (**C1**) can be independently split while minimizing the NLI. Thus, we donot add this constraint in the model, which will take effect in the final step in Sec. 4.3.4. The main variables to be optimized in `Phase 4` are the center frequencies f_p and $\eta^{XCI}_{p,p'}$.

The complexity of the above model mainly depends on the constraints (4.13c) and (4.13d)). The number of constraints could be $\mathcal{O}(Q \cdot |\mathcal{P}_{adopt}|^2)$ if assuming a point-to-point link. The square relationship restricts the application case of channel spacing optimization to a small number of lightpaths. Note that the XCI efficiency could decrease dramatically with the channel spacing and it may be negligible when the channel spacing equals two baud-rates [20, Fig. 4]. That is to say, only the nearest neighbor channel counts the most in terms of XCI efficiency and SNR.

Motivated by the above observation, we propose a low-complexity method to evaluate the NLI using the nearest neighbor channels. The starting FS index γ_i is used to denote the spectrum position of the channel of lightpath p. The nearest channel of lightpath p is described as these channels that have the minimal difference of spectrum position. The second-nearest channel of lightpath p is described as these channels that have the nearest channel related to the "nearest" channel of lightpath p. We use $y^{(1)}_{p,p'}$

and $y^{(2)}_{p,p'}$ to denote whether the nearest and second-nearest channel of lightpath p is p', respectively, which are obtained by the following algorithms `Algorithm 4.1` and `4.2`. In `Algorithm 4.1`, from lines 3 to 5, we determine the minimal FS difference (left side) $FS_p^{<left>}$ of lightpath p. From lines 6 to 8, we determine the nearest channels. From 12 to 18, we use the same process for the right nearest channel. In `Algorithm 4.2`, we determine the second-nearest channel p' if there exists a third channel p'' that is not only near to p but also near to p'. Finally, with the obtained $y^{(1)}_{p,p'} + y^{(2)}_{p,p'}$, we replace the parameter $y_{p,p'}$ in Eqs. (4.13c) and (4.13d). By doing so, we can conservatively assume the nearest and second-nearest neighbor channels when optimizing the center frequency rather than all lightpaths sharing a common link, so as to lower the complexity from $\mathcal{O}(Q \cdot |\mathcal{P}_{adopt}|^2)$ to $\mathcal{O}(Q \cdot |\mathcal{P}_{adopt}| * 4)$ (in the case of a point-to-point link).

Algorithm 4.1: The nearest neighbor channel

Input : $\mathcal{P}_{adopt}, \boldsymbol{y}$
Output: $\boldsymbol{y}^{(1)}$

1 Intialize $\boldsymbol{y}^{(1)} \Leftarrow \mathbf{0}$;
2 % Determine the left closest channel of lightpath p;
3 **for** $p \in \mathcal{P}_{adopt}$ **do**
4 $\quad \mathcal{P}^{p,<left>}_{adopt} \Leftarrow \{p' \in \mathcal{P}_{adopt} \,|u_{p,p'} = 1, y_{p,p'} = 1\}$;
5 $\quad FS_p^{<left>} \Leftarrow \min_{p' \in \mathcal{P}^{p,<left>}_{adopt}} \{\gamma_p - \gamma_{p'}\}$;
6 $\quad$ **for** $p \in \mathcal{P}_{adopt}, p' \in \mathcal{P}_{adopt}/\{p\}$ **do**
7 $\quad\quad$ **if** $y_{p,p'} = 1$ *and* $\gamma_p - \gamma_{p'} = FS_p^{<left>}$ **then**
8 $\quad\quad\quad y^{(1)}_{p,p'} \Leftarrow 1$;
9 $\quad\quad$ **end**
10 $\quad$ **end**
11 $\quad$ % Determine the right closest channel of lightpath p;
12 $\quad$ **for** $p \in \mathcal{P}_{adopt}$ **do**
13 $\quad\quad \mathcal{P}^{p,<right>}_{adopt} \Leftarrow \{p' \in \mathcal{P}_{adopt} \,|u_{p,p'} = 0, y_{p,p'} = 1\}$;
14 $\quad\quad FS_p^{<right>} \Leftarrow \min_{p' \in \mathcal{P}^{p,<right>}_{adopt}} \{\gamma_{p'} - \gamma_p\}$;
15 $\quad$ **end**
16 $\quad$ **for** $p \in \mathcal{P}_{adopt}, p' \in \mathcal{P}_{adopt}/\{p\}$ **do**
17 $\quad\quad$ **if** $y_{p,p'} = 1$ *and* $\gamma_{p'} - \gamma_p = FS_p^{<right>}$ **then**
18 $\quad\quad\quad y^{(1)}_{p,p'} \Leftarrow 1$;
19 $\quad\quad$ **end**
20 $\quad$ **end**
21 **end**

Besides the channel spacing optimization model, we present methods to implement the traditional fixed channel spacing strategy and candidate channel spacing strategy,

Algorithm 4.2: The second-nearest neighbor channel

Input : $\boldsymbol{y}^{(1)}, \mathcal{P}_{adopt}, \boldsymbol{y}$
Output: $\boldsymbol{y}^{(2)}$

```
Initialize y^(2) ⇐ 0;
for p ∈ P_adopt, p' ∈ P_adopt/{p} do
    if y_{p,p'} = 1 then
        if ∃ p'' ∈ P_adopt/{p, p'} that satisfies y^(1)_{p,p''} = 1 and y^(1)_{p',p''} = 1 then
            y^(2)_{p,p'} ⇐ 1;
        end
    end
end
```

which are implemented by adding the following constraints into (`Phase 4`). The candidate channel spacing set is denoted as $\mathcal{H}$. Here, we call CSO as the optimization of the LP model, FIX as fixed channel spacing strategy, CAN as the candidate channel spacing strategy. In addition, CAN(optimized) uses the same objective function of CSO, while CAN(random) and FIX use no objective function.

- **FIX**: Each channel follows a fixed channel spacing h, $h \in \mathcal{H}_{FIX}(|\mathcal{H}_{FIX}| = 1)$. For the networks that support lightpath using different FSs, we force the small bandwidth channel to follow an integer times of the channel spacing h to keep a paradigm similar to WDM. Thus, for any $p \in \mathcal{P}_{adopt}, p' \in \mathcal{P}_{adopt}/\{p\}$,

$$0 \leq (f_p - f_{p'} - h)u_{p,p'} \cdot y^{(1)}_{p,p'} \leq (n_{p,p'} - 1) \cdot h. \tag{4.14}$$

$$1 \leq n_{p,p'} \leq |\mathcal{T}_B|, \qquad n_{p,p'} \in \mathbb{N}^+. \tag{4.15}$$

  Here, $|\mathcal{T}_B|$ is the number of bandwidth type B_t of transceiver set $\mathcal{T}$.

- **CAN(opt)**: We allow the channel spacing $f_p - f_{p'}$ to vary among the interval $[\inf(\mathcal{H}), \sup(\mathcal{H})]$ if the channel of p' is the nearest neigbor channel of p. Thus, for any $p \in \mathcal{P}_{adopt}, p' \in \mathcal{P}_{adopt}/\{p\}$,

$$0 \leq (f_p - f_{p'} - \inf(\mathcal{H}))u_{p,p'} \cdot y^{(1)}_{p,p'} \leq \sup(\mathcal{H}) - \inf(\mathcal{H}) \tag{4.16}$$

- **CAN(random)**: Similar to CAN(optimized), we allow the channel spacing $f_p - f_{p'}$ to vary among the set $[h_p, \sup(\mathcal{H})]$ if the channel of p' is the nearest neigbor channel of p, where h_p is a random value in the set $\mathcal{H}$. Thus, for any $p \in \mathcal{P}_{adopt}, p' \in \mathcal{P}_{adopt}/\{p\}$,

$$0 \leq (f_p - f_{p'} - h_p)u_{p,p'} \cdot y^{(1)}_{p,p'} \leq \sup(\mathcal{H}) - h_p \tag{4.17}$$

4.3.4 Tuning SNR margin

Finally, we deal with the excessive SNR margin. We create a control loop and decrease the preserved SNR margin M_p such that SNR margin requirement (**C1***) still holds

when generating the candidate lightpath but with the slack parameter M_p, $p \in \mathcal{P}$. With such a slack parameter M_p, all lightpaths will be reoptimized, namely the network starts a new provisioning from `Phase 1` to `Phase 4`. By using the slack parameter M_p rather than $\mathcal{X}_p^{worst}$, we can iteratively decrease the overestimation of SNR margin to the just-enough level. In case there is a lightpath after `Phase 4` that cannot satisfy the QoT in Eq. (4.6), this loop will stop and the algorithm terminates. For simplicity, we set a gradient step of 0.5 dB. Normally, at most six iterations are observed in our simulations.

4.4 Heuristic for throughput maximization problem

In this section, we devise a sequential loading algorithm to efficiently solve the throughput maximization problem in Sec. 4.2.2. The baud-rate optimization is also incorporated.

According to the common sense, we can increase the provisioning capacity between (s, d) by using the following options, i) upgrade the transmission mode of the working lightpath, ii) adjust the baud-rate or the route of the working lightpath, iii) establish a new lightpath directly. We denote by Δ_{TH}^{mod}, Δ_{TH}^{trans}, and Δ_{TH}^{new} the bit-rate gain of these three options, respectively. According to the adopted GN model in [66], option i) increases the bit-rate without incurring additional NLI to other lightpaths, which is regarded as the first choice. Options ii) and iii) both degrade the QoT of other existing lightpaths. To reduce the extra interference from the new lightpath, we give priority to option ii) and then choose option iii).

Based on the aforementioned discussion, we explain the lightpath provisioning algorithm in `Algorithm 4.3`. The main idea is to sequentially increase the bit-rate demand until the provisioning capacity cannot satisfy it. Specifically, in line 1, we manually set the throughput increment Δ_{TH} (25 Gbps is used). From lines 3 to 14, we try to increase the provisioning capacity to satisfy the bit-rate demand of node pair (s, d) by sequentially using options i), ii), and iii). Specifically, in line 5, we use option i) to increase the provisioning traffic. Then, either option ii) or iii) is adopted if the provisioning capacity is smaller than the bit-rate demand, as shown from lines 6 to 9. Finally, the algorithm terminates if the maximum provisioning capacity is smaller than the bit-rate demand, as shown in line 11. It should be noted that the different network traffic loads are implemented by restricting the available channel indexes *ch* when establishing a new lightpath or adjusting the channel position.

4.5 Simulation results

In this section, we use numerical simulations to verify the throughput improvement by optimizing channel spacing and using just-enough SNR margin. First, we compare the throughput difference between just-enough SNR margin and excessive SNR margin in single baud-rate networks. The comparison of channel spacing strategies *FIX*, *CAN(opt)*, *CAN(random)*, and the proposed *CSO* is also made in terms of throughput. Next, we investigate the throughput difference in flexible baud-rate networks lever-

Algorithm 4.3: Sequential loading algorithm for throughput maximization

Input : $G(V, E), \hat{\boldsymbol{D}}, \mathcal{T}, \mathcal{M}, W_{cur}, W, \mathcal{P}, \mathcal{C}, \beta_{s,d,k,l}$
Output: TH, $\mathcal{P}_{adopt}$

1 $TH \Leftarrow 0$, $\Delta_{TH} \Leftarrow 25$ Gbps, Terminate $\Leftarrow$ false;
2 **while** *!Terminate* **do**
3 **for** *Node pair* (s, d) **do**
4 Calculate current provisioning capacity $T_{s,d}$;
5 Option i): upgrade transmission mode m for existing lightpaths to obtain Δ_{TH}^{mod};
6 **if** $T_{s,d} + \Delta_{TH}^{mod} < (TH + \Delta_{TH}) \cdot \hat{D}_{s,d}$ **then**
7 Try either one of the following:
8 Option ii): adjust route k, baud-rate R, or move the channel ch to gain Δ_{TH}^{trans} ;
9 Option iii): establish a new lightpath to gain Δ_{TH}^{new};
10 **if** $T_{s,d} + \Delta_{TH}^{mod} + max(\Delta_{TH}^{new}, \Delta_{TH}^{trans}) < (TH + \Delta_{TH}) \cdot \hat{D}_{s,d}$ **then**
11 Go to line 20 to terminate the algorithm;
12 **end**
13 **else**
14 Upgrade the lightpaths of options ii) and iii) into lightpath set $\mathcal{P}_{adopt}$;
15 **end**
16 **end**
17 **end**
18 $TH = TH + \Delta_{TH}$;
19 **end**
20 Output TH and the lightpath set $\mathcal{P}_{adopt}$;

aging just-enough SNR margin provisioning and CSO. Finally, we investigate the impact of power setting for different channel spacing strategies in terms of the network throughput.

4.5.1 Simulation setup

The simulations use three network topologies, including 4-node ring (400 km per link), Cost239 network (11 nodes, 52 links)[68], and NSF network (14 nodes, 44 links)[68]. It should be noted that the NSF network are scaled with a factor of 0.5 to guarantee the node pair with the longest shortest path can be transmitted. To guarantee that the ILP models in `Phase 2` and `Phase 3` are solvable within a reasonable time, we assume that the available spectrum resource per link of 4-node ring is F = 750 GHz (W = 60 FSs). While in the mesh network, we assume the available spectrum resource is F = 3,000 GHz (W = 240 FSs). Other network parameters are stated as follows. The network traffic load is varied with the available spectrum resources, W_{cur} from 20%$\times W$ to 100%$\times W$. The number of candidate routes K equals 10. Similar to the prior

studies[62, 139, 149], we adopt the widely used assumption of uniform traffic for the normalized demand matrix, i.e., $\hat{D}_{s,d} = \frac{1}{n \cdot (n-1)}$.

Our simulations run on an Intel Core PC with 3.6 GHz CPU and 64 GB RAM. Specifically, the LP/ILP models and heuristic algorithm are solved with Gurobi 9.0 and MATLAB 2017a. For each LP/ILP model, we set the optimality gap of 5% to guarantee the computational efficiency. The typical single-mode fiber is assumed for physical layer calculation, i.e., fiber attenuation ratio α=0.2 dB/km, second order dispersion coefficient $|\beta_2|$=21.7 ps^2/km, frequency of optical signal ν = 192.5 THz, and fiber nonlinear coefficient γ=1.3 (W·Km)$^{-1}$. For the optical amplifiers, the noise figure n_{sp} = 5 dB and L_{span}=100 km. The PSD for all transceivers is assumed with a constant 25 μW/GHz, which is slightly larger than the power calculated by the LOGON strategy (15.3 μW/GHz among 3,000 GHz). The impact of different PSD settings will be illustrated in the simulations. In this study, we have adopted four different MFs (PM-QPSK, PM-16QAM, and PM-64QAM, PM-256QAM) and at most five FECs overhead for each MF so that we can obtain the bit-rate from 50 to 375 Gbps with a step of 25 Gbps[63]. Besides, the SNR threshold of each transmission mode has been individually superimposed with a small and fixed margin of 2 dB compared to the data in [63] in order to avoid the unexpected electrical noise that has not been considered. Three baud-rates are also assumed[104, Table 3]: 16, 32, and 64 Gbaud. The SNR threshold is assumed to be the same for different baud-rates.

For ease of illustration, we use JP and EP to denote the just-enough SNR margin provisioning and traditional excessive SNR margin provisioning.

4.5.2 JP vs. traditional EP in single baud-rate networks

First, we compare the throughput difference between JP and EP for networks adopting single baud-rate (16 Gbaud). The latter is implemented by breaking the iterative loop of Fig. 4.3. The results from different lightpath provisioning algorithms are compared in order to validate the performance of JP, including the heuristic in `Algorithm 4.3`, and the ILP models in `Phase 2` and `Phase 3`.

JP(CSO) vs. traditional EP(CSO) in small network

Figures 4.4 illustrates the throughput, counts the number of adopted transmission modes, and shows the margin as well as the channel spacing when network traffic load increases. JP outperforms the EP under the resource over-provisioning scenarios in terms of the throughput (network traffic load between 20% and 80% in Fig. 4.4(a)). The observed increase in throughput could be attributed to the more usage of high-order transmission modes with high spectral efficiency (H-16QAM) (Fig. 4.4(b)). Another observation in Fig. 4.4(a) is that the relative throughput gain of JP decreases with the network traffic load. This phenomena could be explained using the conclusion of [117, Sec. 5 and 6] that the fraction ratio of achievable capacity is approximately linearly with the overestimation of network SNR margin. As network traffic load increases, less SNR margin overestimation (Fig. 4.4(c)) between resource over-provisoning and

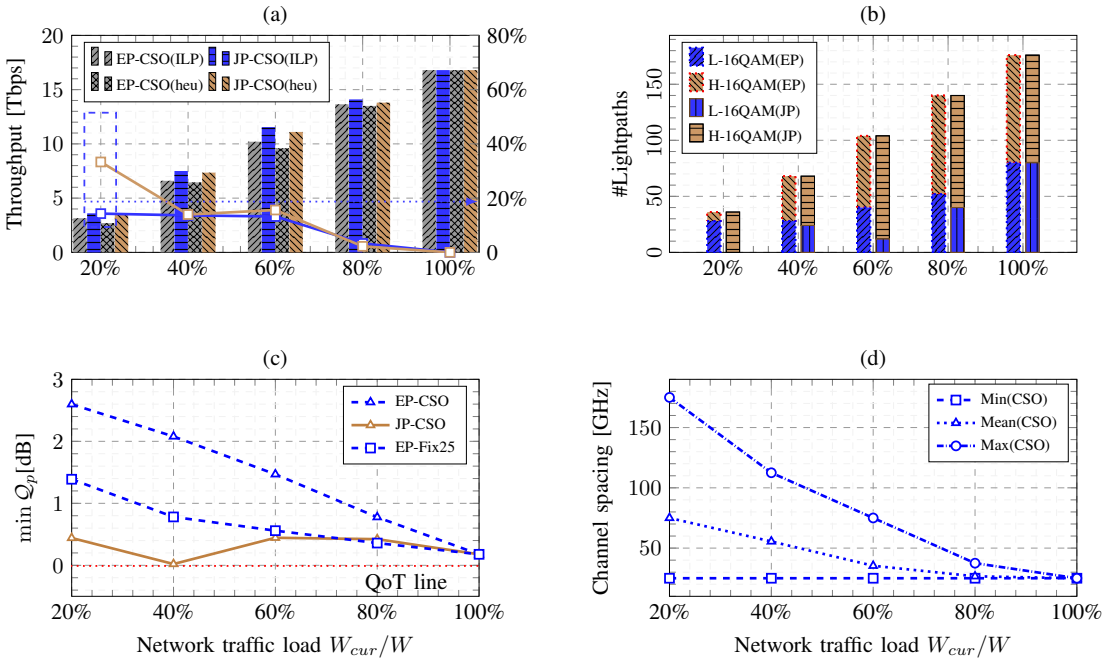

Figure 4.4: *Comparison of JP and EP with CSO for 4-node ring. (a) Throughput vs. network traffic load. The relative gain ratio between JP and EP is also plotted on right y-axis. (b) Adopted transmission modes vs. network traffic load. L-16QAM includes 16QAM with FEC 0.62 and 0.72, while H-16QAM includes 16QAM with FEC 0.82 and 0.92. The spectral efficiency of H-16QAM is higher than L-16QAM; (c) Minimum QoT metric vs. network traffic load; (d) Channel spacing statistics of CSO.*

resource under-provisoning means less throughput gain (Fig. 4.4(a)). It should be also mentioned that the higher throughput of JP is achieved by using the high spectral efficiency transmission mode without increasing the number of lightpaths (Fig. 4.4(b)). However, it cannot be ruled out that in some special cases, the heuristic algorithm may generate extra lightpaths even under the same network traffic load to obtain the higer throughput. We will point out the cost-effective performance ratio in Sec. 4.5.2. In Fig. 4.4(d), we find that the channel spacing statistics value (minimum channel spacing, average channel spacing, and maximum channel spacing) varies with the different network traffic loads. Moreover, the traditional channel spacing with one guard band cannot adopt the large channel spacing over than 37.5 GHz, which is a suggested value of CSO. The throughput difference between different channel spacing strategies will be presented in the following.

JP(FIX, CAN, CSO) vs. traditional EP(CSO) in large networks

Next, we investigate the throughput of different channel spacing strategies. $\mathcal{H} = \{37.5\}$ GHz for FIX, $\mathcal{H} = \{25, 37.5, 50\}$ GHz for CAN(opt) and CAN(random).

In Fig. 4.5(a), the largest throughput gain ratio among the existing channel spacing strategies (FIX, CAN, CSO) is obtained by CSO, 50% at the network traffic load of 20%.

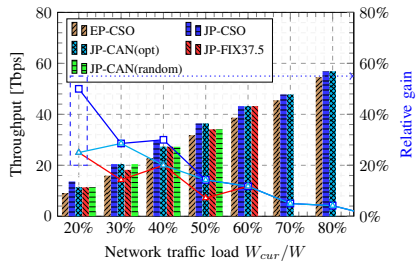

(a) Throughput (NSF)

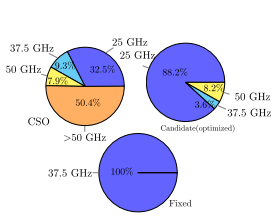

(b) Channel spacing under 20% load (NSF)

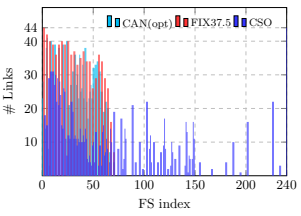

(c) Link spectrum usage (20% load) (NSF)

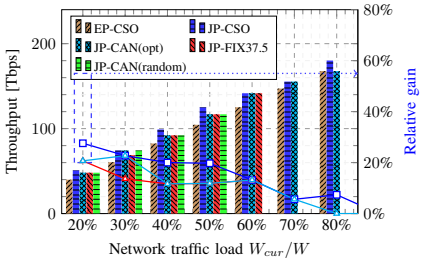

(d) Throughput (Cost239)

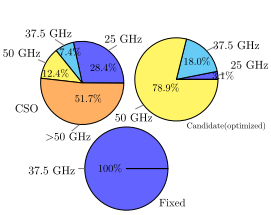

(e) Channel spacing under 20% load (Cost239)

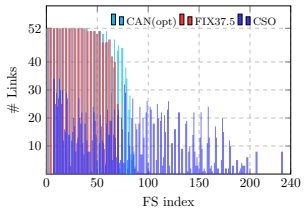

(f) Link spectrum usage (20% load) (Cost239)

Figure 4.5: *Throughput with different channel spacing strategies.*

This is expected because CSO uses no artificial constraint of channel spacing and allows the transceiver to use the idle spectrum resources to enhance the physical layer performance and consequently upgrade the high-order transmission mode. To gain more insight, we plot the number of adopted channel spacing statistics in Fig. 4.5(b) as well as the link statistics on each FS in Fig. 4.5(c). We see that the suggested channel spacing of $\geq$50 GHz should be over than 50%, which is out of the scope of the other strategies (FIX and CAN). The above findings can be also observed in the Cost239 network.

In addition, we analyze the cost-effective factor of the feedback tuning algorithm. Taken Cost239 network as an example, the relative increase of lightpaths and throughput from EP to JP are shown in Fig. 4.6. The cost ratio varies from -1% to 5%, while the throughput gain ratio varies from 7% to 27%. However, the throughput gain ratio is always higher than the cost ratio, which reveals that the JP is more cost-effective.

4.5.3 JP vs. traditional EP in multiple baud-rates networks

Next, we study the throughput of different baud-rates and compare the baud-rate selection policies (Fig. 4.7). The comparison of different channel spacing strategies is also made (Table 4.1).

Different single baud-rates

The network throughput of three different single baud-rate are illustrated in Fig. 4.7(a). While a larger throughput (295 Tbps) can be achieved by the 64 Gbaud at 100% load, the

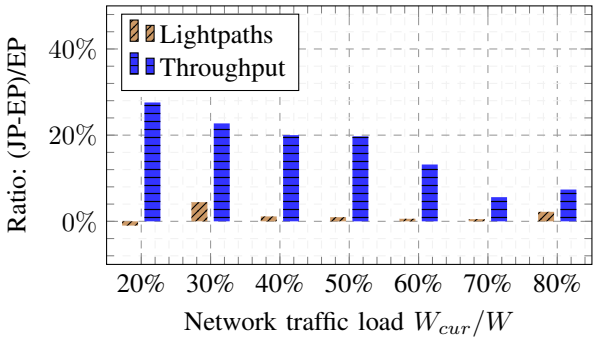

Figure 4.6: *Cost-effective ratio of JP-CSO and EP in Cost239 network.*

same throughput (210 Tbps) is observed for the 16 and 32 Gbaud. It is expected because the spectral efficiency of 64 Gbaud transceiver is 2.7 bps/Hz, while it is 2.0 bps/Hz for both 16 and 32 Gbaud (50 Gbps for 16 Gbaud on 25 GHz, 100 Gbps for 32 Gbaud on 50 GHz, 200 Gbps for 64 Gbaud on 75 GHz [63, 104].). An interesting observation in Fig. 4.7(b) is that the maximal absolute gain (33/22/19.5 Tbps) is achieved in the medium network traffic load for these single baud-rate networks. It can be explained by using the previous finding on throughput gain ratio in Figs. 4.4 and 4.5. On one hand, the available spectrum resources increase with the network traffic load. On the other hand, the relative throughput gain ratio (or relative net spectral efficiency gain ratio) decreases (see Figs. 4.5(a) and (d)). Therefore, their product, namely absolute throughput gain, could achieve the maximum when the network traffic load is medium.

Baud-rate selection strategies (low baud-rate first, high baud-rate first, vs. random baud-rate)

Figure 4.7(c) shows the network throughput using different baud-rate selection policies. The utilization of prioritizing the higher baud-rate (higher baud-rate means higher spectral efficiency in this case) has a larger throughput performance. Such a result gives a guideline for the efficient utilization of the flexible baud-rates to achieve the higher throughput.

JP(FIX, CAN, CSO) vs. traditional EP(CSO)

We compare the throughput of different channel spacing strategies in networks supporting flexible baud-rates. Table 4.1 illustrates the relative throughput gain ratio of different channel spacing strategies. The performance of CAN (opt) is closer to the proposed CSO if the size of candidate channel spacing set increases. Moreover, the FIX and CAN (random) can be applied to increase the network throughput only under the scenarios of low network traffic load. These results show the advantage of CSO with a larger throughput gain ratio and with more network traffic load scenarios.

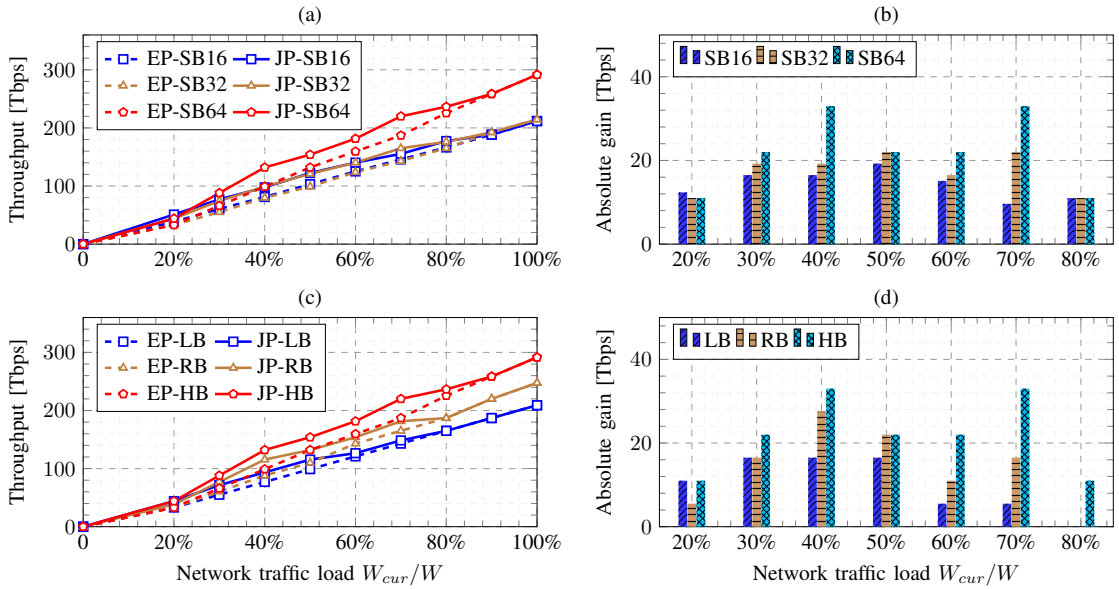

Figure 4.7: *Throughput in Cost239 network with different baud-rate configurations. (a) Different single baud-rates (SB16: only single 16 Gbaud); (b) Absolute throughput gain of JP with single baud-rate; (c) Different selection strategies of flexible baud-rates (LB: low baud-rate first. RB: random baud-rate. HB: high baud-rate first); (d) Absolute throughput gain of JP with different selection policies.*

Table 4.1: *Relative throughput gain ratio in Cost239 network with single baud-rate (above) and with flexible baud-rates (below)*

Single baud-rate (32 Gbaud)							
Load	FIX		CAN(random)		CAN(opt)		CSO
	{50}	{100}	{12.5,...,50}	{12.5,...,100}	{12.5,...,50}	{12.5,...,100}	
20%	17%	17%	17%	17%	17%	17%	33%
40%	0%	21%	0%	10%	0%	21%	24%
60%	0%	-	0%	-	0%	13%	13%
80%	0%	-	0%	-	0%	7%	7%
100%	0%	-	0%	-	0%	0%	0%
Flexible baud-rates (16, 32, and 64 Gbaud)							
Load	FIX		CAN(random)		CAN(opt)		CSO
	{75}	{150}	{12.5,..,75}	{12.5,..,150}	{12.5,..,75}	{12.5,..,150}	
20%	24%	32%	24%	24%	20%	28%	36%
40%	10%	-	-	-	1%	14%	14%
60%	-	-	-	-	6%	14%	14%
80%	-	-	-	-	0%	0%	4%
100%	-	-	-	-	0%	0%	0%

- It signifies the channel spacing strategy is infeasible due to the limited spectrum resources.

4.5.4 Impact of physical layer parameters

This section discusses the impact of different initial PSDs on channel spacing optimization. In Fig. (4.8), we see that the the throughput increases with the initial PSD in the linear regime where the PSD is lower than 15 μW/GHz, and decreases in the nonlinear regime where the PSD exceeds 15 μW/GHz. The higher throughput can be maintained if we adopt the CSO. Such results imply that the channel spacing optimization can tolerate a higher PSD where the NLI increases.

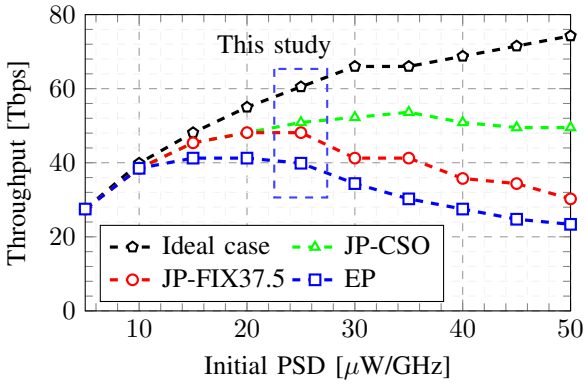

Figure 4.8: *Throughput vs. different initial PSDs under 20% network loads in Cost239 network (PSD=25μW/GHz is adopted in the simulations). "Ideal case" means no NLI in the networks.*

4.6 Conclusion

In this chapter, we studied the problem of *throughput maximization leveraging just-enough SNR margin provisioning and channel spacing optimization*. Based on the analysis of the lightpath's parameters, we developed an iterative feedback tuning algorithm to provide a just-enough SNR margin. We also established an ILP model and a heuristic algorithm to maximize the network throughput with using flexible baud-rate. Furthermore, we devised an LP model that enables to optimize the channel spacing for each lightpath.

Through the simulations, we verify the throughput improvement of just-enough SNR margin provisioning compared to the conventional excessive SNR margin provisioning. The relative gain reaches the maximum (over 20%) under low network traffic load, while the absolute gain reaches the maximum under medium network traffic load. These observations highlight that the importance of just-enough SNR margin provisioning under low and medium network traffic load. Compared to the existing channel spacing strategies (fixed, random, candidate), our channel spacing optimization also demonstrates a clear advantage on two aspects: (1) it can be applied with more resource over-provisioning scenarios; (2) it has a larger relative throughput gain ratio. We also find that the higher baud-rate with larger spectral efficiency should be prioritized to gain a larger throughput when implementing the lightpath provisioning. Taken together, our findings highlight an important role for just-enough SNR margin

provisioning and channel spacing optimization in FONs with flexible baud-rates.

Chapter 5

Revenue Maximization Leveraging Elastic Service Provisioning

Contents

5.1 Introduction

According to recent traffic reports, network traffic (fueled by network services like video on demand, file sharing, online gaming, and video conferencing) is growing exponentially on today's Internet[36]. A solution to accommodate the tremendous traffic growth is using the FON[49]. Network traffic in FONs is transported from the source node to the destination node along a selected lightpath. An adequate amount of spectrum resources should be also allocated to establish a lightpath, e.g., multiple continuous FSs. With the advance of the commercially available ADCs and DACs, advanced MFs (e.g., traditional MF, FEC, probabilistic shaping, and TDHMF) are also available for these channels to reach the theoretical maximum spectral efficiency defined by Shannon theory[18]. The opportunity offered by the flexibilities of routing, on-demand FS allocation, and advanced MF, allows the network to reach the maximum capacity. However, the capacity crunch problem will probably occur in the near future[12], or when optical equipment is temporarily unavailable[112]. We are expected to use the current network infrastructure for a while before the new optical fibers (e.g., multi-core, multi-mode), new transmission bands (e.g., O, E, S, C, and L band), and new optical equipment (e.g., the supported amplifiers, and tunable lasers) are deployed[12, 135]. With such limited resources, the network will become heavily loaded and fail to satisfy all requests, which potentially limits the revenue of a network.

The services in today's networks have different requirements (e.g., latency tolerance, and bandwidth) and characteristics (revenue or importance). Luckily, some services are sensitive to the bandwidth and latency, while others services are *elastic* and operational when degrading the bit-rate[109, 112, 119], e.g., a lower resolution video or a longer file transfer time. In addition, the video services still dominate the majority of network traffic (about 82% predicted by [86]). We use the metric of revenue to denote the QoS parameter when the service is degraded throughout this study. Thus, using the elastic services can release a small portion of spectrum resources, and consequently accommodating more requests, thus improving the overall network revenue. The management of such elastic services will become a key for network operators to maintain the high network revenue in case of capacity crunch. However, such a resource allocation problem becomes more difficult when incorporating the lightpath provisioning problem in FON, which is already NP-hard.

One of the greatest benefits of elastic services is to spare the spectrum resources. Such resources are especially important in a high load scenario, in which the revenue will be lost if the network fails to provision a lightpath for the coming requests. The process of releasing spectrum resources requires network operators to reconfigure the existing lightpaths with different techniques, such as rerouting and spectrum retuning. The two techniques differ in cost, speed, service quality, and hardware implementation [25]. For example, traffic interruption is a well-known issue for rerouting, while it can be avoided by spectrum retuning, such as *make-before-break*, *hop-tuning*, and *push-and-pull* [25]. In order to make full play of the network reconfiguration, an intuitive method is to simultaneously use these two techniques. However, it is time-consuming, costly, and difficult for network operators. The first question arises that *1) how to reconfigure the*

network to maintain a high revenue when part of these reconfiguration techniques is available, e.g., the spectrum retuning technique that ensures uninterrupted communication. In addition, network reconfiguration seems only desired for revenue improvement in a high traffic load scenario, while it is too complex to operate in a low network load scenario for the frequent reconfiguration and little revenue improvement. Thus, another question arises, *2) when to reconfigure the existing lightpaths in order to avoid the frequent network reconfiguration*. Recently, the statistical approach acts as a new paradigm to investigate the physical layer resources[38]. It assumes an unloaded network initially, and progressively loads the traffic, which is regarded as a reliable and powerful approach to obtain the *progressive network load* and statistically evaluate the various load-dependent metrics (network throughput, link status, and network blocking probability). Therefore, the *progressive* network loads offered by this approach are also promising to evaluate the load-dependent revenue performance of elastic requests. However, as far as we know, the current studies using the progressive network load have never incorporated the network reconfiguration. To fill this gap, we will propose an auto-degrading scheme and investigate how to use a progressive load to statistically assess the network performance and address the above two questions, namely how to and when to reconfigure the existing lightpaths.

In short, this chapter will investigate how to manage the elastic services in order to maximize the network revenue of FON with various flexibilities. Both the scenarios of static and progressive network load are to be explored. The main contributions of this chapter are summarized as follows:

- First, in a static FON that supports the variable MF, FEC, and baud-rate, we formulate the lightpath provisioning problem for the elastic services. The objective is to maximize the total revenue of a network by leveraging elastic services. Then, we design an ILP model. An efficient decomposition method is also proposed.
- Next, we propose an auto-degrading provisioning scheme to determine the progressive network load and incorporate different network reconfiguration strategies in an effort to maximize the revenue[38, 63, 115], thus addressing the issue of when and how to reconfigure the network. This algorithm consists of a normal operation to progressively load the lightpath, as well as a reconfiguration operation to automatically reconfigure the network. Additionally, several quantitative metrics (network revenue and total accepted requests) are provided to evaluate how much performance gain can be achieved by different network reconfiguration strategies.
- Last, through numerical simulations, we validate the revenue improvement of elastic services. Besides, in our example network, we make the following observation: the spectrum retuning is more beneficial than rerouting when choosing the reconfiguration strategies.

The rest of this chapter is organized as follows. In Sec. 5.2, we present the problem of lightpath provisioning of revenue maximization leveraging elastic service, and formulate it as a mathematical model. A decomposition method is also proposed. Then, we propose an auto-degrading provisioning scheme to automatically trigger the net-

work reconfiguration in Sec. 5.3. Illustrative numerical results are presented in Sec. 5.4. Finally, Sec. 5.5 concludes this chapter.

5.2 Problem Statement

In this section, we present the lightpath provisioning problem of *revenue maximization leveraging elastic service*. Different flexibilities can be adopted by the lightpath in FONs, including MF, FEC, baud-rate, as well as the elastic service level requirement. Next, we present the ILP model with the objective of revenue maximization. Additionally, the decomposition method is presented.

5.2.1 Problem statement

An FON is denoted by a graph $G(V, E)$. Each node $v \in V$ represents an optical cross connects (OXC). Each link $e \in E$ represents two optical fibers vu and $vu(u, v \in V)$ that carry traffic in opposite directions. The spectrum resource of each fiber is denoted as F FSs with a bandwidth of 12.5 GHz per FS, $F \in \mathbb{N}^+$.

In the FON, a request i needs a lightpath from the source node s_i to the destination node d_i, and uses several contiguous FSs B_i along that lightpath[26]. To service this request, the provisioned capacity C_i of such lightpath should be no smaller than the required bit-rate R_i, i.e., $C_i \geq R_i$. The provisioned capacity depends on the baud-rate, MF, and FEC. The combination of MF and FEC is named as *transmission mode* in this study. Each transmission mode has the maximum transmission reach D_m for the lightpath. Once the request i is served, its revenue η_i will be collected by network operators. When network congestion occurs, blocking and revenue loss could be caused due to insufficient spectrum resources.

To alleviate this issue, we introduce the *elastic request*. The difference between elastic request and conventional request lies in that the former can select a degraded bit-rate from a given set $\mathcal{R}_i$ ($|\mathcal{R}_i| \geq 2$, e.g., $\mathcal{R}_i = \{R_i, 0.8R_i, 0.5R_i\}$), while the latter can only select one rigid bit-rate R_i ($|\mathcal{R}_i| = 1$). If the elastic request is serviced by a bit-rate lower than R_i, we call *the request is degraded or the QoS decreases*. Throughout this study, we use the terms "service level" and "QoS level" interchangeably. All degraded service levels are stored in the service level set $\mathcal{L}_i$ ($|\mathcal{L}_i| = |\mathcal{R}_i|$), which are all operational for request i. Recall that the revenue could decrease when the request is degraded, thus we introduce the service level-dependent revenue $\eta_{i,l}$ ($\eta_{i,l} \leq \eta_i, l \in \mathcal{L}_i$), which mainly depends on the final serviced bit-rate $R_{i,l}$ ($R_{i,l} \leq R_i, l \in \mathcal{L}_i$).

The objective of this problem is to maximize the total revenue of all requests. Here, we see that this problem consists of service level, routing, transmission mode, baud-rate and spectrum assignment (SL-RMBSA).

5.2.2 ILP model

Given a set of elastic requests I, we aim to maximizing the total revenue of these requests. The objective is written as follows,

$$\begin{aligned} & \max \quad \sum_{i \in I} \eta_i \quad \texttt{(SL-RMBSA)} \\ \textbf{\textit{s.t.}} \quad & (5.1) - (5.6) \end{aligned}$$

where η_i is the revenue of elastic request i. For the sake of readability, we use $\forall i$, $\forall uv$, $\forall m$, $\forall b$, $\forall l$ to denote $\forall i \in I$, $\forall uv \in E$, $\forall m \in \mathcal{M}$, $\forall b \in \mathcal{B}$, $\forall l \in \mathcal{L}_i$.

Parameters

- $G(V, E)$: optical network with node sets V and link set E.
- $\mathcal{N}(v)$: neighbor set of node v.
- uv and $vu \in E$: two opposite optical fibers that connect node v and u. $u \in \mathcal{N}(v)$.
- D_{uv}: span length of link uv ($\times$100 km/span).
- $s_i \in V, d_i \in V/\{s_i\}$: source node and destination node of request i.
- $\mathcal{L}_i$: service level set of elastic request i, $l \in \mathcal{L}_i$.
- $\mathcal{R}_i$: bit-rate set of elastic request i, $R_{i,l} \in \mathcal{R}_i$.
- $\eta_{i,l}$: revenue of elastic request i at service level l.
- $\mathcal{M}$: transmission mode set, $m \in \mathcal{M}$.
- D_m: transmission reach of transmission mode m.
- $\mathcal{B}$: baud-rate set, $b \in \mathcal{B}$.
- B_b: number of required FSs of a certain baud-rate b.
- $C_{m,b}$: capacity of the lightpath at the baud-rate b and transmission mode m.

Variables

- $\delta_{i,l}$: equals 1 if the request i the chooses l-th service level, 0 otherwise.
- $\beta_{i,m,b}$: equals 1 if the (lightpath of) request i chooses transmission mode m and baud-rate b, 0 otherwise.
- x^i_{uv}: equals 1 if the request i uses the fiber link uv, 0 otherwise.
- γ_i: starting FS index of request i;
- $u_{i,j}$: equals 1 if the starting FS index of request i is lower than request j, 0 otherwise.
- $y_{i,j}$: equals 1 if requests i and j share a common link, 0 otherwise.
- B_i: number of allocated FSs of request i.

- C_i: provisioned capacity of request i.
- η_i: revenue of request i.

Constraints

- *Network flow constraint*: Here, we assign the route for each request by using the flow-based approach rather than path-based approach[10]. The flow-based approach ensures all possible routes can be generated for the lightpath. The flow of each request i comes from the source node s_i and ends at destination node d_i. While on the rest nodes, the incoming flow equals the outgoing flow.

$$\sum_{v \in \mathcal{N}(u)} x_{uv}^i - \sum_{v \in \mathcal{N}(u)} x_{vu}^i = \begin{cases} 1, & u = s_i \\ -1, & u = d_i \\ 0, & u \in V/\{s_i, d_i\}. \end{cases}, \forall i \tag{5.1}$$

- *One baud-rate and one transmission mode constraint*: Each lightpath can flexibly choose a baud-rate and transmission mode. We use Eq. (5.2a) to guarantee only one transmission mode and one baud-rate is used by the lightpath. Eq. (5.2b) obtains the occupied FSs of each lightpath, while (5.2c) obtains its provisioned bit-rate.

$$1 = \sum_{m \in \mathcal{M}, b \in \mathcal{B}} \beta_{i,m,b}, \qquad \forall i \tag{5.2a}$$

$$B_i = \sum_{m \in \mathcal{M}, b \in \mathcal{B}} B_b \beta_{i,m,b}, \qquad \forall i \tag{5.2b}$$

$$C_i = \sum_{m \in \mathcal{M}, b \in \mathcal{B}} C_{m,b} \beta_{i,m,b}, \qquad \forall i \tag{5.2c}$$

- *Spectrum non-overlapping constraint*: Eq. (5.3a) determines whether the requests i and j share a common link. Eq. (5.3b) determines the relative spectrum order of the requests i and j, i.e., either i is on the left or j is on the left. Eq. (5.3c) guarantees the requests are spectrum non-overlapping if they share a common link.

$$x_{uv}^i + x_{uv}^j - 1 \leq y_{i,j}, \qquad \forall uv, \forall i \neq j \tag{5.3a}$$

$$u_{i,j} + u_{j,i} = 1, \qquad \forall i < j \tag{5.3b}$$

$$\gamma_i + B_i + (y_{i,j} + u_{i,j} - 2) \cdot F \leq \gamma_j, \qquad \forall i, \forall j \tag{5.3c}$$

- *Resource limit constraint*: Eq. (5.4) guarantees the spectrum of each lightpath is within the available spectrum resources.

$$\gamma_i + B_i - 1 \leq F, \qquad \forall i \tag{5.4}$$

- *Transmission reach constraint*: Eq. (5.5) requires the length of the chosen lightpath is shorter than the maximum reach of the adopted transmission mode.

$$\sum_{uv \in E} x_{uv}^i D_{uv} \leq \sum_{m \in \mathcal{M}, b \in \mathcal{B}} D_m \beta_{i,m,b}, \qquad \forall i \tag{5.5}$$

- *QoS level requirement*: Eq. (5.6a) guarantees that each request needs to adopt one and only one service level. Its revenue is calculated by Eq. (5.6b). Eq. (5.6c) guarantees the transmission capacity of the lightpath should satisfy the required bit-rate. Eq. (5.6d) restricts that the serviced bit-rate is monotonically decreasing for the requests on the same node pair. By specifying a service-level order for elastic requests, we can reduce the solution space and accelerate the solution. The requirement is that these requests should be sorted according to their service levels in advance.

$$1 = \sum_{l \in \mathcal{L}_i} \delta_{i,l}, \qquad \forall i \tag{5.6a}$$

$$\eta_i = \sum_{l \in \mathcal{L}_i} \delta_{i,l} \eta_{i,l}, \qquad \forall i \tag{5.6b}$$

$$C_i \geq \sum_{l \in \mathcal{L}_i} \delta_{i,l} R_{i,l}, \qquad \forall i \tag{5.6c}$$

$$\sum_{l \in \mathcal{L}_i} \delta_{i,l} R_{i,l} \geq \sum_{l \in \mathcal{L}_j} \delta_{j,l} R_{j,l}. \qquad \forall \left(s_i, d_i\right) = \left(s_j, d_j\right), i < j \tag{5.6d}$$

Complexity analysis: We analyze the number of variables and constraints of the above ILP model. There are mainly three types of variables, including route-related variables x_{uv}^{i}, spectrum-related variables (γ_i, $u_{i,j}$, and $y_{i,j}$), and the flexibility-related variables ($\delta_{i,l}$ and $\beta_{i,m,b}$). Thus, the total number of these variables, $|I| \cdot (|E| + 1 + |\mathcal{M}| \cdot |\mathcal{B}| + 2|I|) + \sum_i |\mathcal{L}_i|$, will increase with the network scale and the number of requests. In addition, the number of constraints from (5.1) to (5.6) is $\mathcal{O}\left(|I| \cdot (|I| + |E|)\right)$.

5.2.3 Decomposition method

To reduce the complexity of the SL-RMBSA, we divide it into two subproblems, i.e., *SL-RMB* and *SA*. Specifically, the first subproblem solves the route, transmission mode, baud-rate, and service level assignment with the objective of maximizing the revenue. Using the obtained results, the second subproblem solves the remaining problem, i.e., spectrum assignment. Here, we present the techniques to solve the two subproblems.

SL-RMB

Before solving this subproblem, we use Yen's algorithm to pre-calculate K candidate routes for the lightpath between node pair (s, d) in order to increase the computation efficiency[141].

Parameters

- $\sigma_{uv} \in \mathbb{N}$: a small constant to restrict the available FSs of link uv in `SL-RMB`, $0 \leq \sigma_{uv} \leq F$.
- $\alpha_{i,k,uv}$: equals 1 if the k-th route of node pair (s_i, d_i) uses link uv, 0 otherwise.

Variables

- $\beta_{i,k,m,b,l}$: equals 1 if the k-th route of request i chooses transmission mode m, baud-rate b, and service level l.

Constraints

- *One route, one baud rate, and one service level constraint*: It combines the multiple constraints into one, including network flow constraints in Eq. (5.1), one baud-rate, one transmission constraint in Eq. (5.2a), and one service level constraint in Eq. (5.6a).

$$\sum_{k,m,b,l} \beta_{i,k,m,b,l} = 1, \qquad \forall i \tag{5.7}$$

- *Resource limit constraint*: This constraint plays the same role as Eq. (5.4) that restrict the spectrum usage on each link among F. Note that the exact spectrum location for each request has not been determined yet in this problem. Thus, the spectrum continuity and contiguous constraint are temporarily neglected when we use the following constraints. It should be noted that the parameter σ_{uv} in Eq. (5.8) is used to spare a small portion of redundant spectrum resources. This is used to increase the possibility of the successful spectrum assignment when considering the spectrum continuity and contiguous constraints in the next subproblem.

$$\sum_{i,k,m,b,l} B_b \alpha_{i,k,uv} \beta_{i,k,m,b,l} \leq F - \sigma_{uv}, \forall uv \tag{5.8}$$

- *Transmission reach constraint*: This constraint plays the same role as Eq. (5.5) to limit the length of each lightpath.

$$\sum_{k,m,b,l,uv} D_{uv} \alpha_{i,k,uv} \beta_{i,k,m,b,l} \leq \sum_{k,m,b,l} \beta_{i,k,m,b,l} D_m, \forall i \tag{5.9}$$

- *QoS level constraint*: This plays the same role as Eq. (5.6c), in which the provisioned capacity of each lightpath needs to satisfy its chosen service level. The service-level order in Eq. (5.6d) is also maintained by using Eq. (5.11).

$$\sum_{k,m,b,l} \beta_{i,k,m,b,l} C_{m,b} \geq \sum_{k,m,b,l} \beta_{i,k,m,b,l} R_{i,l}, \quad \forall i \tag{5.10}$$

$$\sum_{k,m,b,l} \beta_{i,k,m,b,l} R_{i,l} \geq \sum_{k,m,b,l} \beta_{j,k,m,b,l} R_{j,l}, \qquad \forall (s_i, d_i) = (s_j, d_j) \tag{5.11}$$

Objective

$$\begin{aligned} \max \quad & \sum_{i \in I} \eta_i \quad \texttt{(SL-RMB)} \\ \textbf{\textit{s.t.}} \quad & (5.7) - (5.11) \end{aligned}$$

where $\eta_i = \sum_{k,m,b,l} \eta_{i,l} \beta_{i,k,m,b,l}$.

SA

This subproblem assigns the exact spectrum position for the above lightpaths. The obtained results in SL−RMB are passed to the ILP model of SL−RMBSA. The required variables x^i_{uv}, $\delta_{i,l}$, and $\beta_{i,m,b}$ in SL−RMBSA are extracted by using the variables $\beta_{i,k,m,b,l}$. Finally, through the ILP model of SL−RMBSA, the value of the variables γ_i, $y_{i,j}$, and $u_{i,j}$ are found.

Complexity analysis: We analyze the number of variables in the decomposition method. The number of variables in the first subproblem, which mainly depends on $\beta_{i,k,m,b,l}$, is $\sum_{i \in I} |\mathcal{L}_i| \cdot K \cdot |\mathcal{M}| \cdot |\mathcal{B}|$. Meanwhile, the number of variables in the second subproblem, which mainly depends on γ_i and u_{ij}, is $\mathcal{O}(|I| + |I|^2)$.

5.3 Auto-degrading provisioning scheme for revenue maximization

The previous section has formulated an ILP model as well as the two-step decomposition method for the SL-RMBSA problem. They have the advantage of providing a global optimal result. However, these models seem only suitable for the static lightpath provisioning with a given set of requests, because they may easily cause heavy tasks of network reconfiguration when a new request comes or leaves. This section focuses on the lightpath provisioning and network reconfiguration of a progressive traffic load, in which the network only reconfigure the lightpath when a request is unable to find the satisfied spectrum resources. Besides, the advantage of the ILP model (global resource optimization) is also considered when reconfiguring the existing lightpaths.

The proposed provisioning scheme is shown in Fig. 5.1. The main idea of this framework is to sequentially add the requests. Each request can be individually treated and accepted by either the "normal operation" using a classical heuristic algorithm, or the "reconfiguration operation" using the ILP model. The sequential adding process will not terminate until a request is blocked. The request blocking occurs only when the network reconfiguration fails to provision a suitable lightpath. The aim of such reconfiguration operation is to spare the current network spectrum resources to accommodate the current request. Different algorithms in the normal operation and the reconfiguration operation will be presented in the following, respectively. Note that the operation without reconfiguration is similar to the proposed simulation framework in the existing studies [23, 63]. A minor difference consists in that our study focuses on supporting elastic request rather than the transmission capacity[63], and the process of sequential loading terminates once a request is blocked[23].

For readability, we call normal operation (NO) and reconfiguration operation (RO). Next, we present the algorithms proposed for NO and RO, respectively.

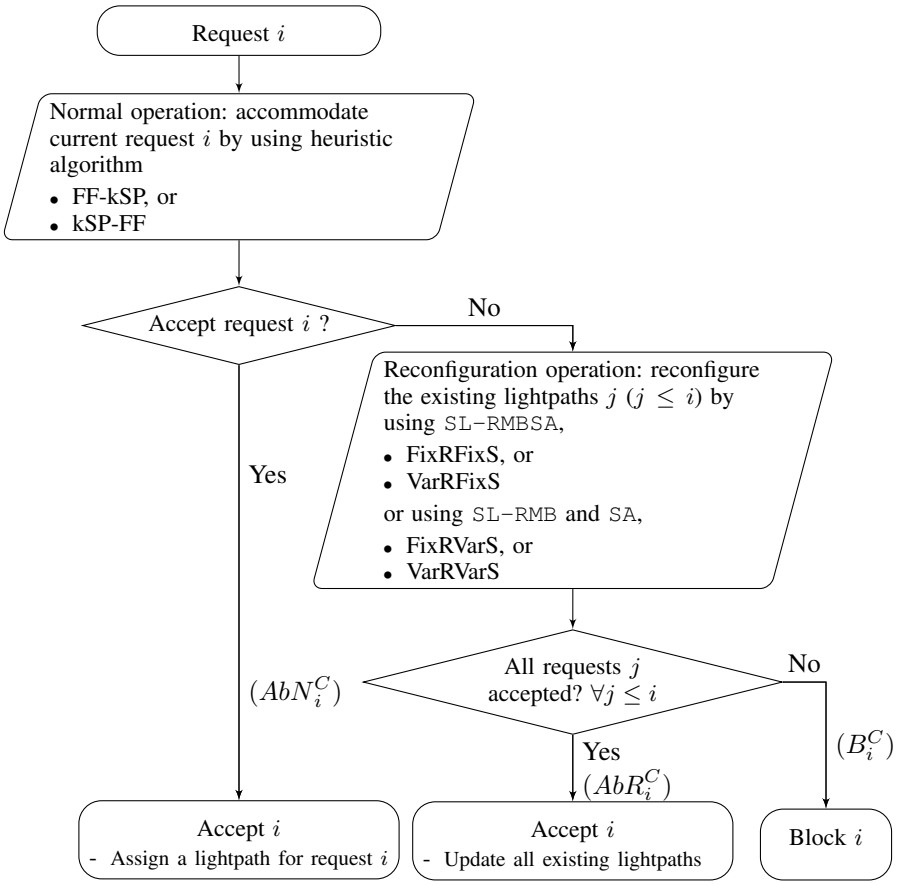

Figure 5.1: *Flowchart of the auto-degrading provisioning scheme.*

5.3.1 Algorithms in auto-degrading provisioning scheme

NO

The NO configures the current request i using the classical heuristic algorithm, such as kSP-FF or FF-kSP[26, 148]. The former priorities the shortest route and search available FSs on that route, while the latter priorities to search a given contiguous FSs on different routes.

Besides route and spectrum assignment, SL-RMBSA problem also includes the decision-making of some other parameters including service level, transmission mode, and baud-rate. This study assumes that both kSP-FF and FF-kSP select these parameters using the following order: service level from high to low, baud-rate from low to high, transmission mode from high to low. The performance comparison of different selection orders can refer to [26, 37, 132].

RO

The RO is triggered only if NO fails to provision a lightpath for the current request. This process will adjust the parameters of already provisioned or established lightpaths

j ($j < i$) in an effort to release the spectrum resources to accommodate the current request i. Thus, the parameters of route, baud-rate, transmission mode, and spectrum are to be adjusted. According to the network reconfiguration capability of rerouting and spectrum retuning, our study uses the following four network reconfiguration strategies,

- *FixRFixS*: The route, spectrum[1], and baud-rate of the existing lightpaths are all fixed. This strategy differs with the *no reconfiguration* in the algorithm employed to the current request i. For example, FixRFixS can find more routes for request i with the ILP model `SL-RMBSA`, while the kSP-FF and FF-kSP cannot.
- *VarRFixS*: Only the route of the existing lightpaths will be adjusted, while the spectrum and baud-rate are still fixed.
- *FixRVarS*: Both the spectrum and baud-rate of the existing lightpaths will be adjusted, while the route is fixed.
- *VarRVarS*: All the parameters: route, baud-rate, and spectrum could be all adjusted.

For the previous two strategies, we directly use the ILP model to maximize the revenue, while for the last two strategies, we apply the decomposition version. The reason why we adopt the decomposition method for the latter two strategies is that the computation time of `SL-RMBSA` on spectrum retuning is found to increase exponentially with the number of requests (observed from the simulations). In addition, it is worth noted that the reconfiguration algorithms in the existing studies[148] is completed by a heuristic algorithm, which may fail to globally optimize spectrum resources with respect to the maximal metrics of revenue.

5.3.2 Evaluation metrics

Similar to the existing study in [38, 63], these metrics are mainly based on statistical. The requests will be sequentially added to the network until a request is blocked. For the serviced request i, we record the cumulative network revenue η_i^C, cumulative accepted requests AbN_i^C and AbR_i^C (accepted requests by normal operation and accepted requests by reconfiguration operation, $A_i^C = AbN_i^C + AbR_i^C$), and cumulative blocking requests B_i^C ($B_i^C + A_i^C \equiv i$). These metrics are averaged by independent simulations of N^{rep} times.

5.4 Illustrative Simulation Results

In this part, we use numerical simulations to illustrate the revenue performance of elastic request and network reconfiguration strategies in both static networks and networks with a progressive traffic load. First, we validate the performance in a static network. Both the ILP model `SL-RMBSA` and decomposition method `SL-RMB+SA` are compared in terms of computational efficiency and total revenue. Also, the difference between

[1]The fixed spectrum signifies that the starting FS index γ_i is fixed.

the elastic requests and the conventional requests is compared. Second, we compare the performance difference under a progressive network load. The difference between the elastic request and conventional request, between different network reconfiguration strategies, are both illustrated.

5.4.1 Simulation setup

To guarantee that the ILP models are solvable within a reasonable time, we assume that a 6-node mesh network [151, Fig. 1] and the available spectrum resources in each optical fiber are 50 FSs. All simulations are carried out by Gurobi 9.0 and MATLAB 2017a on an Intel Core PC with 2.3 GHz CPU and 8 GB RAM. In order to guarantee computational efficiency, the maximum limitation time of the ILP model is 120 seconds, while the optimal gap is 1%. The parameter $\sigma_{uv} = 6$ FSs. The results of auto-degrading scheme are averaged with 10 independent simulations, $N^{rep} = 10$. The requests are uniformly distributed.

For each request, we provide three baud-rates for the baud-rate set $\mathcal{B}$: 16, 32, and 64 Gbaud, which needs 2, 4, and 6 FSs, respectively [104, Table 3]. 5 routes can be used for each request, i.e., $1 \leq k \leq 5$. The transmission mode set $\mathcal{M}$ in this study is adopted from [63], which assumes a transceiver at 32 Gbaud[63]. Specifically, we use four different MFs (PM-QPSK, PM-16QAM, and PM-64QAM) and at most five FECs overhead for each MF, so that the bit-rate varies from 50 to 300 Gbps with a step of 25 Gbps. The transmission reach (unit:span, one span = 100 km) is 158, 87, 49, 31, 22, 15, 11, 7, 5, 4, and 3, respectively. These parameters are calculated with the GN model using the worst-case assumption[66]. Next, the candidate bit-rate for elastic request $\mathcal{L}_{elastic}$ is $\mathcal{R} = \{50, 100, 150\}$Gbps, while the candidate bit-rate for conventional request $\mathcal{L}_{fix}$ is $\mathcal{R} = \{150\}$Gbps. Here, all requests are assumed to use the same service level set in a network, i.e., either adopt $\mathcal{L}_{fix}$ or adopt $\mathcal{L}_{elastic}$. The study of the mixed service levels will be made in the future work. Then, the resulting revenue of each accepted service is obtained by the power law [154],

$$\eta_l = \eta_0 {R_l}^{\alpha} \tag{5.12}$$

where η_0 is a constant value, α is a quantity number ($\alpha < 1$), and R_l is the required bit-rate of a service level l. We also neglect the impact of distance in [154]. Note that the price parameters should be specified by a specified pricing model. For simplicity, here, we assign the following value, $\alpha = 0.4$, $\eta_0 = 1.27$. Thus, $\eta_l \in \{6.07, 8.01, 9.42\}$ for $\mathcal{L}_{elastic}$.

5.4.2 Elastic requests in static network

Computational efficiency of ILP model and decomposition method

First, we compare the computational efficiency of the ILP model `SL-RMBSA` and decomposition method `SL-RMB+ SA` on the 6-node network. Figure 5.2 illustrates the revenue and computational time of two methods as the number of requests increases. The lower

computation time and the higher revenue of the two-step SL−RMB + SA confirms the efficiency of the decomposition method. Therefore, the proposed decomposition method is more time-efficient than ILP model.

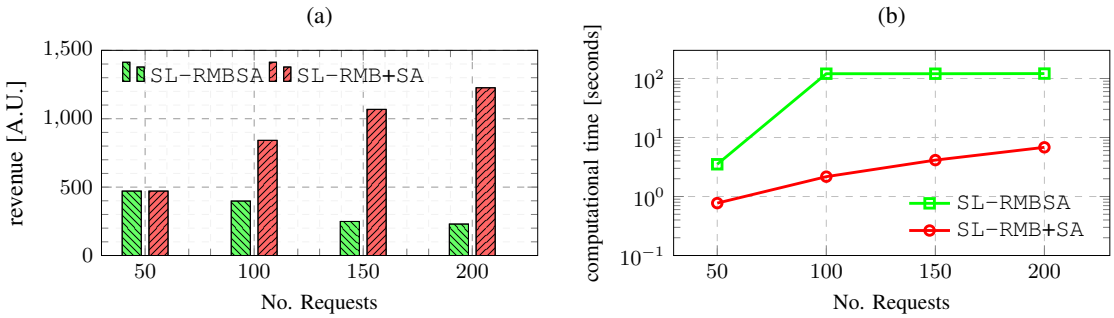

Figure 5.2: *Comparison of revenue and computational time in 6-node network.*

Elastic request vs. conventional request ($\mathcal{L}_{elastic}$ vs. $\mathcal{L}_{fix}$)

Here, we evaluate the performance improvement through supporting elastic service provisioning. The improvement of revenue and total accepted requests in Fig. 5.3 confirms the advantage of elastic request. Besides, the improvement of total accepted requests increases from 0% to 46% when the number of requests increases from 50 to 500, while the total revenue increases from 0% to 64%.

5.4.3 Elastic requests in progressive network load

Next, we compare the performance of elastic requests under progressive network load. No network reconfiguration has been assumed in the existing studies[38]. Thus, in order to make a fair comparison, we present the simulation results without network reconfiguration firstly, and with network reconfiguration in the following.

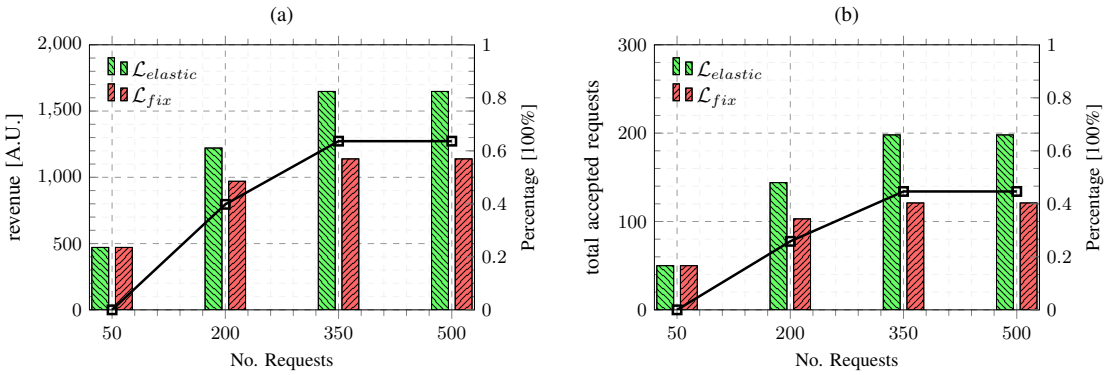

Figure 5.3: *Elastic vs. conventional request in terms of revenue and total accepted requests in static network.*

Without network reconfiguration ($\mathcal{L}_{elastic}$ vs. $\mathcal{L}_{fix}$)

The improvement of $\mathcal{L}_{elastic}$ of the total revenue (9.6% in Fig. 5.4(a)) and total accepted requests (10% in Fig. 5.4(b)) shows the advantage of using elastic requests under progressive network load.

With network reconfiguration ($\mathcal{L}_{elastic}$ vs. $\mathcal{L}_{fix}$)

Performance improvement of network reconfiguration is achieved for both $\mathcal{L}_{elastic}$ and $\mathcal{L}_{fix}$, as shown in Fig. 5.4. Besides, a higher improvement of the maximum revenue (80% in Fig. 5.4(a)) and the maximum accepted requests (104% in Fig. 5.4(b)) is observed when compared to the previous results of 9.6% and 10% without network reconfiguration. Such results imply the larger benefit when using network reconfiguration for $\mathcal{L}_{elastic}$. However, it will be expensive and complex for network operators to implement the network reconfiguration with both rerouting and spectrum retuning. Thus, we compare the performance with different network reconfiguration strategies in the following.

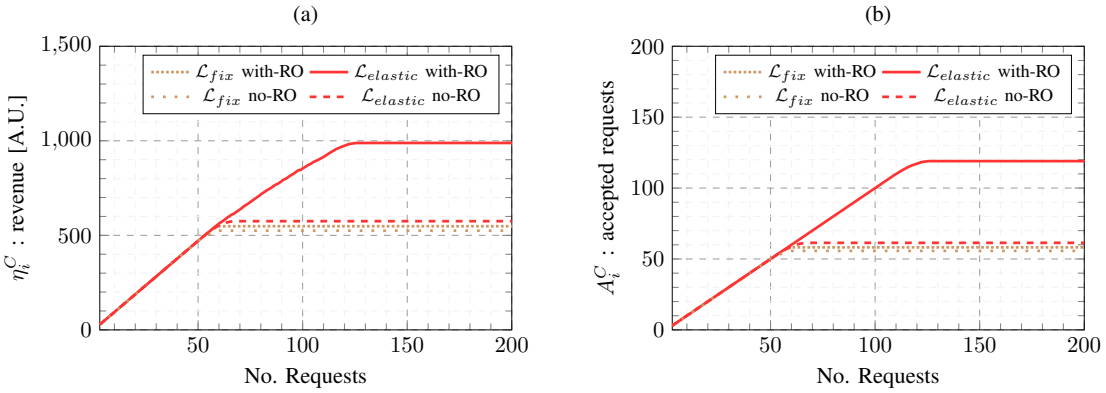

Figure 5.4: *Performance comparison under a progressive network load (NO=kSP-FF, RO=VarRVarS).*

With different network reconfiguration strategies (FixRFixS, FixRVarS, VarRFixS, VarRVarS, vs. no-RO)

In Fig. 5.5, for the normal operation of kSP-FF algorithm, the improvement of the maximum revenue of four ROs follows this order, *no-RO(0%) < FixRFixS(3.7%) ≤ VarRFixS(4.0%) < FixRVarS(32.0%) < VarRVarS(72.0%)*. While for FF-kSP algorithm, the improvement of the maximum revenue follows this order, *no-RO(0%) < FixRFixS(0.7%) ≤ VarRFixS(0.7%) < FixRVarS(28.0%) < VarRVarS(64.9%)*. In addition, the improvement of spectrum retuning could be mainly attributed to the released spectrum resources of the lightpath of the existing elastic requests. Such results imply that the network reconfiguration of spectrum retuning outperforms the rerouting.

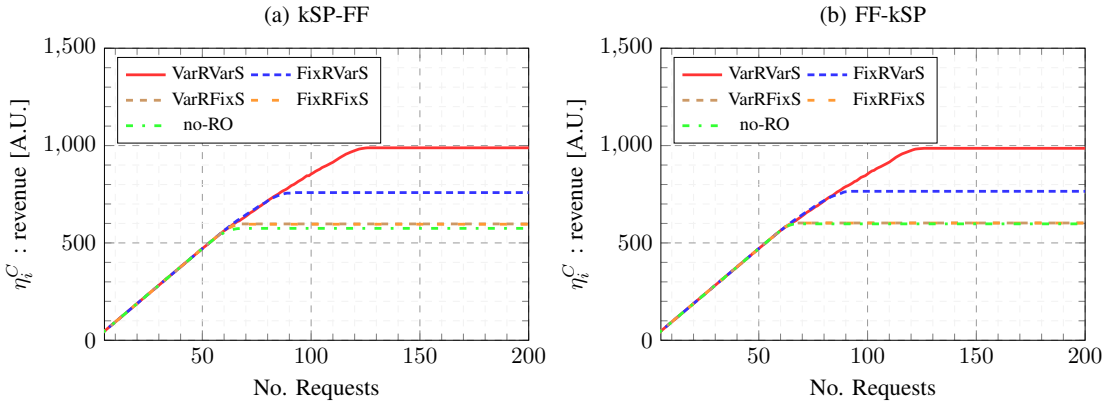

Figure 5.5: *Performance comparison of different ROs for $\mathcal{L}_{elastic}$ under a progressive network load.*

5.5 Conclusions

In this chapter, we studied the problem of revenue maximization leveraging QoS-aware elastic services. This problem is formulated as an ILP model that simultaneously combines the selection of service level, route, baud-rate, MF, FEC, as well as the spectrum assignment. A time-efficient decomposition method is also proposed to address this problem. Through simulations, we validate the benefit of supporting elastic requests in both scenarios, namely static FON and FON with a progressive network load. In static network load, compared to the conventional requests, the number of total accepted requests of elastic requests can increase to up to 46%, while the total revenue can increase up to 64%. This result shows that the benefit of elastic requests in terms of accommodating more requests. While for a progressive network load, a similar improvement of these two metrics is also observed. Specifically, the improvement of total accepted requests is 10%. This number increases up to 104% if the network reconfiguration strategies are considered. In addition, by comparing four different network reconfiguration strategies (FixRFixS, FixRVarS, VarRFixS, and VarRVarS) through employing the proposed auto-degrading scheme in our example network, we find that the FixRVarS with spectrum retuning outperforms the VarRFixS with rerouting.

Chapter 6

Conclusions and Perspectives

6.1 Conclusions

This thesis has investigated how the network parameter flexibility can be used to enhance the overall network performance. Specially, we investigate MF, FEC, channel spacing, and baud rate in physical layer, and the elastic service in network layer. When employing these flexibilities for the lightpath provisioning, we consider the impact of actual PLI rather than the worst-case PLI.

Before conducting the studies, we establish a PLI model to evaluate the PLIs of lightpath. These PLIs influence the QoT of each lightpath and determine the available parameters. Both the NLI of fibers and the crosstalk at OXCs are incorporated for the SNR evaluation, in order to obtain an accurate result. When evaluating the NLI on fibers, the recent widely adopted GN model is used.

The first study investigated the flexibility of MF and FEC. An MILP model is proposed to incorporate the PLI calculation and resource allocation. With this model, the impact of MF, FEC, and PSD were investigated. Simulation results in two typical large networks (NSF and Cost239) validate the revenue improvement by optimizing the selection of MF and FEC. Besides, the results also show that the adaptive MF can obtain more revenue in high SNR scenario, while FEC can obtain more revenue in low SNR scenario. These observations emphasize that the multiple FECs can obtain much tolerance in different PSD settings, while adaptive MFs obtain higher revenue performance.

The second study investigated the optimization of channel spacing and baud-rate. An iterative feedback tuning algorithm was proposed to combine the baud-rate selection and channel spacing optimization. With this algorithm, the excess SNR margin can be iteratively tuned to the just-enough level, thus improve the network throughput. Simulation results validate the throughput improvement of the proposed algorithms. The results also reveal that the channel spacing optimization has two advantages compared to the existing fixed and candidate channel spacing strategy: (1) it can be applied with more resource over-provisioning scenarios; (2) it has a larger relative throughput gain ratio. As for baud-rate optimization, the simulation results advised to prioritize

the higher baud-rate with larger spectral efficiency to gain a larger throughput when implementing the lightpath provisioning. These findings highlight an important role of just-enough SNR margin provisioning and channel spacing optimization in FONs with flexible baud-rates.

Different from the previous studies that assume 100% bit-rate provisioning for each request, the third study focus on the elastic service provisioning with degraded bit-rate. This problem is formulated as an ILP model that simultaneously optimizes the selection of service level, route, baud-rate, MF, FEC, as well as the spectrum assignment. A time-efficient decomposition method is also proposed to address this problem. The benefit of supporting elastic requests are validated in both scenarios, static FON and FON with an incremental load. Besides, we find that the network reconfiguration of spectrum retuning outperforms the network reconfiguration of rerouting.

6.2 Future works

Many issues need further investigations for better utilization of the flexibility as well as the physical layer resources.

Scalable algorithm to handle various flexibilities

This thesis aims at the different flexibility of FONs. Due to the limit of hardware, only a set of discrete MFs and discrete FECs can be chosen. Let us denote the number of these flexibilities by N_{MF}, and N_{FEC}. It can be expected that the performance of these flexibilities will increase with N_{MF} and N_{FEC} [7, 87]. Meanwhile, a problem will arise that the size of solution space could increase exponentially, thus leads to insufficient solution speed of current algorithms. Thus, a large-scale algorithm is required to deal with the issue of scalability, such as meta-heuristic algorithm, fast greedy algorithms, and column generation[10, 11, 70, 72].

Performance comparison for different reconfiguration strategies in a high traffic load

In the third study, further works should be implemented to compare the existing re-configuration strategy of hop-tuning, make-before-break, and push-and-pull. These three techniques have different hardware requirement [25]. For example, the hop-tuning technique requires an arrayed waveguide grating (AWG) to track the wave-length changes, make-before-break requires an additional redundant transceiver at the source node to finish the new established lightpath, and the spectrum tuning requires the transceivers with capability of fast frequency sweeping to move the center fre-quency. For a specified FON, it may adopt only one of these techniques considering the equipment cost.

Energy-efficiency aware re-provisioning

Energy saving is still an important issue in optical networks. We have considered the flexibility of MFs and FECs in this thesis. According to the study in [69, 89, 93], the

energy consumption of these different parameters may vary with their hardware implementations, including encoder, Fourier transform component, as well as other DSP modules. Therefore, the power consumption of different flexibilities varies with the chosen parameter for each transceiver. However, the power consumption model in these studies only provides the data with one or a few MFs, or several baud-rates, which can be insufficient to character the future transceiver with flexible parameters. Thus, a proper energy consumption model for different flexibility is still required when allocating the spectrum resources with different lightpaths.

With the obtained power consumption model, we are allowed to achieve the energy efficiency designed optical networks. According to the data in [67, 93], the power consumption of a transceiver will increase with the order of MF, while the unit power consumption per bit-rate seems to decrease. This observation can be used to find a balance between energy consumption and network throughput. For example, in the high network load scenario, the transceiver tends to use the high-order MF to compress the bandwidth, leading to a higher power consumption. The low-order MF could be adopted to reduce the power consumption when the network load becomes low. Therefore, we can obtain the desired high bit-rate transmission for low network load, as well as the desired low power consumption in low network load.

Appendix A

Piece-wise linear fitting algorithm

We linearize the NLI by taking the least square algorithm from [83].

First, we collect m samples ($1 \leq i \leq m$) by using 2.9 with frequency step of 1 GHz on $[0, F]$ [66, Eq. (11)]. These samples are partially described by K lines, $1 \leq j \leq K$, whose slope and interception are (a_j, b_j). Thus, the approximate NLI $\tilde{G}^{NLI}(f)$ is expressed as,

$$G^{NLI}(f) \approx \tilde{G}^{NLI}(f) = \max_{1 \leq j \leq K} (a_j f + b_j) \tag{A.1}$$

The objective of piece-wise linear fitting is to minimize the error sum e_i by adjusting parameters (a_j, b_j), where $e_i = \left(G^{NLI}(f_i) - \tilde{G}^{NLI}(f_i) \right)^2$,

$$\min e = \sum_{i=1}^{m} \left(G^{NLI}(f_i) - \max_{1 \leq j \leq K} \left(a_j f_i + b_j \right) \right)^2 \tag{A.2}$$

The heuristic algorithm to solve the parameters (a_j, b_j) is based on the least-square method. Next, we explain the algorithm step by step.

First, we denote by $P_j^{(l)}$ the set of sample indices that are uniquely controlled by the j-th line at l iteration. We have $\cup_{j=1}^{j=K} P_j^{(l)} = \{1, 2, ..., m\}$ and $P_j^{(l)} \cap P_i^{(l)} = \emptyset$.

Then, the partition set of $P_j^{(0)}$ is initialized randomly by using the Voronoi set. Specifically, for each $P_j^{(0)}$, the point f_i belongs to the set P_j if it is closest to the point p_j, where the frequency points $p_1, ..., p_K$ are randomly generated. The initial set $P_j^{(0)}$ is expressed as follows,

$$P_j^{(0)} = \left\{ i \,||f_i - p_j| < |f_i - p_s|, \forall s \neq j \right\}, j = 1, ..., K. \tag{A.3}$$

When obtaining the initial partition set, we start the iteration. To guarantee that the error of each partition set $P_j^{(l)}$ is locally minimized, namely,

$$\min \sum_{i \in P_j^{(l)}} (af_i + b - G^{NLI}(f_i))^2 \tag{A.4}$$

we can use the *least square fitting* to calculate the parameter $(a_j^{(l+1)}, b_j^{(l+1)})$,

$$\begin{pmatrix} a_j^{(l+1)} \\ b_j^{(l+1)} \end{pmatrix} = \begin{pmatrix} \sum_i f_i^2 & \sum_i f_i \\ \sum_i f_i^T & |P_j^{(l)}| \end{pmatrix}^{-1} \cdot \begin{pmatrix} \sum_i G^{NLI}(f_i) f_i \\ \sum_i G^{NLI}(f_i) \end{pmatrix} \tag{A.5}$$

If the matrix to be inverted in Eq. (A.5) is singular, we set the parameters $\left(a_j^{(l+1)}, b_j^{(l+1)}\right)$ with a constant slope, i.e. $a_j^{(l+1)} = a_j^{(l)}$, $b_j^{(l+1)} = G^{NLI}(f_i) - a_j^{(l)} \cdot f_i$.

At the end of each iteration, we update the partition $P_j^{(l+1)}$ by trying to assign sample indice i to $P_s^{(l+1)}$, if the equation holds,

$$a_s^{(l+1)} f_i + b_s^{(l+1)} = \max_{j=1,\ldots,K} \left(a_j^{(l+1)} f_i + b_j^{(l+1)}\right) \tag{A.6}$$

The above equation means that only the affine function $a_s^{(l+1)} f_i + b_s^{(l+1)}$ is active at point f_i.

Finally, we repeat the calculation of the parameters $\left(a_j^{(l)}, b_j^{(l)}\right)$ by using Eq. (A.5) and Eq. (A.6), until the maximum number of iteration is achieved, or the partitions sets $P_j^{(l+1)}$ of the current iteration are all identical to the partition set $P_j^{(l)}$ of the last iteration.

The following figures illustrate the iteration step of PWL for two iterations. Each point is uniquely controlled by the line that has the same color.

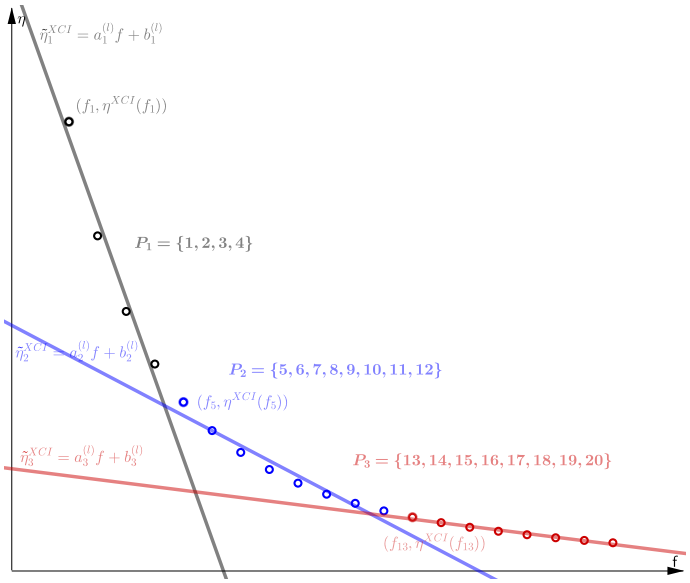

(a) iteration l

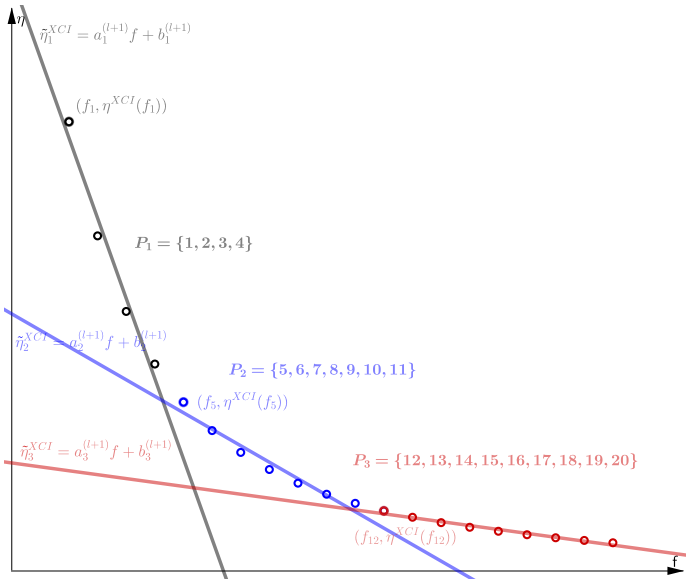

(b) iteration $l + 1$

Figure A.1: *Illustration for PWL fitting algorithms.*

Appendix B

Network topologies

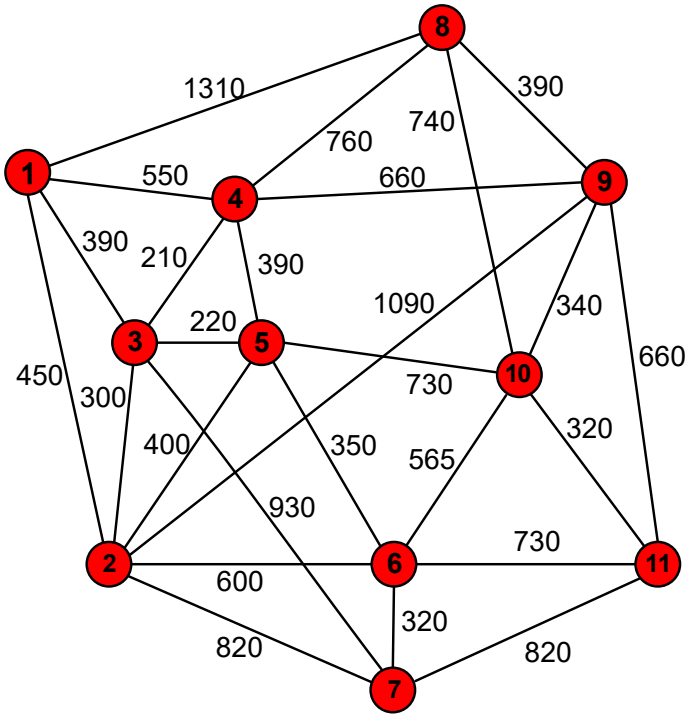

Figure B.1: *Cost239 with 11 nodes and 52 directed links.*

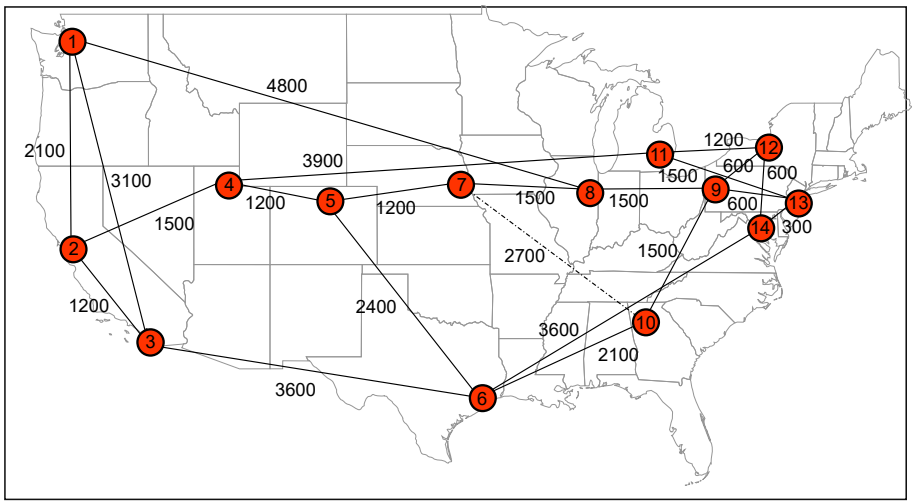

Figure B.2: *NSF with 14 nodes and 42 directed links. The number associated with each link denotes its length in kilometers.*

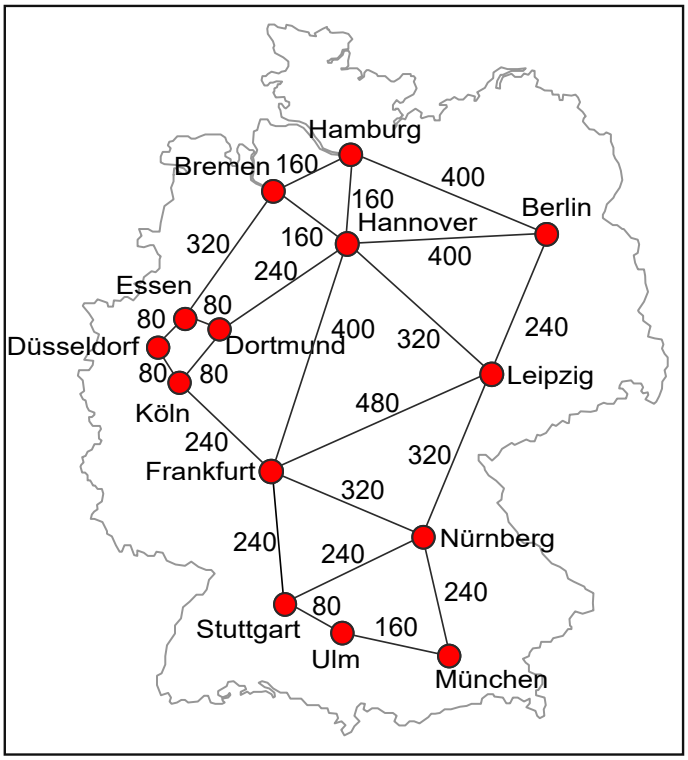

Figure B.3: *German network with 14 nodes and 46 links.*

Acronyms

AD	Add and Drop
ADC/DAC	Analog-to-Digital Converter/Digital-to-Analog Converter
ASE	Amplified Spontaneous Emission
ARPU	Average Revenue Per User
BER	Bit Error Ratio
BPSK	Binary Phase Shift Keying
BVT	Bandwidth-Variable Transceiver
BV-OXC	Bandwidth-Variable Optial Cross-Connect
BV-WSS	Bandwidth-Variable Wavelength-Selective Switches
CAN	CANdidate channel spacing strategy
CD	Chromatic Dispersion
CSO	Channel Spacing Optimization strategy without candidates
CWDM	Coarse Wavelength Division-Multiplexing
DEC-ALG	Decompostion Algorithm
DSP	Digital Signal Processing
DWDM	Dense Wavelength Division-Multiplexing
EDFA	Erbium-Doped Fiber Amplifier
FEC	Forward Error Correction
FF-kSP	First Fit and K Shortest Path algorithm
FIX	FIX channel spacing strategy
FON	Flexible Optical Network
FS	Frequency Slot
GN	Gaussian Noise

GSNR	Generalized SNR
ILP	Integer Linear Programming
kSP-FF	K Shortest Path and First Fit algorithm
MF	Modulation Format
MILP	Mixed Integer Linear Programming
***m*-QAM**	*m*-ary Quadrature Amplitude Modulation
NLI	Non-Linear Interference
OFDM	Orthogonal Frequency-Division Multiplexing
OH	Overhead
OSNR	Optical Signal to Noise Ratio
OTU	Optical Transport Unit
PDL	Polarization Dependent Loss
PLI	Physical Layer Impariment
PMD	Polarization Mode Dispersion
PS	Power Splitter
PSD	Power Spectral Density
QAM	Quadrature Amplitude Modulation
QoS	Quality of Service
QoT	Quality of Transmission
QPSK	Quadrature Phase Shift Keying
RSA	Routing and Spectrum Assignment
RMFSA	Routing, Modulation format, FEC, and Spectrum Assignment
RMSA	Routing, Modulation format, and Spectrum Assignment
RTMA	Routing and Transmission Mode Assignment
ROADM	Reconfigurable Optical Add Drop Multiplexer
RWA	Routing and Wavelength Assignment
SA	Spectrum Assignment
S-BVT	Sliceable Bandwidth-Variable-Transceiver
SCI	Self Channel Inteference
SNR	Signal-to-Noise-Ratio

TDHM Time-domain Hybrid Modulation format

TFP Time and Frequency Packing

WDM Wavelength Division-Multiplexing

XCI Cross Channel Inteference

List of Publications

International Journals:

[J1]: Yuanhao Liu, Fen Zhou, **Cao Chen**, Zuqing Zhu, Tao Shang, Juan-Manuel Torres-Moreno. Disaster Protection in Inter-DataCenter Networks leveraging Cooperative Storage. IEEE Transactions on Network and Service Management, pp 1-14, June. 2021.

[J2]: Yunhao Zhang, Shilin Xiao, Yinghong Yu, **Cao Chen**, et al. Experimental study of wideband in-band full-duplex communication based on optical self-interference cancellation. Optics Express, 2016, 24(26), pp.30139-30148.

International Conferences:

[C1]: **Cao Chen**, Fen Zhou, Shilin Xiao. "Revenue Maximization Leveraging Elastic Service Provisioning in Flexible Optical Networks". Accepted by the conference *IEEE Local Computer Networks (IEEE LCN, 2021)*, pp1-8, Edmonton, Canada, Oct. 2021.

[C2]: Yuanhao Liu, Fen Zhou, **Cao Chen**, Zuqing Zhu, Tao Shang, Juan-Manuel Torres-Moreno. "Disaster Protection in Inter-DataCenter Networks leveraging Cooperative Storage". *The IEEE Global Communications Conference (IEEE Globecom, 2020)*, pp1-6, Taipei, Dec. 2020.

[C3]: **Cao Chen**, Fen Zhou, Yuanhao Liu, Shilin Xiao. "Channel Frequency Optimization in Optical Networks Based on Gaussian Noise Model". *24th international conference on optical network design and modelling* (IFIP ONDM, 2020), pp1-6, Barcelona, Spain, May 2020.

[C4]: **Cao Chen**, Fen Zhou, Shilin Xiao. "Maximizing Revenue with Adaptive Modulation and Multiple FEC in Flexible Optical Networks". *The 21st IEEE International Conference on High Performance Computing and Communications* (IEEE HPCC, 2019), pp1-6, China, August. 2019.

[C5]: **Cao Chen**, Min Ju, Shilin Xiao, Fen Zhou, Xuelin Yang. "Minimizing total blocking by setting optimal guard band in nonlinear Elastic Optical Networks." *The 19th International Conference on Transparent Optical Networks* (IEEE ICTON, 2017), Girona, Spain, July 2017, pp. 1-4.

[C6] Yinghong Yu, Shilin Xiao, Yunhao Zhang, Shaojie Zhang, Lu Zhang, Ling Liu,

and **Cao Chen**. Experimental Demonstration of Wireless In-Band Full-Duplex with DML-Based Self-Interference Cancellation. OSA Asia Communications and Photonics Conference 2016 (IEEE/OSA ACP, 2016), pp. AF3H.6.

[C7] Yinan Hou, Yuankai Xue, **Cao Chen**, Shilin Xiao. A RSS/AOA based indoor positioning system with a single LED lamp. IEEE International Conference on Wireless Communications and Signal Processing (IEEE WCSP, 2015), 2015: 1-4.

Submissions:

[S1]: **Cao Chen**, Fen Zhou, Massimo Tornatore, Shilin Xiao. "Maximizing Revenue with Adaptive Modulation and Multiple FEC in Flexible Optical Networks". submitted to *IEEE Transactions on Networking* in Oct. 2020, under review.

[S2]: **Cao Chen**, Fen Zhou, Yuanhao Liu, Shilin Xiao. "Throughput Maximization Leveraging Just-Enough SNR Margin and Channel Spacing Optimization". submitted to *IEEE/OSA Journal of Lightwave Technology*, Jul. 2021, under review.

Bibliography

[1] Interfaces for the optical transport network, Mar. 2003.

[2] Spectral grids for WDM applications: DWDM frequency grid, Feb. 2012.

[3] O. (2021). Fixed broadband subscriptions. https://data.oecd.org/broadband/fixed-broadband-subscriptions.htm.

[4] G. P. Agrawal. Nonlinear fiber optics. In P. L. Christiansen, M. P. Sørensen, and A. C. Scott, editors, *Nonlinear Science at the Dawn of the 21st Century*, pages 195–211, Berlin, Heidelberg, 2000. Springer Berlin Heidelberg.

[5] G. P. Agrawal. *Fiber-optic communication systems*, volume 222. John Wiley & Sons, 2012.

[6] A. Alvarado, E. Agrell, D. Lavery, R. Maher, and P. Bayvel. Replacing the soft-decision FEC limit paradigm in the design of optical communication systems. *IEEE/OSA J. Lightwave Technol.*, 33(20):4338–4352, Jun. 2015.

[7] A. Alvarado, D. J. Ives, S. J. Savory, and P. Bayvel. On the impact of optimal modulation and FEC overhead on future optical networks. *IEEE/OSA J. Lightw. Technol.*, 34(9):2339–2352, Jan. 2016.

[8] J. Augé. Can we use flexible transponders to reduce margins? In *Proc. Opt. Fiber Commun. Conf. (OFC)*, page OTu2A.1, Anaheim, USA, Mar. 2013.

[9] S. Azodolmolky, M. Klinkowski, E. Marin, D. Careglio, J. S. Pareta, and I. Tomkos. A survey on physical layer impairments aware routing and wavelength assignment algorithms in optical networks. *Computer networks*, 53(7):926–944, May 2009.

[10] D. Banerjee and B. Mukherjee. A practical approach for routing and wavelength assignment in large wavelength-routed optical networks. *IEEE J. Sel. Area. Comm.*, 14(5):903–908, 1996.

[11] N. Banerjee, V. Mehta, and S. Pandey. A genetic algorithm approach for solving the routing and wavelength assignment problem in wdm networks. In *Proc. IEEE international conference on networking, ICN*, pages 70–78, 2004.

[12] P. Bayvel, R. Maher, T. Xu, G. Liga, N. A. Shevchenko, D. Lavery, A. Alvarado, and R. I. Killey. Maximizing the optical network capacity. *Phil. Trans. R. Soc. A.*, 374(2062):20140440, Mar. 2016.

[13] S. Behera, A. Deb, G. Das, and B. Mukherjee. Impairment aware routing, bit loading, and spectrum allocation in elastic optical networks. *IEEE/OSA J. Lightw. Technol.*, 37(13):3009–3020, Apr. 2019.

[14] S. Behera, J. George, and G. Das. Effect of transmission impairments in CO-OFDM based elastic optical network design. *Elseiver Comput. Netw.*, 144:242–253, Oct. 2018.

[15] L. Beygi, E. Agrell, J. M. Kahn, and M. Karlsson. Rate-adaptive coded modulation for fiber-optic communications. *IEEE/OSA J. Lightwave Technol.*, 32(2):333–343, Jan. 2014.

[16] H. Beyranvand and J. A. Salehi. A quality-of-transmission aware dynamic routing and spectrum assignment scheme for future elastic optical networks. *IEEE/OSA J. Lightw. Technol.*, 31(18):3043–3054, 2013.

[17] C. Bhar, E. Agrell, K. Keykhosravi, M. Karlsson, and P. A. Andrekson. Channel allocation in elastic optical networks using traveling salesman problem algorithms. *IEEE/OSA J. Opt. Commun. Netw.*, 11(10):C58–C66, Oct. 2019.

[18] G. Bosco. Advanced modulation techniques for flexible optical transceivers: The rate/reach trade-off. *IEEE/OSA J. Lightw. Technol.*, 37(1):36–49, Jan. 2019.

[19] G. Bosco, A. Carena, V. Curri, P. Poggiolini, and F. Forghieri. Performance limits of nyquist-wdm and co-ofdm in high-speed pm-qpsk systems. *IEEE Photon. Technol. Lett.*, 22(15):1129–1131, May 2010.

[20] G. Bosco, V. Curri, A. Carena, P. Poggiolini, and F. Forghieri. On the performance of nyquist-WDM terabit superchannels based on pm-bpsk, pm-qpsk, pm-8qam or pm-16qam subcarriers. *IEEE/OSA J. Lightwave Technol.*, 29(1):53–61, Jan. 2011.

[21] F. Buchali, F. Steiner, G. Böcherer, L. Schmalen, P. Schulte, and W. Idler. Rate adaptation and reach increase by probabilistically shaped 64-qam: An experimental demonstration. *IEEE/OSA J. Lightwave Technol.*, 34(7):1599–1609, Apr. 2016.

[22] M. Cantono. *Physical layer aware optical networks*. PhD thesis, Ph. D. thesis, Politecnico di Torino, Apr. 2018.

[23] M. Cantono, R. Gaudino, and V. Curri. Potentialities and criticalities of flexible-rate transponders in DWDM networks: A statistical approach. *IEEE/OSA J. Opt. Commun. Netw.*, 8(7):A76–A85, Jul. 2016.

[24] J. C. Cartledge, F. Matos, C. Laperle, A. Borowiec, M. O'Sullivan, and K. Roberts. Use of extreme value statistics to assess the performance implications of cascaded ROADMs. *IEEE/OSA J. Lightw. Technol.*, 35(23):5208–5214, Dec. 2017.

[25] B. C. Chatterjee, S. Ba, and E. Oki. Fragmentation problems and management approaches in elastic optical networks: A survey. *IEEE Commun. Surv. Tutor.*, 20(1):183–210, 2018.

[26] B. C. Chatterjee, N. Sarma, and E. Oki. Routing and spectrum allocation in elastic optical networks: A tutorial. *IEEE Commun. Surv. Tutor.*, 17(3):1776–1800, Sep. 2015.

[27] C. Chen, F. Zhou, Y. Liu, and S. Xiao. Channel frequency optimization in optical networks based on Gaussian Noise model. In *Proc. Int. Conf. Opt. Netw. Design and Modeling (ONDM)*, pages 1–6, Barcelona, Spain, May 2020.

[28] K. Cho and D. Yoon. On the general ber expression of one-and two-dimensional amplitude modulations. *IEEE Trans. Commun.*, 50(7):1074–1080, Jul. 2002.

[29] K. Christodoulopoulos, C. Delezoide, N. Sambo, A. Kretsis, I. Sartzetakis, A. Sgambelluri, N. Argyris, G. Kanakis, P. Giardina, G. Bernini, D. Roccato, A. Percelsi, R. Morro, H. Avramopoulos, P. Castoldi, P. Layec, and S. Bigo. Toward efficient, reliable, and autonomous optical networks: the orchestra solution. *IEEE/OSA J. Opt. Commun. Netw.*, 11(9):C10–C24, Aug. 2019.

[30] K. Christodoulopoulos, K. Manousakis, and E. Varvarigos. Offline routing and wavelength assignment in transparent WDM networks. *IEEE/ACM Trans. Netw.*, 18(5):1557–1570, Oct. 2010.

[31] K. Christodoulopoulos, I. Tomkos, and E. A. Varvarigos. Routing and spectrum allocation in ofdm-based optical networks with elastic bandwidth allocation. In *Proc. Global Commun. Conf. (GLOBECOM)*, pages 1–6, Dec. 2010.

[32] K. Christodoulopoulos, I. Tomkos, and E. A. Varvarigos. Elastic bandwidth allocation in flexible OFDM-based optical networks. *IEEE/OSA J. Lightwave Technol.*, 29(9):1354–1366, May 2011.

[33] Ciena. *Transforming Margin into Capacity with Liquid Spectrum*. (Date last accessed 2-February-2021).

[34] Cisco. Cisco NCS 2000 100-Gbps coherent DWDM trunk card with CPAK client interface data sheet. www.cisco.com/c/en/us/products/collateral/optical-networking/network-convergence-system-2000-series/data_sheet_c78-729401.html. Last accessed 2021-01-01.

[35] Cisco. Cisco ONS 15454 100-Gbps CP-DQPSK full c-band tunable DWDM trunk card data sheet. www.cisco.com/c/en/us/products/collateral/optical-networking/ons-15454-series-multiservice-transport-platforms/datasheet-c78-738094.html. Last accessed 2021-01-01.

[36] Cisco. Cisco visual networking index: Forecast and trends, 2017-2022. Technical report, Cisco, Nov. 2018.

[37] L. R. Costa and A. C. Drummond. New distance-adaptive modulation scheme for elastic optical networks. *IEEE Commun. Lett.*, 21(2):282–285, Feb. 2017.

[38] V. Curri, M. Cantono, and R. Gaudino. Elastic all-optical networks: A new paradigm enabled by the physical layer. how to optimize network performances? *IEEE/OSA J. Lightwave Technol.*, 35(6):1211–1221, Mar. 2017.

[39] H. Dai, Y. Li, and G. Shen. Explore maximal potential capacity of WDM optical networks using time domain hybrid modulation technique. *IEEE/OSA J. Lightwave Technol.*, 33(18):3815–3826, May 2015.

[40] A. Ellis, N. MacSuibhne, D. Saad, and D. Payne. Communication networks beyond the capacity crunch. *Philos. Trans. Royal Soc. A*, 374(2062):1–12, Mar. 2016.

[41] J. M. Fabrega, M. S. Moreolo, L. Martín, A. C. Piat, E. Riccardi, D. Roccato, N. Sambo, F. Cugini, L. Potì, S. Yan, E. Hugues-Salas, D. Simeonidou, M. Gunkel, R. Palmer, S. Fedderwitz, D. Rafique, T. Rahman, H. de Waardt, and A. Napoli. On the filter narrowing issues in elastic optical networks. *IEEE/OSA Journal of Optical Communications and Networking*, 8(7):A23–A33, Jul. 2016.

[42] T. Fehenberger, A. Alvarado, P. Bayvel, and N. Hanik. On achievable rates for long-haul fiber-optic communications. *OSA Opt. Express*, 23(7):9183–9191, Apr. 2015.

[43] T. Fehenberger, A. Alvarado, G. Böcherer, and N. Hanik. On probabilistic shaping of quadrature amplitude modulation for the nonlinear fiber channel. *IEEE/OSA J. Lightw. Technol.*, 34(21):5063–5073, 2016.

[44] J. P. Fernández-Palacios, V. López, B. de la Cruz, O. Gerstel, N. Sambo, and E. Riccardi. *Sliceable Bandwidth Variable Transponders*, pages 117–157. Springer Int. Publishing, Cham, 2016.

[45] A. Ferrari, M. Filer, E. Le Rouzic, J. Kundrát, B. Correia, K. Balasubramanian, Y. Yin, G. Grammel, G. Galimberti, and V. Curri. GNPy: an open source planning tool for open optical networks. In *Proc. Optical Network Design and Modeling (ONDM)*, pages 1–6, May 2020.

[46] M. Filer and S. Tibuleac. Generalized weighted crosstalk for DWDM systems with cascaded wavelength-selective switches. *Opt. Express*, 20(16):17620–17631, Jul. 2012.

[47] W. Freude, R. Schmogrow, B. Nebendahl, M. Winter, A. Josten, D. Hillerkuss, S. Koenig, J. Meyer, M. Dreschmann, M. Huebner, et al. Quality metrics for optical signals: Eye diagram, Q-factor, OSNR, EVM and BER. In *Proc. Int. Conf. Transparent Opt. Netw. (ICTON)*, pages 1–4. IEEE, Aug. 2012.

[48] L. Galdino, D. Semrau, D. Lavery, G. Saavedra, C. B. Czegledi, E. Agrell, R. I. Killey, and P. Bayvel. On the limits of digital back-propagation in the presence of transceiver noise. *Opt. Express*, 25(4):4564–4578, Feb. 2017.

[49] O. Gerstel, M. Jinno, A. Lord, and S. B. Yoo. Elastic optical networking: a new dawn for the optical layer? *IEEE Commun. Mag.*, 50(2):s12–s20, Feb. 2012.

[50] G. Gho, L. Klak, and J. M. Kahn. Rate-adaptive coding for optical fiber transmission systems. *IEEE/OSA J. Lightw. Technol.*, 29(2):222–233, Jan. 2011.

[51] G.-H. Gho and J. M. Kahn. Rate-adaptive modulation and coding for optical fiber transmission systems. *IEEE/OSA J. Lightwave Technol.*, 30(12):1818–1828, Feb. 2012.

[52] M. Hadi and M. R. Pakravan. Resource allocation for elastic optical networks using geometric optimization. *IEEE/OSA J. Opt. Commun. Netw.*, 9(10):889–899, Sep. 2017.

[53] E. R. Hartling, P. Pecci, P. Mehta, D. Evans, V. Kamalov, M. Cantono, E. Mateo, F. Yaman, A. Pilipetskii, C. Mott, P. Lomas, and P. Murphy. Subsea open cables: A practical perspective on the guidelines and gotchas. New Orleans USA, Apr. 2019.

[54] E. R. Hartling, A. Pilipetskii, D. Evans, E. Mateo, M. Salsi, P. Pecci, and P. Mehta. Design, acceptance and capacity of subsea open cables. *IEEE/OSA J. Lightwave Technol.*, 39(3):742–756, Feb. 2021.

[55] H. i Lab. Unlocking value for residential broadband services with quality broadband network. www-file.huawei.com/-/media/CORPORATE/PDF/ilab/unlocking-value-for-residential-broadband-services-1017-en.pdf. Last accessed 2021-05-01.

[56] Infinera. *The ultimate guide to higher baud rates.* (Date last accessed 2-November-2020).

[57] informitv. Bbc iplayer viewing average. informitv.com/2018/02/12/bbc-iplayer-viewing-average.

[58] E. Ip and J. M. Kahn. Compensation of dispersion and nonlinear impairments using digital backpropagation. *IEEE/OSA J. Lightw. Technol.*, 26(20):3416–3425, Oct. 2008.

[59] ITU. Fixed-broadband subscriptions. https://www.itu.int/en/ITU-D/Statistics/Pages/stat/default.aspx.

[60] D. J. Ives. *Coherent optical fibre networking in the nonlinear regime*. PhD thesis, UCL (University College London), Dec. 2015.

[61] D. J. Ives, P. Bayvel, and S. J. Savory. Adapting transmitter power and modulation format to improve optical network performance utilizing the Gaussian Noise model of nonlinear impairments. *IEEE/OSA J. Lightw. Technol.*, 32(21):4087–4096, Nov. 2014.

[62] D. J. Ives, P. Bayvel, and S. J. Savory. Routing, modulation, spectrum and launch power assignment to maximize the traffic throughput of a nonlinear optical mesh network. *Photon. Netw. Commun.*, 29(3):244–256, Jun. 2015.

[63] D. J. Ives, P. Wright, A. Lord, and S. J. Savory. Using 25 gbe client rates to access the gains of adaptive bit- and code-rate networking. *IEEE/OSA J. Opt. Commun. Netw.*, 8(7):A86–A91, Jul. 2016.

[64] B. Jaumard and M. Daryalal. Efficient spectrum utilization in large scale rwa problems. *IEEE/ACM Transactions on Networking (TON)*, 25(2):1263–1278, 2017.

[65] M. Jinno, H. Takara, B. Kozicki, Y. Tsukishima, Y. Sone, and S. Matsuoka. Spectrum-efficient and scalable elastic optical path network: architecture, benefits, and enabling technologies. *IEEE Commun. Mag.*, 47(11):66–73, Nov. 2009.

[66] P. Johannisson and E. Agrell. Modeling of nonlinear signal distortion in fiber-optic networks. *IEEE/OSA J. Lightw. Technol.*, 32(23):3942–3950, Oct. 2014.

[67] M. Ju, F. Zhou, S. Xiao, and Z. Zhu. Power-efficient protection with directed *p*-cycles for asymmetric traffic in elastic optical networks. *IEEE/OSA J. Lightwave Technol.*, 34(17):4053–4065, Jul. 2016.

[68] M. Ju, F. Zhou, Z. Zhu, and S. Xiao. Distance-adaptive, low CAPEX cost *p*-cycle design without candidate cycle enumeration in mixed-line-rate optical networks. *IEEE/OSA J. Lightw. Technol.*, 34(11):2663–2676, Apr. 2016.

[69] H. Khodakarami, B. S. G. Pillai, B. Sedighi, and W. Shieh. Flexible optical networks: An energy efficiency perspective. *IEEE/OSA J. Lightw. Technol.*, 32(21):3356–3367, Jun. 2014.

[70] S. Kirkpatrick, C. D. Gelatt, and M. P. Vecchi. Optimization by simulated annealing. *Science*, 220(4598):671–680, 1983.

[71] M. Klinkowski and K. Walkowiak. Routing and spectrum assignment in spectrum sliced elastic optical path network. *IEEE Commun. Lett.*, 15(8):884–886, Aug. 2011.

[72] M. Klinkowski, M. Żotkiewicz, K. Walkowiak, M. Pióro, M. Ruiz, and L. Velasco. Solving large instances of the rsa problem in flexgrid elastic optical networks. *IEEE/OSA J. Opt. Commun. Netw.*, 8(5):320–330, Aug. 2016.

[73] T. Koike-Akino, K. Kojima, D. S. Millar, K. Parsons, T. Yoshida, and T. Sugihara. Pareto optimization of adaptive modulation and coding set in nonlinear fiber-optic systems. *IEEE/OSA J. Lightw. Technol.*, 35(4):1041–1049, Feb. 2017.

[74] S. K. Korotky. Price-points for components of multi-core fiber communication systems in backbone optical networks. *IEEE/OSA J. Opt. Commun. Netw.*, 4(5):426–435, Jun. 2012.

[75] D. D. Le, F. Zhou, and M. Molnár. Minimizing blocking probability for the multicast routing and wavelength assignment problem in wdm networks: Exact solutions and heuristic algorithms. *IEEE/OSA J. Opt. Commun. Netw.*, 7(1):36–48, Jan. 2015.

[76] Y. Li, H. Dai, G. Shen, and S. K. Bose. Adaptive FEC-based lightpath routing and wavelength assignment in wdm optical networks. *Opt. Switching Netw.*, 14:241–249, Aug. 2014.

[77] R. Lin, S. Luo, J. Zhou, S. Wang, A. Cai, W.-D. Zhong, and M. Zukerman. Virtual network embedding with adaptive modulation in flexi-grid networks. *IEEE/OSA J. Lightwave Technol.*, 36(17):3551–3563, Sept. 2018.

[78] A. D. Little. French telecoms economics 2020. www.fftelecoms.org/app/uploads/2021/01/20210121-ADL-FFT-Telecom-Economics-study-2020-vSent.pdf. Last accessed 2021-05-01.

[79] R. B. Lourenço, M. Tornatore, C. U. Martel, and B. Mukherjee. Running the network harder: Connection provisioning under resource crunch. *IEEE Trans. Netw. Service Manag.*, Oct. 2018.

[80] P. Lu, L. Zhang, X. Liu, J. Yao, and Z. Zhu. Highly-efficient data migration and backup for big data applications in elastic optical inter-datacenter networks. *IEEE Netw.*, 29:36–42, Oct. 2015.

[81] D.-S. Ly-Gagnon, S. Tsukamoto, K. Katoh, and K. Kikuchi. Coherent detection of optical quadrature phase-shift keying signals with carrier phase estimation. *IEEE/OSA J. Lightwave Technol.*, 24(1):12, Feb. 2006.

[82] M-lab. Worldwide broadband speed league 2020. https://www.cable.co.uk/broadband/speed/worldwide-speed-league/.

[83] A. Magnani and S. P. Boyd. Convex piecewise-linear fitting. *Optimization and Engineering*, 10(1):1–17, Mar. 2009.

[84] K. Manousakis, K. Christodoulopoulos, E. Kamitsas, I. Tomkos, and E. A. Varvarigos. Offline impairment-aware routing and wavelength assignment algorithms in translucent WDM optical networks. *IEEE/OSA J. Lightw. Technol.*, 27(12):1866–1877, Jun. 2009.

[85] D. M. Marom, P. D. Colbourne, A. Dérrico, N. K. Fontaine, Y. Ikuma, R. Proietti, L. Zong, J. M. Rivas-Moscoso, and I. Tomkos. Survey of photonic switching architectures and technologies in support of spatially and spectrally flexible optical networking [invited]. *IEEE/OSA J. Opt. Commun. Netw.*, 9(1):1–26, Jan. 2017.

[86] S. Media. Video will grow to 82% of internet traffic by 2022: Interdigital/futuresource report. www.streamingmedia.com/Articles/ReadArticle.aspx?ArticleID=144177. Last accessed 2021-06-05.

[87] D. A. Mello, A. N. Barreto, T. C. de Lima, T. F. Portela, L. Beygi, and J. M. Kahn. Optical networking with variable-code-rate transceivers. *IEEE/OSA J. Lightw. Technol.*, 32(2):257–266, Nov. 2014.

[88] A. Morea, J. Renaudier, T. Zami, A. Ghazisaeidi, and O. Bertran-Pardo. Throughput comparison between 50-GHz and 37.5-GHz grid transparent networks. *IEEE/OSA J. Opt. Commun. Netw.*, 7(2):A293–A300, Feb. 2015.

[89] A. Morea, O. Rival, N. Brochier, and E. Le Rouzic. Datarate adaptation for nighttime energy savings in core networks. *IEEE/OSA J. Lightw. Technol.*, 31(5):779–785, Dec. 2013.

[90] A. Nag, M. Tornatore, and B. Mukherjee. On the effect of channel spacing, launch power, and regenerator placement on the design of mixed-line-rate optical networks. *Opt. Switch and Netw.*, 10(4):301 – 311, Nov. 2013.

[91] M. Nakazawa, T. Hirooka, P. Ruan, and P. Guan. Ultrahigh-speed "orthogonal" tdm transmission with an optical nyquist pulse train. *OSA Opt. Express*, 20(2):1129–1140, Jan. 2012.

[92] E. Palkopoulou, G. Bosco, A. Carena, D. Klonidis, P. Poggiolini, and I. Tomkos. Nyquist-WDM-based flexible optical networks: Exploring physical layer design parameters. *IEEE/OSA J. Lightwave Technol.*, 31(14):2332–2339, Jul. 2013.

[93] P. Papanikolaou, P. Soumplis, K. Manousakis, G. Papadimitriou, G. Ellinas, K. Christodoulopoulos, and E. Varvarigos. Minimizing energy and cost in fixed-grid and flex-grid networks. *IEEE/OSA J. Opt. Commun. Netw.*, 7(4):337–351, Apr. 2015.

[94] J. Pedro, N. Costa, and S. Pato. Optical transport network design beyond 100 Gbaud [invited]. *IEEE/OSA J. Opt. Commun. Netw.*, 12(2):A123–A134, Nov. 2020.

[95] S. D. Personick. Receiver design for digital fiber optic communication systems, i. *Bell system technical journal*, 52(6):843–874, Aug. 1973.

[96] P. Poggiolini. The GN model of non-linear propagation in uncompensated coherent optical systems. *IEEE/OSA J. Lightw. Technol.*, 30(24):3857–3879, Dec. 2012.

[97] P. Poggiolini, G. Bosco, A. Carena, R. Cigliutti, V. Curri, F. Forghieri, R. Pastorelli, and S. Piciaccia. The LOGON strategy for low-complexity control plane implementation in new-generation flexible networks. In *Proc. Opt. Fiber Commun. Conf. (OFC)*, page OW1H.3, Anaheim, USA, Mar. 2013.

[98] P. Poggiolini, G. Bosco, A. Carena, V. Curri, Y. Jiang, and F. Forghieri. The GN-model of fiber non-linear propagation and its applications. *IEEE/OSA J. Lightw. Technol.*, 32(4):694–721, Feb. 2014.

[99] P. Poggiolini and Y. Jiang. Recent advances in the modeling of the impact of nonlinear fiber propagation effects on uncompensated coherent transmission systems. *IEEE/OSA J. Lightwave Technol.*, 35(3):458–480, Sep. 2017.

[100] Y. Pointurier. Design of low-margin optical networks. *IEEE/OSA J. Opt. Commun. Netw.*, 9(1):A9–A17, Jan. 2017.

[101] Y. Pointurier, M. Brandt-Pearce, S. Subramaniam, and B. Xu. Cross-layer adaptive routing and wavelength assignment in all-optical networks. *IEEE J. Sel. Areas Commun.*, 26(6):32–44, Aug. 2008.

[102] H. Rabbani, L. Beygi, S. Ghoshooni, H. Rabbani, and E. Agrell. Quality of transmission aware optical networking using enhanced gaussian noise model. *IEEE/OSA J. Lightw. Technol.*, 37(3):831–838, Feb. 2019.

[103] B. Ramamurthy, D. Datta, and H. Feng. Impact of transmission impairments on the teletraffic performance of wavelength-routed optical networks. *IEEE/OSA J. Lightwave Technol.*, 17(10):1713, Oct. 1999.

[104] J. D. Reis, V. Shukla, D. R. Stauffer, and K. Gass. Technology options for 400G implementation. Technical report, The Optical Internetworking Forum, Jul. 2015.

[105] I. Roberts and J. M. Kahn. Efficient discrete rate assignment and power optimization in optical communication systems following the gaussian noise model. *IEEE/OSA J. Lightw. Technol.*, 35(20):4425–4437, Aug. 2017.

[106] I. Roberts, J. M. Kahn, and D. Boertjes. Convex channel power optimization in nonlinear WDM systems using Gaussian Noise model. *IEEE/OSA J. Lightw. Technol.*, 34(13):3212–3222, May 2016.

[107] C. Rottondi, P. Boffi, P. Martelli, and M. Tornatore. Routing, modulation format, baud rate and spectrum allocation in optical metro rings with flexible grid and few-mode transmission. *IEEE/OSA J. Lightw. Technol.*, 35(1):61–70, Jan. 2017.

[108] C. Rottondi, M. Tornatore, A. Pattavina, and G. Gavioli. Routing, modulation level, and spectrum assignment in optical metro ring networks using elastic transceivers. *IEEE/OSA J. Opt. Commun. Netw.*, 5(4):305–315, Apr. 2013.

[109] T. Ruether. Adaptive bitrate streaming: How it works and why it matters. www.wowza.com/blog/adaptive-bitrate-streaming. Last accessed 2021-06-05.

[110] N. Sambo, P. Castoldi, A. D'Errico, E. Riccardi, A. Pagano, M. S. Moreolo, J. M. Fabrega, D. Rafique, A. Napoli, S. Frigerio, et al. Next generation sliceable bandwidth variable transponders. *IEEE Commun. Mag.*, 53(2):163–171, Feb. 2015.

[111] N. Sambo, G. Meloni, F. Cugini, F. Fresi, A. D'Errico, L. Poti, P. Iovanna, and P. Castoldi. Routing, code, and spectrum assignment, subcarrier spacing, and filter configuration in elastic optical networks. *IEEE/OSA J. Opt. Commun. Netw.*, 7(11):B93–B100, Nov. 2015.

[112] S. S. Savas, M. F. Habib, M. Tornatore, F. Dikbiyik, and B. Mukherjee. Network adaptability to disaster disruptions by exploiting degraded-service tolerance. *IEEE Commun. Mag.*, 52(12):58–65, Dec. 2014.

[113] S. J. Savory. Digital coherent optical receivers: Algorithms and subsystems. *IEEE J. Sel. Top. Quantum Electron.*, 16(5):1164–1179, May 2010.

[114] S. J. Savory. Approximations for the nonlinear self-channel interference of channels with rectangular spectra. *IEEE Photon. Technol. Lett.*, 25(10):961–964, Apr. 2013.

[115] S. J. Savory. Congestion aware routing in nonlinear elastic optical networks. *IEEE Photon. Technol. Lett.*, 26(10):1057–1060, Mar. 2014.

[116] S. J. Savory, G. Gavioli, R. I. Killey, and P. Bayvel. Electronic compensation of chromatic dispersion using a digital coherent receiver. *OSA Opt. Express*, 15(5):2120–2126, Mar. 2007.

[117] S. J. Savory, R. J. Vincent, and D. J. Ives. Design considerations for low-margin elastic optical networks in the nonlinear regime [invited]. *IEEE/OSA J. Opt. Commun. Netw.*, 11(10):C76–C85, Oct. 2019.

[118] P. Sayyad Khodashenas, J. M. Rivas-Moscoso, B. Shariati, D. M. Marom, D. Klonidis, and I. Tomkos. Investigation of spectrum granularity for performance optimization of flexible Nyquist-WDM-based optical networks. *IEEE/OSA J. Lightwave Technol.*, 33(23):4767–4774, Dec. 2015.

[119] H. Schwarz, D. Marpe, and T. Wiegand. Overview of the scalable video coding extension of the h.264/avc standard. *IEEE Trans. Circuits Syst. Video Technol.*, 17(9):1103–1120, Sept. 2007.

[120] M. Secondini, T. Foggi, F. Fresi, G. Meloni, F. Cavaliere, G. Colavolpe, E. Forestieri, L. Potí, R. Sabella, and G. Prati. Optical time–frequency packing: Principles, design, implementation, and experimental demonstration. *IEEE/OSA J. Lightwave Technol.*, 33(17):3558–3570, Jun. 2015.

[121] D. Semrau, R. I. Killey, and P. Bayvel. The Gaussian Noise model in the presence of inter-channel stimulated raman scattering. *IEEE/OSA J. Lightw. Technol.*, 36(14):3046–3055, Jul. 2018.

[122] D. F. Semrau. *Physical Layer Modelling of Optical Fibre Communication Systems in the Nonlinear Regime*. PhD thesis, UCL (University College London), Mar. 2020.

[123] A. Sgambelluri, A. Giorgetti, D. Scano, F. Cugini, and F. Paolucci. Openconfig and openroadm automation of operational modes in disaggregated optical networks. *IEEE Access*, 8:190094–190107, Oct. 2020.

[124] N. Shahriar, S. Taeb, S. R. Chowdhury, M. Tornatore, R. Boutaba, J. Mitra, and M. Hemmati. Achieving a fully-flexible virtual network embedding in elastic optical networks. In *Proc. Int. Conf. on Comput. Commun. (ICC)*, pages 1756–1764, Paris, France, Apr. 2019.

[125] G. Shen, Y. Zhang, X. Zhou, Y. Sheng, N. Deng, Y. Ma, and A. Lord. Ultra-dense wavelength switched network: a special EON paradigm for metro optical networks. *IEEE Commun. Mag.*, 56(2):189–195, Feb. 2018.

[126] W. Shieh and I. B. Djordjevic. *OFDM for optical communications*. Elsevier, Burlington, MA, 2009.

[127] M. G. Taylor. Coherent detection method using DSP for demodulation of signal and subsequent equalization of propagation impairments. *IEEE Photon. Technol. Lett.*, 16(2):674–676, Feb. 2004.

[128] I. Tomkos, S. Azodolmolky, J. Solé-Pareta, D. Careglio, and E. Palkopoulou. A tutorial on the flexible optical networking paradigm: State of the art, trends, and research challenges. *Proc. IEEE*, 102(9):1317–1337, Sept. 2014.

[129] F. Vacondio, O. Rival, C. Simonneau, E. Grellier, A. Bononi, L. Lorcy, J.-C. Antona, and S. Bigo. On nonlinear distortions of highly dispersive optical coherent systems. *Opt. Express*, 20(2):1022–1032, Jan. 2012.

[130] L. Velasco, M. Klinkowski, M. Ruiz, and J. Comellas. Modeling the routing and spectrum allocation problem for flexgrid optical networks. *Photon. Netw. Comm.*, 24(3):177–186, Apr. 2012.

[131] L. Velasco, M. Ruiz, J. Perelló, S. Spadaro, and J. Comellas. Service and resource differentiation in shared-path protection environments to maximize network operator's revenues. *IEEE/OSA J. Opt. Commun. Netw.*, 3(2):117–126, Feb. 2011.

[132] R. J. Vincent, D. J. Ives, and S. J. Savory. Scalable capacity estimation for nonlinear elastic all-optical core networks. *IEEE/OSA J. Lightwave Technol.*, 37(21):5380–5391, Sep. 2019.

[133] R. Wang, S. Bidkar, F. Meng, R. Nejabati, and D. Simeonidou. Load-aware nonlinearity estimation for elastic optical network resource optimization and management. *IEEE/OSA J. Opt. Commun. Netw.*, 11(5):164–178, May 2019.

[134] G. Wellbrock and T. J. Xia. How will optical transport deal with future network traffic growth? In *Proc. European Conf. and Exhibition on Opt. Commun. (ECOC)*, pages 1–3, Sept. 2014.

[135] P. J. Winzer, D. T. Neilson, and A. R. Chraplyvy. Fiber-optic transmission and networking: the previous 20 and the next 20 years. *OSA Opt. Express*, 26(18):24190–24239, Sep. 2018.

[136] H. Wu, F. Zhou, Z. Zhu, and Y. Chen. On the distance spectrum assignment in elastic optical networks. *IEEE/ACM Trans. Netw.*, 25(4):2391–2404, Aug. 2017.

[137] Y. Xu, L. Yan, E. Agrell, and M. Brandt-Pearce. Iterative resource allocation algorithm for EONs based on a linearized GN model. *IEEE/OSA J. Opt. Commun. Netw.*, 11(3):39–51, Mar. 2019.

[138] Y. Xu, L. Yan, E. Agrell, and M. Brandt-Pearce. Iterative resource allocation algorithm for EONs based on a linearized GN model. *IEEE/OSA J. Opt. Commun. Netw.*, 11(3):39–51, Mar. 2019.

[139] L. Yan, E. Agrell, M. N. Dharmaweera, and H. Wymeersch. Joint assignment of power, routing, and spectrum in static flexible-grid networks. *IEEE/OSA J. Lightw. Technol.*, 35(10):1766–1774, May 2017.

[140] L. Yan, E. Agrell, H. Wymeersch, and M. Brandt-Pearce. Resource allocation for flexible-grid optical networks with nonlinear channel model [invited]. *IEEE/OSA J. Opt. Commun. Netw.*, 7(11):B101–B108, Nov. 2015.

[141] J. Y. Yen. Finding the k shortest loopless paths in a network. *Manag. Sci.*, 17(11):712–716, Jul. 1971.

[142] Yueqian. Channel capacity with QAM inputs. (Date last accessed 15-June-2020).

[143] T. Zami, K. Benyahya, A. Arnould, H. Mardoyan, J. Renaudier, and B. Lavigne. Impact of crosstalk on 800 gb/s 90 gbaud 64QAM channel. In *Proc. Optical Fiber Communications Conference and Exhibition (OFC)*, page M5C.3, San Francisco, USA, Jun. 2021.

[144] T. Zami and B. Lavigne. Is there a most appropriate channel spacing in wdm networks when individually routing 67 gbaud carriers? In *Proc. Opt. Fiber Commun. Conf. (OFC)*, page M4D.4., San Diego, USA, May 2020.

[145] G. Zervas, E. Hugues-Salas, T. Polity, S. Frigerio, and K.-I. Sato. *Node Architectures for Elastic and Flexible Optical Networks*, pages 117–157. Springer Int. Publishing, Cham, 2016.

[146] G. Zhang, M. De Leenheer, A. Morea, and B. Mukherjee. A survey on ofdm-based elastic core optical networking. *IEEE Commun. Surveys Tut.*, 15(1):65–87, Feb. 2013.

[147] G. Zhang, M. De Leenheer, and B. Mukherjee. Optical grooming in ofdm-based elastic optical networks. In *Proc. Opt. Fiber Commun. Conf. (OFC)*, pages 1–3. IEEE, 2012.

[148] M. Zhang, C. You, H. Jiang, and Z. Zhu. Dynamic and adaptive bandwidth defragmentation in spectrum-sliced elastic optical networks with time-varying traffic. *IEEE/OSA J. Lightw. Technol.*, 32(5):1014–1023, Mar. 2014.

[149] J. Zhao, H. Wymeersch, and E. Agrell. Nonlinear impairment-aware static resource allocation in elastic optical networks. *IEEE/OSA J. Lightw. Technol.*, 33(22):4554–4564, Aug. 2015.

[150] Z. Zhong, N. Hua, M. Tornatore, J. Li, Y. Li, X. Zheng, and B. Mukherjee. Provisioning short-term traffic fluctuations in elastic optical networks. *IEEE/ACM Trans. Netw.*, 27(4):1460–1473, Aug. 2019.

[151] F. Zhou. Multicast provision in transparent optical networks with mixed line rates. In *Proc. Int. Conf. Opt. Netw. Design and Modeling (ONDM)*, pages 125–130, Brest, France, Apr. 2013.

[152] F. Zhou, J. Liu, G. Simon, and R. Boutaba. Joint optimization for the delivery of multiple video channels in Telco-CDNs. *IEEE Trans. Netw. Service Manage.*, 12(1):87–100, Mar. 2015.

[153] X. Zhou, W. Lu, L. Gong, and Z. Zhu. Dynamic rmsa in elastic optical networks with an adaptive genetic algorithm. In *Proc. Global Commun. Conf. (GLOBECOM)*, pages 2912–2917, Dec. 2012.

[154] K. Zhu and B. Mukherjee. Traffic grooming in an optical wdm mesh network. *IEEE J. Sel. Areas Commun.*, 20(1):122–133, Jan. 2002.

[155] Z. Zhu, W. Lu, L. Zhang, and N. Ansari. Dynamic service provisioning in elastic optical networks with hybrid single-/multi-path routing. *IEEE/OSA J. Lightw. Technol.*, 31(1):15–22, Jan. 2013.

[156] Q. Zhuge, M. Morsy-Osman, X. Xu, M. Chagnon, M. Qiu, and D. V. Plant. Spectral efficiency-adaptive optical transmission using time domain hybrid qam for agile optical networks. *IEEE/OSA J. Lightwave Technol.*, 31(15):2621–2628, Aug. 2013.